修士学位論文

題名 The electrical properties of DMET and DIMET radical salts
(DMETおよびDIMETラジカル塩の電気物性)

指導教授 池本 勲 教授

~~平成~~ ~~昭和~~ 4年 1月10日提出

理学研究科 化学 専攻

氏名 吉野治一

論文要旨

「ＤＭＥＴおよびＤ ＩＭＥＴラジカル塩の電気物性」

9083446　　吉野 治一

５つのグループに分類された DMET 塩のうち，各グループの代表的な塩について熱電能を測定した．グループ１の PF_6，AsF_6 塩については半導体的挙動が観測された．これは以前の抵抗測定の結果と一致する．グループ２の BF_4 塩については２種類のドナー・スタックに沿った方向について熱電能を測定した．金属－絶縁体転移（M-I 転移）が約 35 K に観測され，抵抗測定の結果と一致した．熱電能測定の結果，バンド幅が a 軸に沿った方向の方が b 軸に沿った方向よりも大きいということがわかった．また，SDW 状態にある半導体領域で，熱電能の複雑な挙動が観測された．これは新たに行った抵抗率の測定からも確認され，SDW 状態の中でさらにバンド構造が複雑に変化することを示唆するものである．グループ３の塩では $Au(CN)_2$ 塩の熱電能を測定した．約 180 K での相転移，約 28 K での M-I 転移に対応した熱電能の変化が観測された．熱電能は 28 K 以下で急激な減少を示し，約 20 K で極小値をとって増大に転じる．半導体領域のこの温度付近で抵抗の増大の仕方も変化することがわかっており，何らかのバンド構造の変化が起こっているものと思われる．グループ４では I_3 と SCN 塩の熱電能を測定し，低温まで金属的な挙動が観測された．この結果は抵抗測定の結果と一致した．熱電能から得られた I_3 塩と SCN のバンド幅はグループ３の $Au(CN)_2$ 塩に比べて減少しており，グループ４の次元性がグループ３に比べて相対的に高まっていることが実験的に確認できた．この結果を用いて，低次元有機伝導体における超伝導の発現と次元性の関係について考察した．グループ５の $AuBr_2$ 塩は擬二次元的な物性を持つので試料結晶の２種類の方向について熱電能の測定を行った．その結果，絶対値は方向に依存するが，変化の仕方が似た挙動が両方向について観測された．

DMET の誘導体である DIMET の，新しく合成されたラジカル塩について抵抗率と熱電能の測定を行いこれらの塩の性質を特定した．これまでにほとんど報告のない直線型アニオンの塩を多く調べたが，DIMET 塩としてはまれな金属的な塩がいつくか見つかった．その中で I_3 塩はグループ３，４の DMET 塩と類似の結晶構造を持ち，DIMET の IBr_2 および $Cu(NCS)_2$ 塩と同様の特徴的な熱電能の挙動を示した．これらはいずれも約 40 K で M-I 転移を起こすことがわかった．低温の半導体領域では熱電能の符号は負となり，約 30 K で極小値をとるといった $(DMET)_2Au(CN)_2$ によく似た挙動が観測された．この挙動について考察を試みた．また，これらのDIMET 塩は高温側の金属的領域でも熱電能の特徴的な変化を示すことがわかった．この変化は次元性の変化に関連すると推測されたことから，さらに抵抗率の異方性の測定を行い，それについて調べた．他の DIMET 塩は BF_4 塩が金属的だったのを除くと半導体的な挙動が確認された．$AuCl_2$ および AuI_2 塩は I_3 塩と類似の構造をとっているにもかかわらず，電気的な性質が I3 塩と大きく異なっていることがわかったので，これらの塩について次元性と金属的性質の発現について考察を行った．

Contents

Abstract

Thermopower of some DMET radical salts (DMET = dimethyl(ethylenedithio)tetrathiafluvalene, the first unsymmetrical donor which gives organic superconductors) was measured and some band parameters, *i.e.* band-gap, bandwidth, were determined.

Resistivity, thermopower and anisotropy of DIMET salts (DIMET = dimethyl(ethylenedithio)tetrathiafluvalene, a sulfur analog of DMET) were also measured. The characterization of these salts was carried out and the band parameters were determined.

The relation between the superconductivity and/or the appearance of the metallic character and the dimensionality in organic conductors was discussed on the basis of the measurement. Some interesting phenomenon in the resistivity and the thermopower were observed and discussed comparing the behaviors of radical salts.

Chapter 1. Introduction

The search for organic superconductors was accelerated by the successful synthesis of TTF-TCNQ in 1973 and various organic donor/acceptor molecules that give conducting charge transfer (CT) salts have been synthesized.[1] Structural formulas of TTF and TCNQ molecules are shown in Fig. 1.1(a) and (b), respectively. (TTF = tetrathiafluvalene, a donor, TCNQ = tetracyanoquinodimethane, an acceptor) Electrical properties of TTF-TCNQ are metallic from room temperature (RT) down to 60 K. The possibility of superconductivity in organic material was arisen from the wide range metallic behavior that has never been seen in organic materials before that. Since TTF-TCNQ itself undergoes a metal-insulator (M-I) transition at about 60 K, superconductivity is not observed in the material in fact. TTF-TCNQ has both the stack of TTF molecules and the stack of TCNQ ones.[2,3] Neighboring molecules in each stack faces their molecular planes each other, *i.e.* π-orbitals of the molecules overlaps each other. Since both overlap in the TTF stack and the TCNQ stack are well to form bands to contribute for electrical conduction, the material shows metallic behavior. The bands formed in this manner is quasi one-dimensional (1D), because the face-to-face interaction of molecular orbitals is much stronger than the side-by-side interaction. The quasi one-dimensionality in TTF-TCNQ is a cause of the M-I transition. It is well known as the Peierls instability that a 1D system is unstable against the perturbation of the wave number of $2k_F$, where k_F is the Fermi wave number.[4] If a kind of $2k_F$-perturbation exists in a 1D metallic material, the band-gap opens at the wave number $k=\pm k_F$ and the material becomes a semiconductor (or an insulator when the gap is large), *i.e.* a M-I transition occurs. In the case of TTF-TCNQ the perturbation is a charge-density-wave (CDW) that is a kind of wave of charge density coupled to the modulation of the crystal lattice along the stacking direction and the transition is called as "Peierls transition". On cooling down to about 60 K and the Peierls transition occurs in TTF-TCNQ.

Although the superconductivity was not observed in TTF-TCNQ,

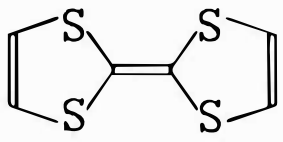

(a) TTF

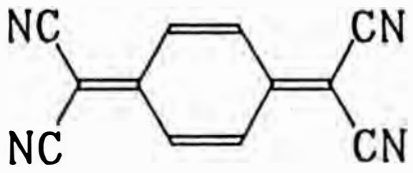

(b) TCNQ

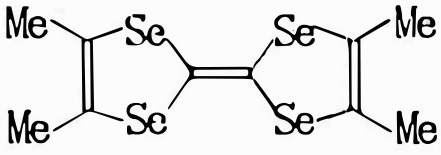

(c) TMTSF

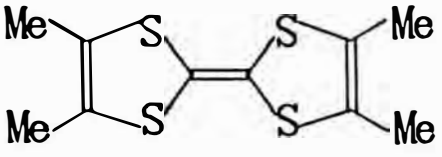

(d) TMTTF

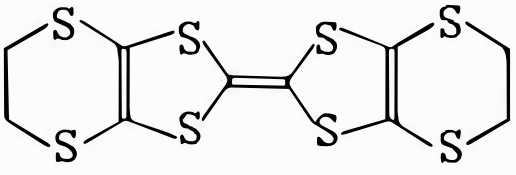

(e) BEDT-TTF

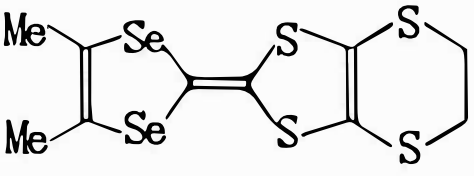

(f) DMET

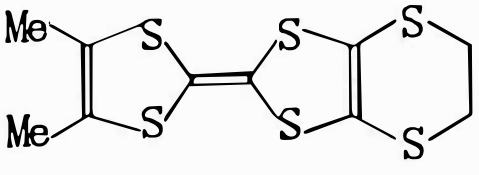

(g) DIMET

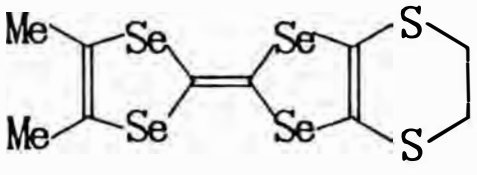

(h) DMET-TSF

Fig. 1.1. Structural formulas of (a) TTF, (b) TCNQ, (c) TMTSF, (d) TMTTF, (e) BEDT-TTF, (f) DMET, (g) DIMET and (h) DMET-TSF.

synthesis of chemical derivatives of TTF has been performed to get organic superconductors with great enthusiasm. As a result, it was found that five kinds of TTF-derivatives give more than thirty kinds of superconducting salts with inorganic anions up to now.[4] Many of these superconductors and conducting (not superconducting) salts of the five and other chemical derivatives of TTF have the composition of two donors and one monovalent inorganic anion. The conduction band of such a 2:1 salt is formed by overlapping of the highest occupied molecular orbital (HOMO) of each donor molecule. The HOMO of a TTF-derivative molecule accepts two electrons. Because one electron is taken from a pair of donors, when the 2:1 salt is composed, three of the four electrons from their HOMO's remain in the conduction band, namely the conduction band is 3/4-filled. The Fermi energy can be known if the band structure is established.

TMTSF (TMTSF = tetramethyl(tetraselena)fluvalene, see Fig. 1.1(c)) was synthesized at first of the five kinds of sources of the organic superconductors. The first observation of superconductivity in organic materials was reported for $(TMTSF)_2PF_6$ at 0.9 K under 12 kbar in 1980.[5] After this discovery, many TMTSF salts of the series of $(TMTSF)_2X$ ($X=AsF_6$, ClO_4, FSO_3 etc. called "Bechgaard salts") including more six superconductors, have been reported and various investigation have been performed. Among them the material that possesses the highest superconducting transition temperature (T_c) is $(TMTSF)_2TaF_6$ (1.4 K under 12 kbar)[6].

Besides superconductivity, one of the most interesting characters of the Bechgaard salts is a quasi-1D character with very high conductivity (400 - 800 S/cm at room-temperature) along one direction.[7] The quasi-1D high conductivity of $(TMTSF)_2X$ is due to the columnar packing of donor molecules in the crystal as shown in Fig. 1.2.[8] Owing to this face-to-face stacking of donor molecules along the direction nearly normal to the molecular plane, their π-orbitals well overlap to each other and construct a band that contributes to the electrical conduction. There are shorter contacts between neighboring donor molecules than the sum of the van der Waals radii of two Se atoms. Such short contacts between chalcogen atoms

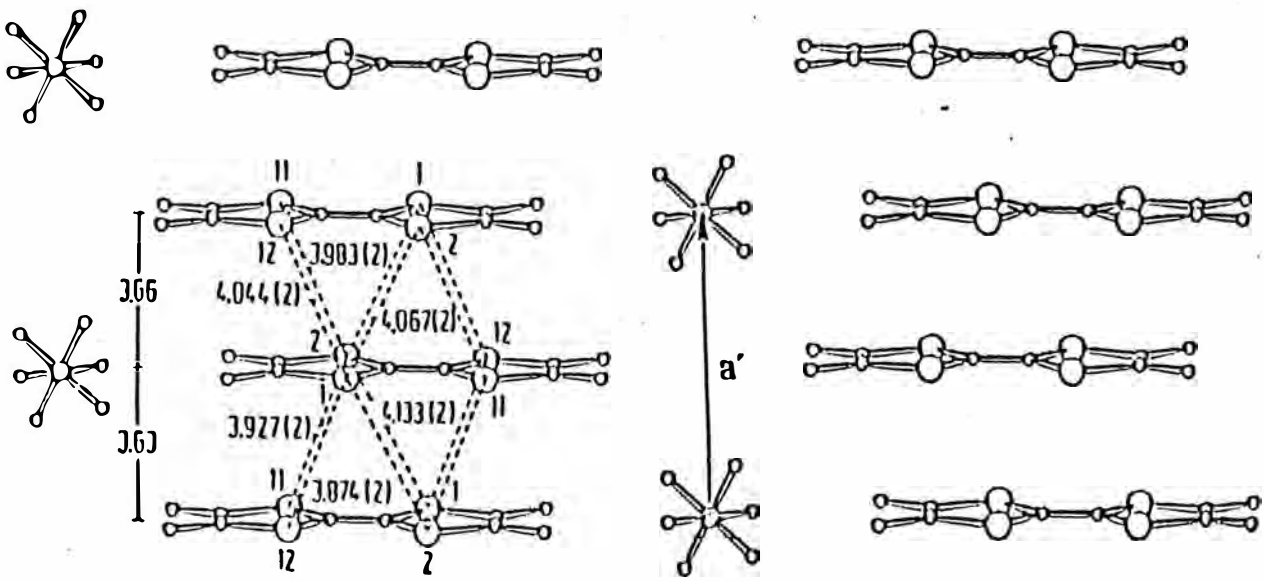

Fig. 1.2. Crystal structure of $(TMTSF)_2PF_6$. Side view of stacks; a' is the projection of a.

play an important role in the properties of organic conductors. However, the overlapping of molecular orbitals (MO) along parallel directions to the molecular plane is much less than the former, though some side-by-side short contacts of Se atoms are observed along almost parallel to the b-axis. As a result, the conductivity ratio at RT is $\sigma_a:\sigma_b:\sigma_c = 100:1:10^{-4}$ (each subscript means a direction along each crystallographic axis).[9-11]

There are observed other interesting phenomena at low temperature in some Bechgaard salts with PF_6, AsF_6 and so on. One of them is SDW (spin-density-wave) state of the 1D system.[12-16] SDW is a wave of spin density of electrons in a conduction band. If SDW appears, spin density is modulated in the space. In contrast to TTF-TCNQ, the gap-opening in some $(TMTSF)_2X$ is caused by the perturbation due to SDW and the M-I transition is called the SDW transition. In fact the superconductivity of Bechgaard salts is observed under pressure except ClO_4 salts and SDW transition occurs at ambient pressure in PF_6, AsF_6 salts and so on. Under some pressure, however, dimensionality of these salts changes from quasi-1D to slightly quasi-2D character because the increase in the side-by-side interaction of MO is larger than that of face-to-face.[6] As a result, the 1D instability is suppressed and M-I transition disappears.

The brief introduction of salts of TMTTF, the sulfur analog of the former, is necessary for the later discussion. (TMTTF = tetramethyltetraselenafluvalene, see Fig. 1.1(d)) Though the shape of molecular and crystal structures of its salts are similar to those of TMTSF, properties of the two series of salts are very different from each other. Most of TMTTF salts reported are slightly metallic or semiconducting, and no superconductor is found among them.[17-19] This is possibly attributed to the decrease in intracolumn interactions in TMTTF salts as compared to TMTSF ones. Because the van der Waals radius of S is smaller than that of Se, the overlap integral between donor molecules in a donor stacking becomes shorter in TMTTF salts. In other words their band widths must also be smaller. At the point of searching for superconductors, the TMTTF series was in failure. However, TMTTF is important for a deeper

understanding of physical properties of organic conductors, since TMTTF salts produced the information about influence of changing donors from TMTSF to TMTTF.

A series of superconducting TMTSF salts is, so to speak, the first generation of organic superconductors. Although many interesting phenomena other than those mentioned above have been observed and investigated, a desire to get high-T_c superconductors was not satisfied by TMTSF salts. Higher-T_c organic materials have been synthesized with BEDT-TTF (bis(ethylenedithio)tetrathiafluvalene, alternatively abbreviated as ET, see Fig. 1.1(e)). The first observation of superconductivity among them was performed with $(BEDT\text{-}TTF)_2ReO_4$, one of the various structures of ReO_4 salts of BEDT-TTF, whose T_c is 2 K under a pressure of 7 kbar.[20] After this discovery, about 20 salts of superconducting BEDT-TTF salts have been found. Furthermore T_c has been increased up to 12.8 K at 0.3 kbar by the recent synthesis of κ-$(BEDT\text{-}TTF)_2CuN(CN)_2Cl$ (κ means a certain type of crystal structure to be explained below).[21,22]

The important properties of BEDT-TTF salts are the quasi-two-dimensionality of electrical conduction and wide variety in packing of donor molecules, *i.e.* crystal structure. Although almost all conducting $(TMTSF)_2X$ has the same type of structure with 1D donor stacks shown in Fig. 1.2, BEDT-TTF salts have more than eight types of donor packing. One kind of counter anion sometimes gives several structures of crystals. For example, at least four main different structures are known for I_3 salts, and they are symbolized as "α-", "β-", "θ-" and "κ-".[23-25] As a result physical properties of BEDT-TTF salts spread over the wide range.

The wide variety in crystal structure is attributed to the shape of BEDT-TTF molecule to a certain extent.[26] The molecule has two ethylenedithio units on its ends. These units contribute to side-by-side interaction between donor molecules by extending π-electrons over the molecule and contacting its S atoms which have larger van-der-Waals radii than C atom with those of neighbor donor molecules. Furthermore a BEDT-TTF molecule in radical salts is not planer

because the six-membered ring including ethylenedithio unit bends for stability. This results in weakening of face-to-face interaction of donors and increase the dimensionality. The conductivities, β-$(BEDT-TTF)_2I_3$ for instance, measured in the plane of plates of the sample crystal is nearly isotropic and values of them are about 30 S/cm.[27)]

The superconducting DMET salts were discovered in 1987.[28)] (DMET = dimethyl(ethylenedithio)tetrathiafluvalene) As shown in Fig. 1.1(f), DMET has a shape that is formed by connecting a half components of TMTSF and BEDT-TTF molecules each other. A purpose of taking DMET to synthesize radical salts was to get superconductors. Because both TMTSF and BEDT-TTF gave superconductors, it could be expected that DMET which probably inherits a part of their characters would give superconductors. Another purpose was to get a systematic understanding of TMTSF and BEDT-TTF whose salts had very different properties as mentioned before. If it can be expected that a DMET molecule has intermediate character of TMTSF and BEDT-TTF molecules, DMET salts have intermediate properties of salts of their parent donors. The third purpose was to develop a new type of donors, namely unsymmetrical ones. Before the discovery of DMET superconductors, some investigators claimed that no unsymmetrical donor gives superconductors due to the disorder probably made by the unsymmetricity of the molecule and disturb a periodic potential of the crystal. However this was not the case. The fourth purpose was to discover new physical properties as the result of the unsymmetricity. Most of these purposes are also common to investigating other unsymmetrical donors.

Since DMET salts are one of the objects of this study, their known physical properties, especially electrical ones, are briefly summarized. Conducting DMET salts are classified into five groups on the basis of the temperature dependence of electrical resistance and counter anions.[29-31)] The temperature dependence of resistance of typical DMET salts, at ambient pressure, of each group is shown in Fig. 1.3.

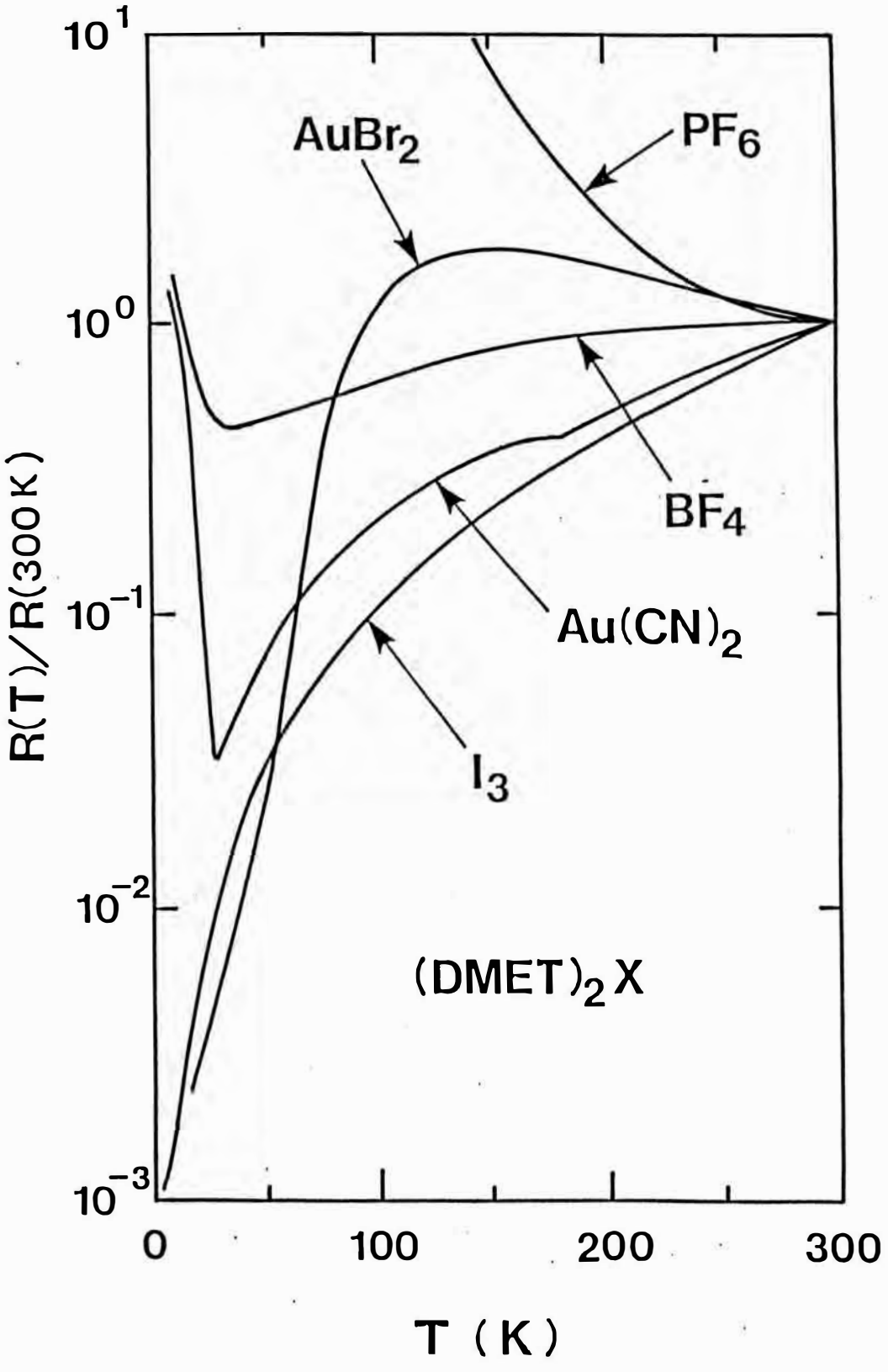

Fig. 1.3. Temperature dependence of resistivity of DMET salts normalized at 300 K.

PF_6, AsF_6 and SbF_6 salts are classified into Group 1. These salts have octahedral counter anions and show semiconducting behavior below RT. Their crystal structure possesses 1D columns of DMET molecule as shown in Fig. 1.4.[32-34] The donor molecules stack turning TMTSF components to opposite directions alternately one by one and the molecular planes tilt from the stacking direction. Though this type of structure is common to DMET and DIMET salts, relatively strong dimerization of donors is characteristic for semiconducting salts like this group.

BF_4 and ClO_4 salts are classified into Group 2, in short they have tetrahedral anions.[30-34] These salts have common features, namely temperature dependence of resistance is metallic down to about 40 K, then becomes semiconducting at a lower temperature. Furthermore each of their crystal has two types of donor stacks, which are almost perpendicular to each other, as shown in Fig. 1.5.[35,36] This structure is also found in salts with a few kinds of unsymmetrical donors, for example $(DIMET)_2ClO_4$ (DIMET = dimethyl(ethylenedithio)tetrathiafluvalene, see Fig. 1.1(g)),[37,38] $(DIMET)_2BF_4$[39] and $(DMET\text{-}TSF)_2BF_4$. (DMET-TSF = dimethyl(ethylenedithio)tetraselenafluvalene, see Fig. 1.1(h)) DIMET and DMET-TSF are derivatives of DMET whose two S atoms of the five-membered rings are substituted by S or Se atoms.

Though ReO_4 salt contains a tetrahedral anion, the salt has a 1D columnar structure and is not classified into any groups.[40] In addition, a period of this donor stack is four molecules, namely tetrameres are formed. As a result, the ReO_4 salt shows semiconducting behavior below 293 K at ambient pressure, because the period is a cause of gap-opening at k_F in 3/4-filled band of 1D material.

Salts in Groups 3 and 4 have linear anions.[30-34] Group 3 is composed of $AuCl_2$, AuI_2 and $Au(CN)_2$ salts. Their crystal structures are like PF_6 salt mentioned above except the dimerization seen in Group 1, although that of $AuCl_2$ salt is slightly different from the others. The crystal structure of $(DMET)_2Au(CN)_2$ is shown in Fig. 1.6. The temperature dependence of resistance is metallic down to a low

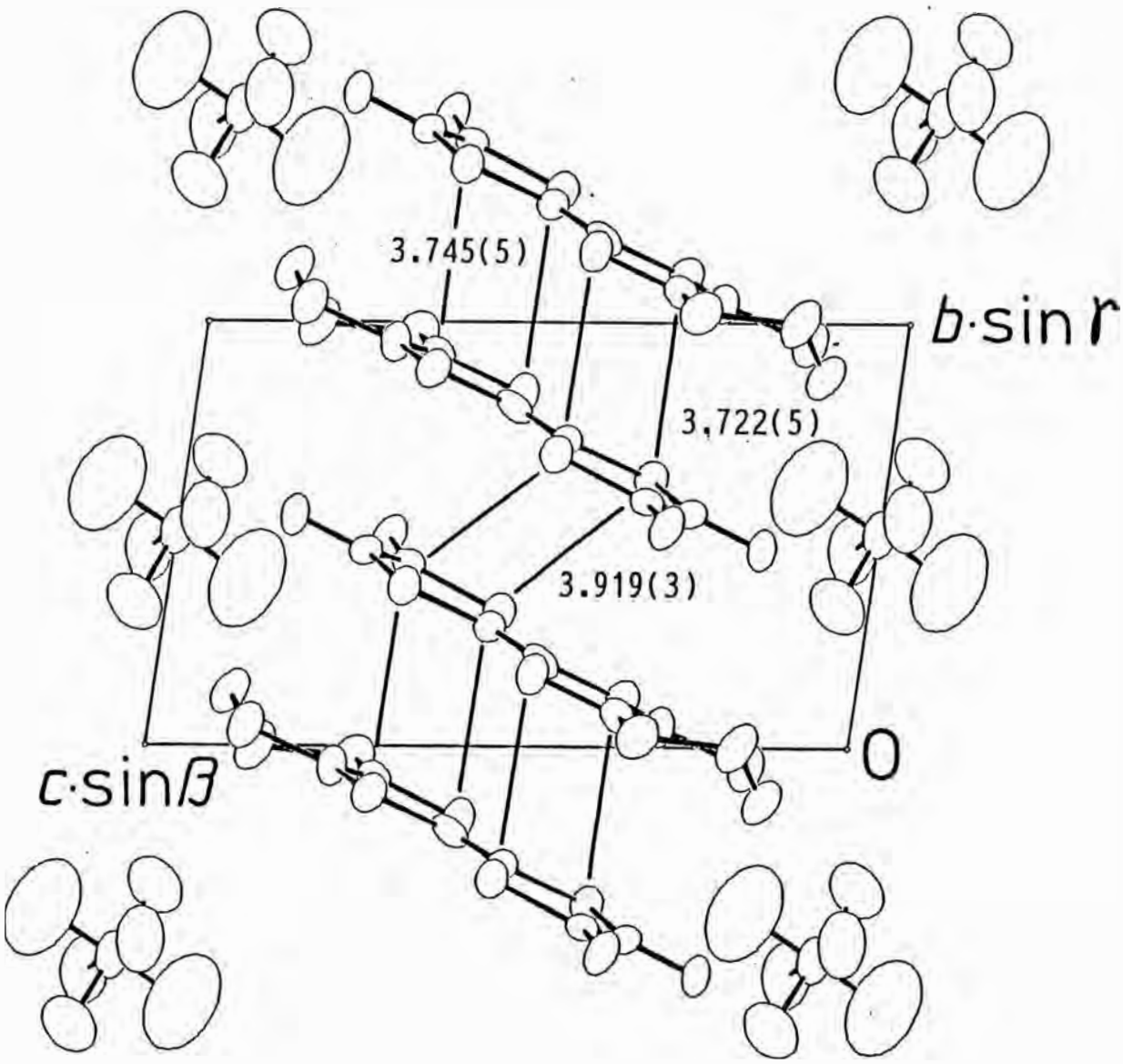

Fig. 1.4. Crystal structure of $(DMET)_2PF_6$ viewed along the a-axis.

(a)

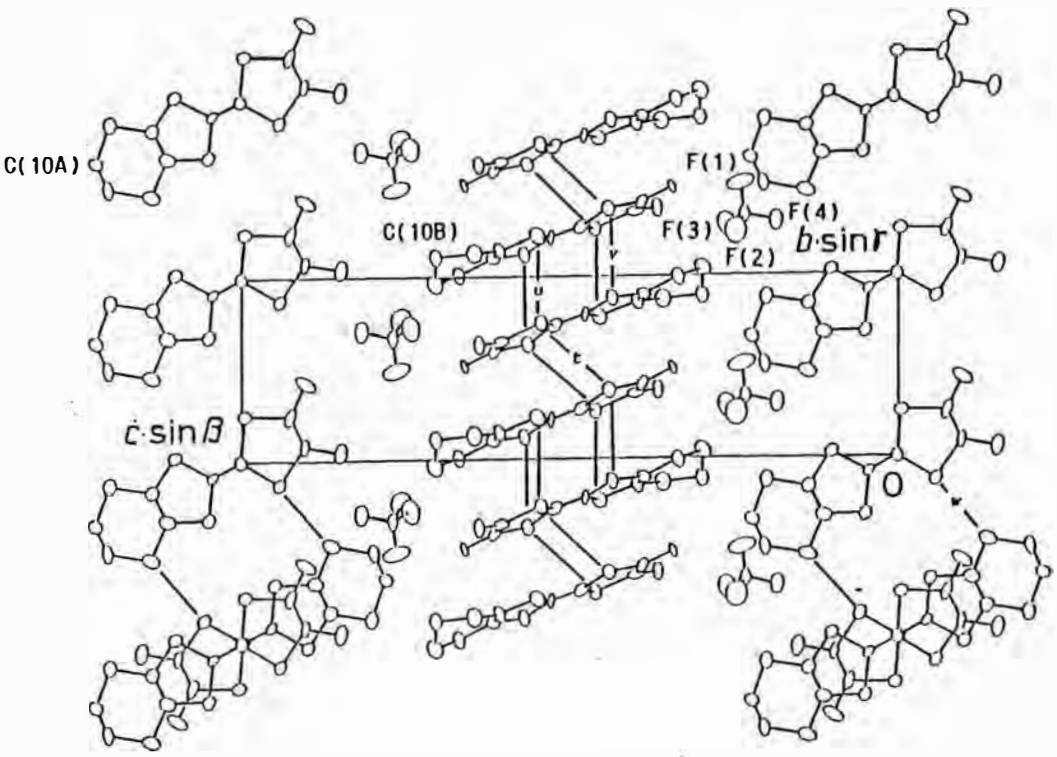

(b)

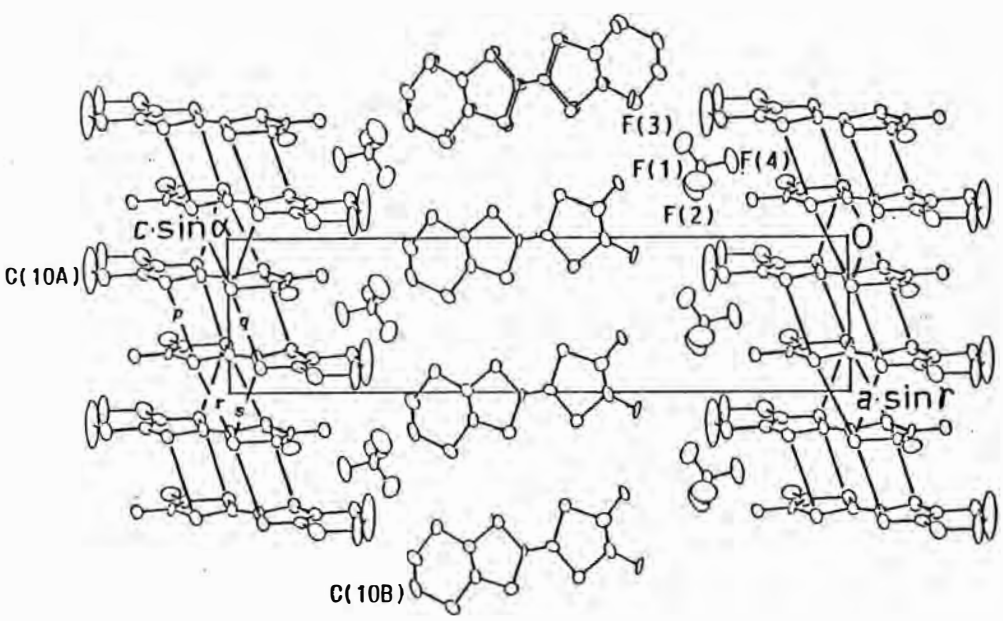

Fig. 1.5. Crystal structure of $(DMET)_2BF_4$ viewed along the b-axis (a) and viewed along the a-axis (b).

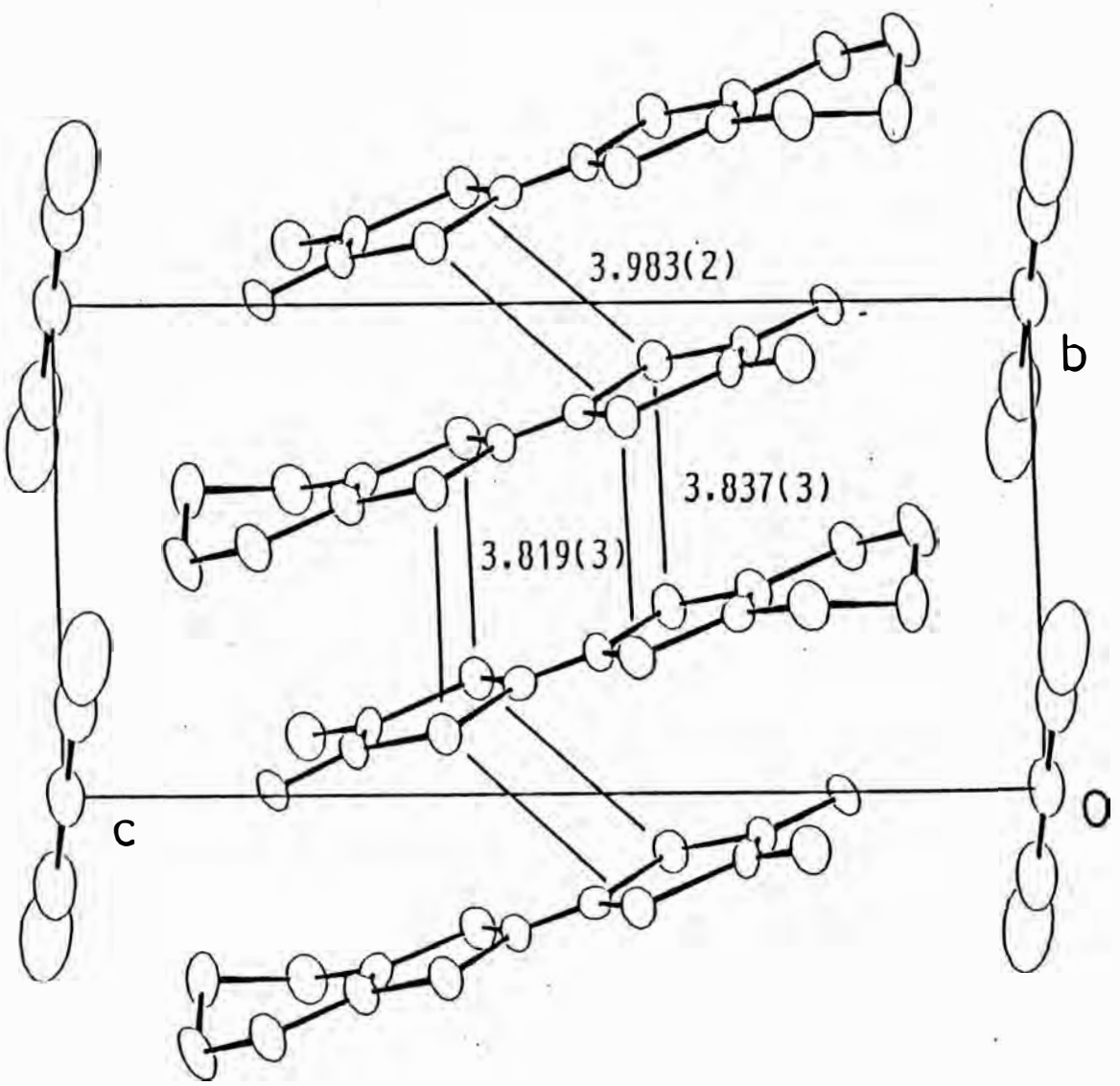

Fig. 1.6. Crystal structure of $(DMET)_2Au(CN)_2$ viewed along the a-axis.

temperature. $AuCl_2$ salt have a minimum in resistance at about 3 K and the resistance slightly increase down to 1 K, at which a superconducting transition occurs under ambient pressure. The weak increase in resistance suggests the presence of the insulating phase in the phase diagram. Under 0 kbar AuI_2 and $Au(CN)_2$ salts undergo a M-I transition at 20 and 28 K, respectively. However they become superconductors at 0.55 K under 5 kbar for the former and 1.1 K under 3.5 kbar for the latter. The common feature of these salts containing Au is the existence of insulating phase. In addition, $Au(CN)_2$ salt has another phase transition at about 180 K in the metallic regime. This is confirmed by the measurement of heat capacity and detected as an anomaly of the temperature dependence of resistance shown in Fig. 1.3.

I_3, I_2Br, IBr_2, SCN and $AuBr_2$ salts is classified into Group 4. They also have linear counter anions and their crystal structures are like that of Group 3. Behavior of resistance with decreasing temperature is metallic down to low temperature and there is no sign of the presence of any insulating phase in the temperature region studied. In Group 4, I_3 and IBr_2 salts become superconducting at 0.47 and 0.58 K, respectively, at ambient pressure. The other salts of this group have residual resistance at the lowest temperature (about 0.5 K).

There is another morphology of $(DMET)_2AuBr_2$.[30-34] This is the only member of Group 5. The crystal structure of this salt is in Fig. 1.7 and is like the κ-type of BEDT-TTF salts.[25,41,42] Each component made of paired donor molecules arrayed perpendicular to one another and constructs 2D donor sheets and neighboring donor sheets are separated by an anion sheet. This 2D structure is BEDT-TTF like, contrary to 1D column structure seen in Groups 1 to 4. This is one of the evidence that DMET have a intermediate character of TMTSF and BEDT-TTF. In agreement with its crystal structure, $(DMET)_2AuBr_2$ of Group 5 shows the similar temperature dependence of resistance to the κ-type BEDT-TTF salts. As seen in Fig. 1.3, at ambient pressure, resistance of this salt gradually increases with decreasing temperature from RT to about 150 K like a semiconductor. Then below

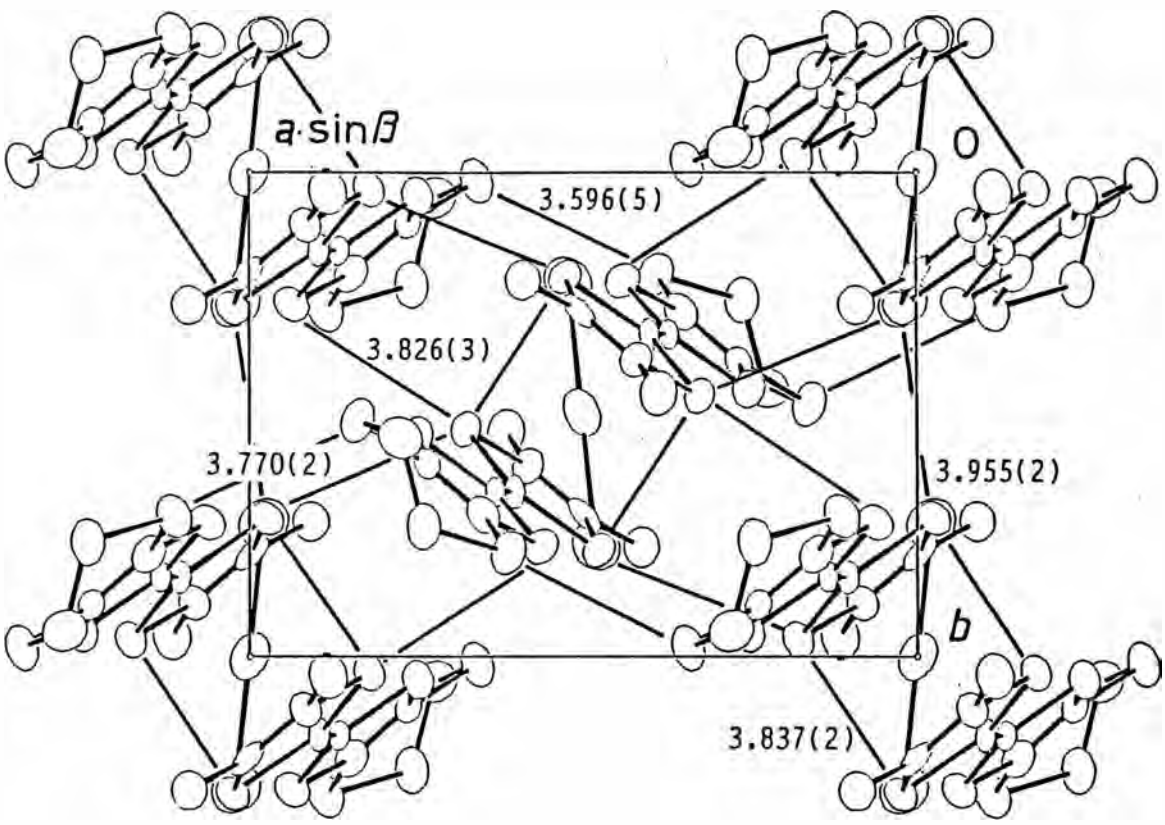

Fig. 1.7. Crystal structure of $(DMET)_2AuBr_2$ (Z=2) viewed along the c-axis.

about 150 K, resistance turns to decrease and the material becomes a superconductor at 1.9 K. This is the highest T_c of DMET salts at present.

There are also other investigations of physical properties of the DMET salts. ESR measurement is one of these studies.[43,44] ESR is a effective tool to get microscopic information about objects, especially it is often used for organic conductors to study SDW, a kind of magnetic ordered state. A knowledge about dimensionality of DMET salts has been brought. An evidence of higher dimensionality of $(DMET)_2I_3$ than those of salts in Groups 1 - 3. It was found from temperature dependence of ESR linewidths.

Though many studies were performed, there exist few experimental information about band structures of DMET salts, for example a bandwidth, a sign of dominant carrier and so on. If the band structure is revealed, we can discuss about dimensionality of the materials. Furthermore, we will get a guide to synthesize a new material such as superconductors with higher T_c. For these reasons, thermopower of the typical DMET salts of each group, namely PF_6. AsF_6 (Group 1), BF_4 (Group 2), $Au(CN)_2$ (Group 3), I_3, SCN (Group 4), $AuBr_2$ (Group 5) and ReO_4 salts, were measured.

The shape of DIMET molecule has already been shown in Fig. 1.1. Since DIMET is composed of each halves of BEDT-TTF and TMTTF, it contains only S as heteroatoms, though its shape is similar to DMET. A purpose to investigate DIMET salts is, therefore, to get knowledge about influence of changing donor properties for radical salts through the comparison of their properties. Another purpose is to know what happens when BEDT-TTF, a source of superconductors, and TMTTF, giving no superconductors, are combined. There is a possibility to find new organic superconductors or new phenomena in DIMET salts.

The first report of DIMET salts precedes those of DMET salts in fact. DIMET salts of PF_6, AsF_6, SbF_6, ClO_4, ReO_4, AuI_2, Br, etc. have been reported since 1985.[37,38,45-48] Many of them have similar crystal structures to the corresponding DMET salts. No superconductor has been found in these DIMET salts and even metallic

salts are few. This is a similar case of TMTSF and TMTTF. However most of counter anions of the salts reported are octahedral or tetrahedral, and only few studies were done on salts with linear. In the case of DMET salts, superconductors were obtained only using linear anions. For this reason, DIMET salts with linear counter anions must be investigated.

In this study, on DIMET salts of I_3, IBr_2, Br_3, $AuCl_2$, AuI_2. $Ag(CN)_2$, $Cu(NCS)_2$ (linear), BF_4 (tetrahedral) and PF_6 (octahedral) synthesized at this laboratory, measurement of resistance and thermopower were carried out. Discussion was performed through comparing a DIMET salts with other DIMET and DMET salts and so on.

After this chapter, experimental details are described in the second chapter. In the third chapter, results of the measurement are shown in order and properties found in this study are explained for each salt. The resulting discussion is given in the fourth chapter and the last chapter concludes this thesis.

References to Chapter 1

1 L. B. Coleman, M. J. Cohen, D. J. Sandman, F. G. Yamagishi, A. F. Garito and A. J. Heeger, Solid State Commun. 12, 1125(1973).

2 T. E. Phillips, T. J. Kistenmacher, J. P. Ferraris and D. O. Cowan, J. Chem. Soc. Chem. Commun., 471(1973).

3 T. J. Kistenmacher, T. E. Phillip and D. O. Cowan, Acta Cryst. B30, 763(1974).

4 See, for example, T. Ishigro and K. Yamaji: *Organic Superconductors*, Springer. Ser. Solid-State. Sci. Vol.88(Springer, Berlin, Heidelberg 1990).

5 D. Jerome, A. Mazaud. M. Ribault and K. Bechgaard, J. Physique Lett. 41, L95(1080).

6 S. S. P. Parkin, M. Ribault, D. Jerome and K. Bechgaad, J. Physique, C14, L445(1981).

7 K. Bechgaad, C. S. Jacobsen, K. Mortensen, J. H. Pederson and N. Thorup, Solid State Commun., 33, 1119(1980).

8 N. Thorup, G. Rindorf, H. Soling and K. Bechgaad, Acta Cryst., B37, 1236(1981).

9 C. S. Jacobsen, K. Mortensen, M. Weger and K. Bechgaad, Solid State Commun., 38, 423(1981).

10 K. Murata, H. Anzai, G. Saito, K. Kajimura and T. Ishiguro, J. Phys. Soc. Jpn., 50, 3529(1981).

11 R. L. Greene, P. Haen, S. Z. Huang, E. M. Engler, M. -Y. Choi and P. M. Chaikin, Mol. Cryst. Liq. Cryst., 79, 183(1982).

12 K. Mortensen, Y. Tomkiewicz and K. Bechgaad, Phys. Rev, 25, 3319(1982).

13 W. M. Walsh Jr., F. Wudl, G. A. Thomas, D. Nalewajek, J. J. Hauser, P. A. Lee and T. Poehler, Phys. Rev. Lett., 45. 829(1980).

14 A. Andrieux, D. Jerome and K. Bechgaad, J. Physique Lett., 42, L87(1982).

15 J. C. Scott, H. J. Pedersen and K. Bechgaad,

Phys. Rev., B24, 475(1981).

16 J. B. Torrance, H. J. Pedersen and K. Bechgaad, Phys. Rev. Lett., 49, 881(1982).

17 B. Liautard, S. Peytaven, G. Brun and M. Maurin, J. Physique, 44, C3-951(1983).

18 K. Mortensen, E. M. Conwell and J. M. Fabre, Phys. Rev., B28, 5856(1983).

19 K. Mortensen and E. M. Engler, Mol. Cryst. Liq. Cryst., 119, 293(1985).

20 S. S. P. Parkin, E. M. Engler, R. R. Schumaker, R. Lagier, V. Y. Lee, J. C. Scott and R. L. Greene, Phys. Rev. Lett., 50, 270(1983).

21 J. M. Williams, A. M. Kini, H. H. Wang, K. D. Carlson, U. Geiser, L. K. Montgomery, G. J. Pyrka, D. M. Watkins, J. M. Kommers, S. J. Boryschuk, A. V. Striby Crouch, W. K. Kwok, J. E. Schilber, D. L. Overmyer, D. Jung and M. -H. Wangbo, Inorg. Chem. 29, 3272(1990).

22 H. H. Wang, K. D. Carlson, U. Geiser, A. M. Kini, A. J. Schultz, J. M. Williams, L. K. Montgomery, W. K. Kwok, U. Welp, K. G. Vandervoort, S. J. Boryschuk, A. V. Strieby Crouch, J. M. Kommers and D. M. Watkins, Synth. Metals 42, 1983(1991).

23 I. Hennig, K. Bender, D. Schweitzer, K. Diez, H. Endres, H. J. Keller, A. Gleiz and H. W. Helberg, Mol. Cryst. Liq. Cryst., 119, 337(1985).

24 H. Kobayashi, R. Kato, A. Kobayashi, Y. Nishino, K. Kajita and W. Sasaki, Chem. Lett., 1986, 2017(1986).

25 A. Kobayashi, R. Kato, H. Kobayashi, S. Moriyama, Y. Nishino, K. Kajita and W. Sasaki, Chem. Lett., 1987, 459(1987).

26 P. C. W. Leung, T. J. Emge, M. A. Beno, H. H. Wang, J. M. Williams, V. Patrick and P. Coppens, J. Am. Chem. Soc., 107, 6184(1985).

27 E. B. Yagubskii, I. F. Shchegolev, V. N. Laukhin, P. A. Kononovich, M. V. Karsovnic, A. V. Zvarykina

and L. I. Bubarov, JETP Lett., 39, 12(1984).
28 K. Kikuchi, M. Kikuchi, T. Namiki, K. Saito, I. Ikemoto, K. Murata, T. Ishigro and K. Kobayashi, Chem. Lett., 931(1987).
29 K. Murata, K. Kikuchi, T. Takahashi, K. Kobayashi, Y. Honda, K. Saito, K. Kanoda, T. Tokiwa, H. Anzai, T. Ishiguro and I. Ikemoto, J. Mol. Electron., 4, 173(1988).
30 K. Kikuchi, K. Saito, I. Ikemoto, K. Murata, T. Ishiguro and K. Kobayashi, Synth. Metals, 27, B269(1988).
31 K. Kikuchi, Y. Ishikawa, K. Saito, I. Ikemoto, and K. Kobayashi, Synth. Metals, 27, B391(1988).
32 I. Ikemoto, K. Kikuchi, K. Saito, K. Kanoda, T. Takahashi, K. Murata, K. Kobayashi, Mol. Cryst. Liq. Cryst., 181, 185(1990).
33 K. Kikuchi, I. Ikemoto and K. Kobayashi, Synth. Metals., 19, 551(1987).
34 Y. Ishikawa, M. Sc. Thesis, Department of Chemistry, Faculty of Sc., Tokyo Metropolitan University(1989).
35 Y. Ishikawa, K. Saito, K. Kikuchi, K. Kobayashi and I. Ikemoto, Bull. Chem. Soc. Jpn., 64, 212(1991).
36 T. G. Takhirov, O. N. Karasochka, O. A. D'Yachenko, L. O. Atovmyan, M. L. Petrov, I. K. Pubtsova and R. N. Lyubovskaya, Zh. Atrukt. Khim. 30, 114(1989).
37 M. Z. Aldoshina, L. O. Atovmyan, L. M. Goldenberg, O. N. Krasochka, R. N. Lubovskaya, R. B. Lubovskii, V. A. Marzhanov and M. L. Khidekel, J. Chem. Soc., Chem., Commun., 1658(1985).
38 H. Endres, R. Heid, H. J. Keller, I. Heinen and D. Schweitzer, Acta Cryst., C43, 115(1987).
39 H. Itoh, B. Sc. Thesis, Department of Chemistry, Faculty of Sc., Tokyo Metropolitan University(1991).
40 K. Saito, Y. Ishikawa, M. Ishibashi, K. Kikuchi, K. Kobayashi and I. Ikemoto, Bull. Chem. Soc. Jpn., 63, 1865(1990).

41 H. Urayama, H. Yamochi, G. Saito, S. Saito, A. Kawamoto, J. Tanaka, T. Mori, Y. Maruyama, H. Inokuchi, Chem. Lett., 436(1988).

42 G. Saito, H. Urayama, H. Yamochi, K. Oshima, Synth. Metals, 27, A331(1988).

43 K. Kanoda, T. Takahashi, K. Kikuchi, K. Saito, I. Ikemoto and K. Kobayashi, Synth. Metals, 27, B385(1988).

44 K. Kanoda, T. Takahashi, T. Tokiwa, K. Kikuchi, K. Saito, I. Ikemoto and K. Kobayashi, Phys. Rev., B38, 39(1988).

45 R. Laversanne, E. Dupart and P. Delhaes, Mol. Cryst. Liq. Cryst., 137, 179(1986).

46 R. Laversanne, C. Coulon, J. Amiell, E. Dupart, P. Delhaes, J. P. Morand and C. Manigand, Solid State Commun., 58, 765(1986).

47 B. Gallois, J. Gaulitier, F. Bechtel, D. Chasseau, C. Hauw and L. Duchasse, Synth. Metals, 19, 419(1987).

48 K. Bender, H. Endres, S. Gärtner, E. Gogu, R. Heid, I. Heinen, H. J. Keller, A. Kraatz and D. Schweitzer, Synth. Metals, 19, 559(1987).

Chapter 2. Experimental

2.1 Measurement of resistivity

2.1.1 Purpose

One of the most basic measurements for studying organic conductors is measurements of resistivity. When one wants to know whether a material conducts electricity well or not, he should measure the resistivity. If the resistivity of the material decreases with decreasing temperature, it is apparently "metallic". If the resistivity, on the contrary, increases with decreasing temperature, it is "semiconducting". The magnitude of the resistivity itself is important information about the material. However, the temperature dependence of the resistivity is another point, *i.e.* there exist a metallic material and a semiconducting one both of which have a comparable magnitude of the resistivity. The temperature dependence of resistance is therefore usually studied.

After one found a new metallic material, the measurement down to lower temperatures is usually made to know whether the superconducting transition occurs or not. One of the characteristics of superconductivity is the zero-resistivity. If the abrupt decrease in resistivity is observed at a low temperature and the resistivity becomes less than the lower limit of the measurement, it is possibly the superconductivity, although other experiments, the Meissner effect for instance, must be made for the confirmation.

An anomaly in resistivity is also observed at other transitions. An M-I transition is general in studying low dimensional conductors. When the transition occurs, the temperature dependence changes from metallic to semiconducting behavior. (Note that an insulator is a kind of semiconductor.) Measurements of the temperature dependence of the resistivity is useful to get the information about such a transition or a change in the electronic state of a material.

The resistivity as a function of pressure is also interesting. The superconductivity in some organic materials is observed only under some pressure. The measurement of resistivity at a low

temperature under pressure is important to find a new superconductor, although there are some difficulties.

All described above is the first purpose, namely to know a behavior of a material. There is also another use in measuring resistivity. That is to estimate the anisotropy (or dimensionality) of the electrical property. The dimensionality of the system sometimes determines the behavior of low-dimensional (quasi-1D or 2D) materials. Measurement of reflectance spectra is often performed to get information about band parameters such as the effective mass of the carrier, the band width of a metal, the band gap of a semiconductor and so on. From the reflectance spectra using polarized light, one can also elucidate the anisotropic nature of the crystal. Although the optical technique including the measurement of the reflectance spectra is almost conclusive method to get information about the band structure, the optical technique is rather exaggerated for only knowing the temperature dependence of the resistivity and its anisotropy. One had better use the electrical and the optical method properly. To estimate the anisotropy is only one example of the information from measurements of resistivity and there are also others. However more detailed explanation about the principle, the instrument, the methods of some kind of measurements and the analyses are described in later subsections.

2.1.2 Principles

2.1.2.1 Four-probe method

If two kinds of materials are contacted and the electrical current runs through the connection, the contact resistance usually arises there. It is a obstacle to measure the intrinsic resistance of the sample. The four-probe (or four-wire) method is often used to overcome the difficulty.

In the four-probe method, four wires are connected on the sample, *e.g.* a cylinder as shown in Fig. 2.1. The electrical current I runs through the wire 1, the sample and the wire 2. The voltage V between the wires 3 and 4 is measured with a voltmeter. It is worth noting that the current does not run through the connection of

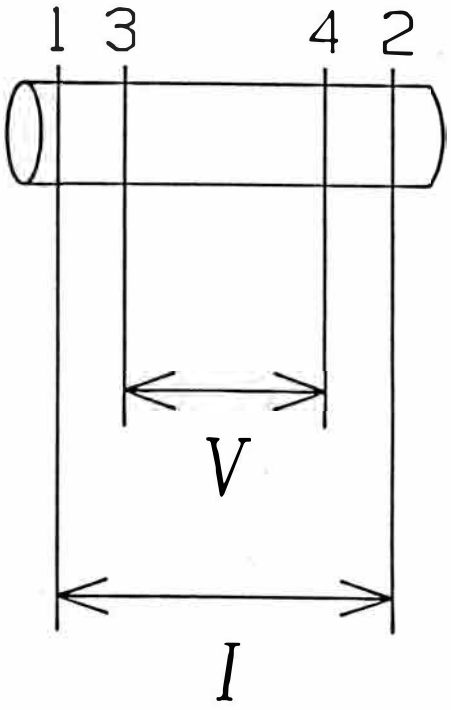

Fig. 2.1. Resistivity measurement with the four-probe method.

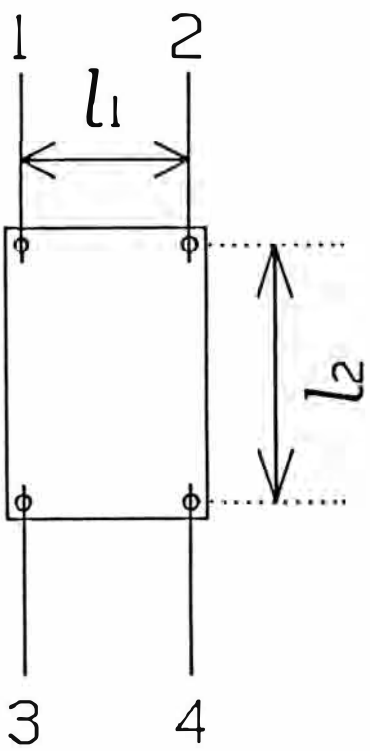

Fig. 2.2. Resistivity measurement with the Montgomery method.

the sample and the wire 3 or 4. Namely the contact resistance does not arise there. From the Ohm's low, $V=RI$, the resistance R of a material is the ratio of the voltage V versus the electrical current I. Also the resistance R is proportional to the length l between the wires 3 and 4 and to the inverse of the cross section of the sample S. Namely Eq.(2.1) holds in general.

$$R=\rho l/S \tag{2.1}$$

Since the resistivity ρ is the coefficient of them, it can be calculated after Eq.(2.1), if one knows V, I, l and S.

2.1.2.2 Montgomery method[1,2)]

The Montgomery method was developed by Montgomery *et al.*[1,2)] The method is useful to measure the resistivity along two directions perpendicular to each other at the same time. Four wires are contacted on four corners of the plate-like sample one by one as shown in Fig. 2.2. To obtain the measurements of the resistivity along the two directions, the shorter and the longer distances between the corner probes along edges of the sample crystal, l_1 and l_2, and the thickness of the sample l_3 must be measured previously. At first the current I_1 is supplied between the terminals 1 and 2, then the voltage V_1 between the terminals 3 and 4 is measured. After that the current I_2 is through between the terminals 1 and 3, then the voltage V_2 between the terminals 2 and 4 is measured. Now R_1 and R_2 are defined as Eqs.(2.2).

$$R_1=V_1/I_1, \tag{2.2(a)}$$
$$R_2=V_2/I_2. \tag{2.2(b)}$$

The quantities used for the determination of the resistivity along the short edges ρ_1 and along the long edges ρ_2 of the plate are l_1, l_2, l_3, R_1 and R_2.

Several equations to calculate ρ_1 and ρ_2 has been derived in the Refs. 1 and 2. For an "isotropic" material with the four probes as

same as Fig. 2.2., the resistivity ρ is calculated from the shorter and the longer distances between the two probes along the edges of the isotropic material a and b, the thickness of the material c and R_1 using Eqs.(2.3) to (2.5).

$$\rho=(\pi/4)[c/(cM)_0](V_1/I_1), \tag{2.3}$$

$$(cM)_0=2\sum_{n=0}^{\infty}\ln[(1+q^{2n+1})/(1-q^{2n-1})], \tag{2.4}$$

$$q=\exp(-\pi b/a). \tag{2.5}$$

In the case of the isotropic material, the resistivity ρ is proportional to R_1 or R_2.

$$\rho=H_{b/a}ER_1, \tag{2.6(a))}$$
$$=H_{a/b}ER_2. \tag{2.6(b))}$$

In Eqs.(2.6), E is the effective thickness of the sample; $H_{b/a}$ is a function of b/a and $H_{a/b}$ is also a function of a/b. With comparing Eqs.(2.3) and (2.6(a)), one can get the next relation.

$$H_{b/a}=(\pi/4)[(cM)_0]^{-1}. \tag{2.7}$$

With comparing Eqs.(2.6(a)) and (2.6(b)), one can also get the next relation.

$$R_2/R_1=H_{b/a}/H_{a/b} \tag{2.8}$$

Using Eqs.(2.7) and (2.8), one can calculate R_2/R_1 as a function of b/a. Contrary to this, if the table of R_2/R_1 versus b/a is given, one can also get b/a from R_2/R_1 measured.

For the "anisotropic" material, the resistivity ρ_1 and ρ_2 are related to the measurements l_1, l_2, l_3, R_1 and R_2 with the parameter b/a.

$$(\rho_2/\rho_1)^{1/2}=(b/a)(l_1/l_2), \tag{2.9}$$

$$(\rho_2\rho_1)^{1/2}=H_{b/a}l_3R_1. \tag{2.10}$$

All quantities in the right hand side in Eqs.(2.9) and (2.10) are the measurable or the calculable quantities. Then one can get the resistivity ρ_1 and ρ_2 solving Eqs.(2.9) and (2.10) as the simultaneous equations.

2.1.2.3 Metals and semiconductors

From Boltzmann theory, the temperature dependence of the resistivity of metals or semiconductors can be expressed with some equations under some assumptions. However there are too many factors that influence the resistivity. According to the Bloch's theorem, in ideal, there is no electrical resistance for a perfect crystal at 0 K. The perfect periodicity of the crystal does not become a cause of electrical resistance. In reality, even in the case of a metal with very high quality, there are many factors that break the periodicity, for example the lattice vibration, many kinds of defects (each of them contributes in the different manner) and so on. The equations fully expresses the magnitude or temperature dependence of the resistivity do not exist up to now due to the complex reasons. Then, in this subsection, only some important qualitative general facts are summarized.

For crystals of metals, the lattice vibrations contribute to electrical resistance near around RT, because it breaks the periodicity of the lattice. Since the lattice vibrations are thermally excited, the resistance due to them decreases with decreasing temperature. The resistance of metals, therefore, decreases with decreasing temperature. When temperature is low enough, for instance below about 1/3 of the Debye temperature, the excited modes of the lattice vibrations and also the resistance due to them decrease rapidly. And the residual resistance exists at 0 K. The reason of the residual resistance is defects or impurities in the crystal that also break the periodicity. In general, their contribution to resistance is smaller than that of the lattice

vibrations and temperature independent, because their concentration is almost constant when temperature is varied for the metals of normal quality.

In short speaking, there exist two kinds of important factors contributing to electrical resistance of metals and the resistance of metals decreases with decreasing temperature.

For semiconductors, the most dominant factor to the electrical resistance is the number of carriers. The conclusive character of a semiconductor is the existence of the band gap. Only electrons, which are excited from the valence to the conduction band, and holes generated in the valence band at the same time contribute to the electrical conduction in the semiconductor. Since the excitation of the carriers is a thermal process, the number of carriers strongly depends on temperature. If the magnitude of the band gap is independent of temperature, the concentration of the carriers varies exponentially with temperature. Then the most simplest expression for the resistance of the semiconductors is

$$R=R_0 \exp(E_a/k_B T). \qquad (2.10)$$

R_0 is a constant, the limit of resistance at the high temperature, and $E_a=E_g/2$ (E_g:the band gap) is the activation energy. In general, including the dependency of the scattering mechanism, the next form is used.

$$R\propto T^{\alpha-0.5} \exp(E_a/k_B T). \qquad (2.11)$$

Since the exponential temperature dependence is dominant in most cases, Eq.(2.10) is used for the estimation of E_a. There also exist many factors, some of them are common to those in the case of metals, that influence the resistance of semiconductors. For example, even though a small number of impurities or defects vary the carrier concentration of semiconductors very much, furthermore the temperature dependence of the resistivity becomes very complicated. However the more developed expressions for semiconductors are not

used in this study.

2.1.2.4 Resistance jump

In the resistivity measurement of organic conductors with varying temperature, the abrupt jump of resistance is sometimes observed. The degree of the jump is strongly affected by the condition of cooling or heating the sample and the magnitude of the electrical current. Although the mechanism of the jump has not been fully elucidated, that is known to be an extrinsic phenomenon to the sample. Furthermore, if it occurs, the intrinsic behavior of the sample becomes unclear, for example the temperature region of the M-I or superconducting transition is broadened. It is a difficulty in the measurement of the resistivity.

2.1.3 Instruments and methods

In this subsection, the instruments used for the measurement of resistivity and the methods are explained.

2.1.3.1 Four-probe method at ambient pressure

A sample-holder for the measurement of resistivity with four-probe method at ambient pressure is shown in Fig. 2.3(a). Four Au wires (B) (10 μm in diameter) are contacted on the sample (A) with carbon paste (XC-12, Fujikurakasei Co., Ltd.) and the sample is held with the Au wires above the central hole of the holder. The Au wires are softened by annealing with some current to decrease the damage against the sample. Each of Au wires is connected with another Au wire (C) (20 μm in diameter) with Ag paste (Ohmiyakasei Co., Ltd.). Each of the four thicker wires is contacted on the soldered copper (D) at each corner of the plate with Ag paste. Both the carbon paste and the Ag one are conducting material and they are used for connecting electrically with the sample and the wires one another. The contact resistance using the Ag paste is smaller than that using the carbon paste. However, silver is reactive with halogens and it is known that silver also often reacts with halogens of the counter anions of organic conductors and damages the sample. To prevent this problem the carbon paste is used when the sample and Au wires are

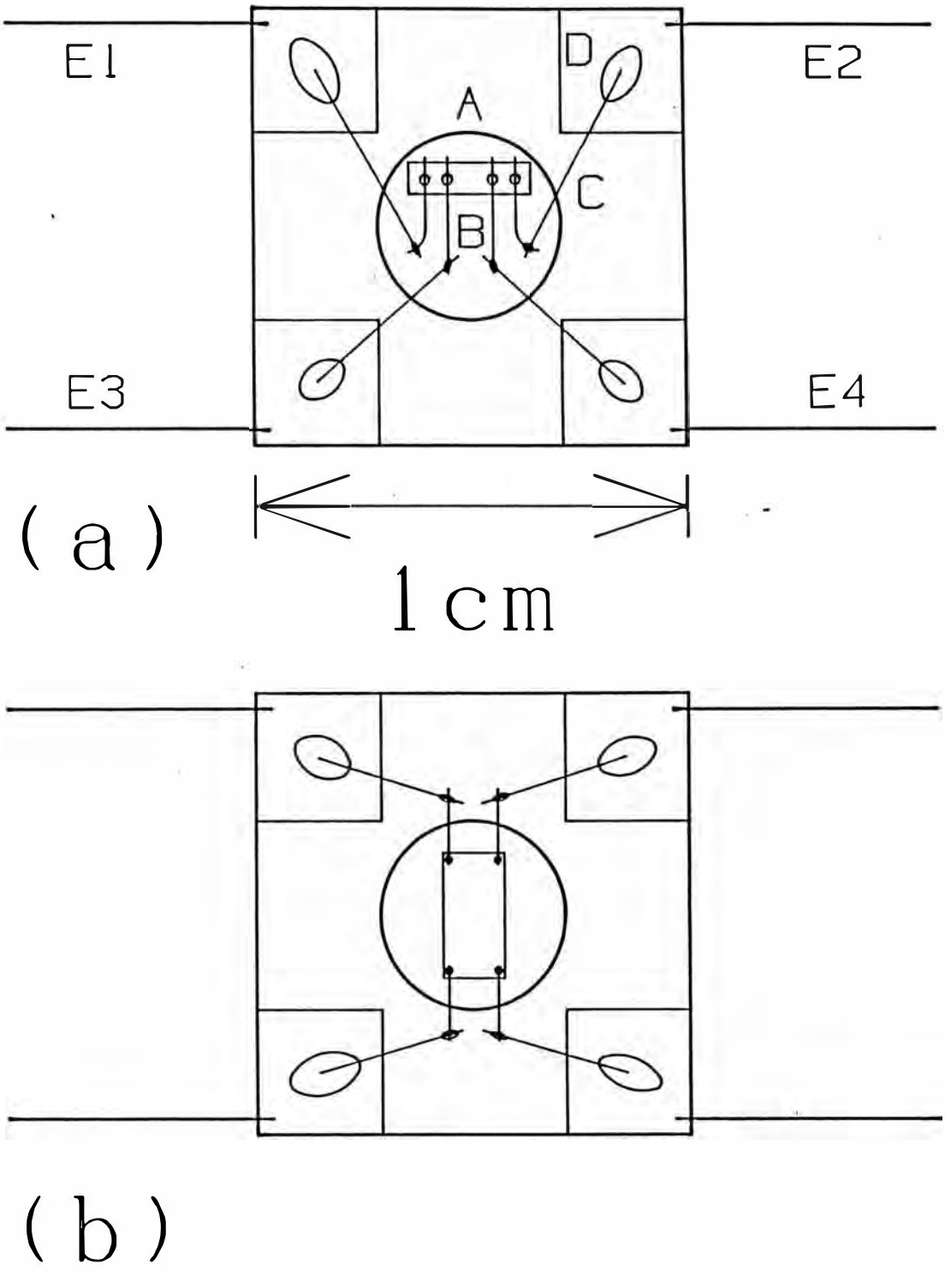

Fig. 2.3. Sample holders for the resistivity measurement at ambient pressure. (a) For the four-probe method. (b) For the Montgomery method.

connected with each other. A Cu wire (E1 - 4) is soldered on the copper corner. The electric current generated by a current-generator (TR6142 or R6142, ADVANTEST Corp.) runs through E1, the sample and E2. E3 and E4 are connected to a digital multi meter (3478A, Hewlett Packard Co.).

The holder is put in the sample-chamber made of Cu of the cryostat.[3] The sample-chamber is held in the inner-vacuum-chamber (IVC) made of stainless steel. Both the chamber are evacuated with a rotary pump and an oil-diffusion pump during the measurement. The current used for the measurement is controlled so as to get below about a few hundreds μV of the output voltage to keep the sample from the damage. To cancel the stray electromotive force (EMF), furthermore, the current is varied from 10 % to 110 % of the set value and the resistance is determined from the variation of the voltage vs. the current. In many cases in this study, the measurement is performed for three samples at the same time. Three current-generators are used. However only one voltmeter is used for the measurement of the output voltage. Each output voltage is switched over using a scanner to the voltmeter. All these instruments are controlled with a personal computer. Sampling of the data is also done with the computer.

2.1.3.2 Montgomery method

The sample-holder for the measurement of Montgomery method is common to that for the measurement of the four-probe method. The positions of the contact is different from each other. For the Montgomery method the sample is mounted on the sample-holder as shown in Fig. 2.3(b). The holder is put in the cryostat as described in subsection 2.1.3.1. The measurement is made only at ambient pressure in this study.

Two current-generators are used corresponding to the two direction of the measurement. At first R_1 is determined, then the connection is switched over and R_2 is determined after the way explained in subsection 2.1.2.2. The distances between contacts and the thickness of the sample are previously measured with a

microscope. The resistivity for the two perpendicular directions in the plane of the sample crystal are also calculated in the described manner.

2.1.3.3 Temperature

In the early times of this study, temperature of the sample is determined using only a Pt and a Ge resistance thermometers put near by the samples. Their resistances are measured by Multimeters (195A, Keithley Instruments, Inc.). When a resistance thermometer is used, temperature is determined from a table or equations, in which resistance is determined as a function of temperature. In this study, temperature in the region from 40 K to RT is measured with the Pt thermometer. Below 40 K, the Ge thermometer is used. (The resistance of Pt decreased with decreasing temperature, since Pt is metallic. Contrary to this, the resistance of Ge increases with decreasing temperature, because Ge is semiconducting.)

However, there exists some difference between the temperatures of the sample and the thermometers in fact. If the temperature is varied gradually, for example less than 10 K/h, the difference is less than 0.5 K (often nearly equals to zero). However, if the speed of varying temperature becomes more than 20 K/h, the difference sometimes becomes more than 2 K. To avoid this, the most important thing is to suppress the speed of varying temperature below 10 K/h. In addition, it is also important to measure the temperature nearer the samples.

To solve the problem, thermocouples are used in this study. The Au-0.07 at% Fe-chromel thermocouple has high enough sensitivity from RT down to 4.2 K (b.p. of liquid He, the lowest limit of the temperature in this study). The resistance thermometers are used to determine the temperature on the stage in the sample-chamber of the cryostat. Then temperature difference between the position and near the sample is measured using the thermocouple. If one use three thermocouples, he can determine temperature of three samples separately. This is a similar way to determine the temperature as described in section 2.2 for the measurement of thermopower.

2.1.3.4 Four-probe method under pressure

The sample-holder of the resistivity under pressure is shown in Fig. 2.4(a).[3] The sample (A) is held with four Au wires as mentioned in 2.1.3.1. Each Au wire (B) is electrically connected with a manganin wire (C) goes through the cupronickel tube (D) welded to the brass disk (E) on its center hole to pass the tube through. The Teflon tube (F), whose one end is closed, covers the disk tightly. The space in the tube is filled with the oil (Daphne #7373, Idemitsu Oil Co., Ltd.).

The copper-beryllium cell (G), including the sample-holder in it, to hold the pressure in the Teflon cell is shown in Fig. 2.4(b). The brass disk (E) is on the copper-beryllium carrier (H). The carrier is set tightly with the copper-beryllium screw (J1). The tungsten-carbide cylinder (I1) is on the closed end of the Teflon tube. The another copper-beryllium screw (J2) presses the another tungsten-carbide cylinder (I2) and, as a result, presses also the sample-holder.

Pressuring is made with a press and the pressure is monitored with a gauge attached to the press. The region of pressure is below 15 kbar at RT in this study. After pressuring up to the wanted pressure at RT, the cell is removed from the press. Because the measurement is made with varying temperature, the pressure in the cell also varies. The variation is almost negligible above the temperature where the oil in the Teflon tube solidifies. The oil used solidifies at about 200 K and the pressure decreases after the solidification. In the case of this study, the release is about 1.5 kbar for each pressure below about 200 K.

Temperature above 40 K is determined with the Pt thermometer that is in the sample-holder with the sample ignoring the pressure effect on the Pt thermometer. Below 40 K, the Ge thermometer thermally contacted on the cell is used. The Ge thermometer is too large and delicate to set in the sample-holder. The temperature difference between the Ge thermometer and the sample is considered to be negligibly small (< 1K) while temperature is slowly varied.

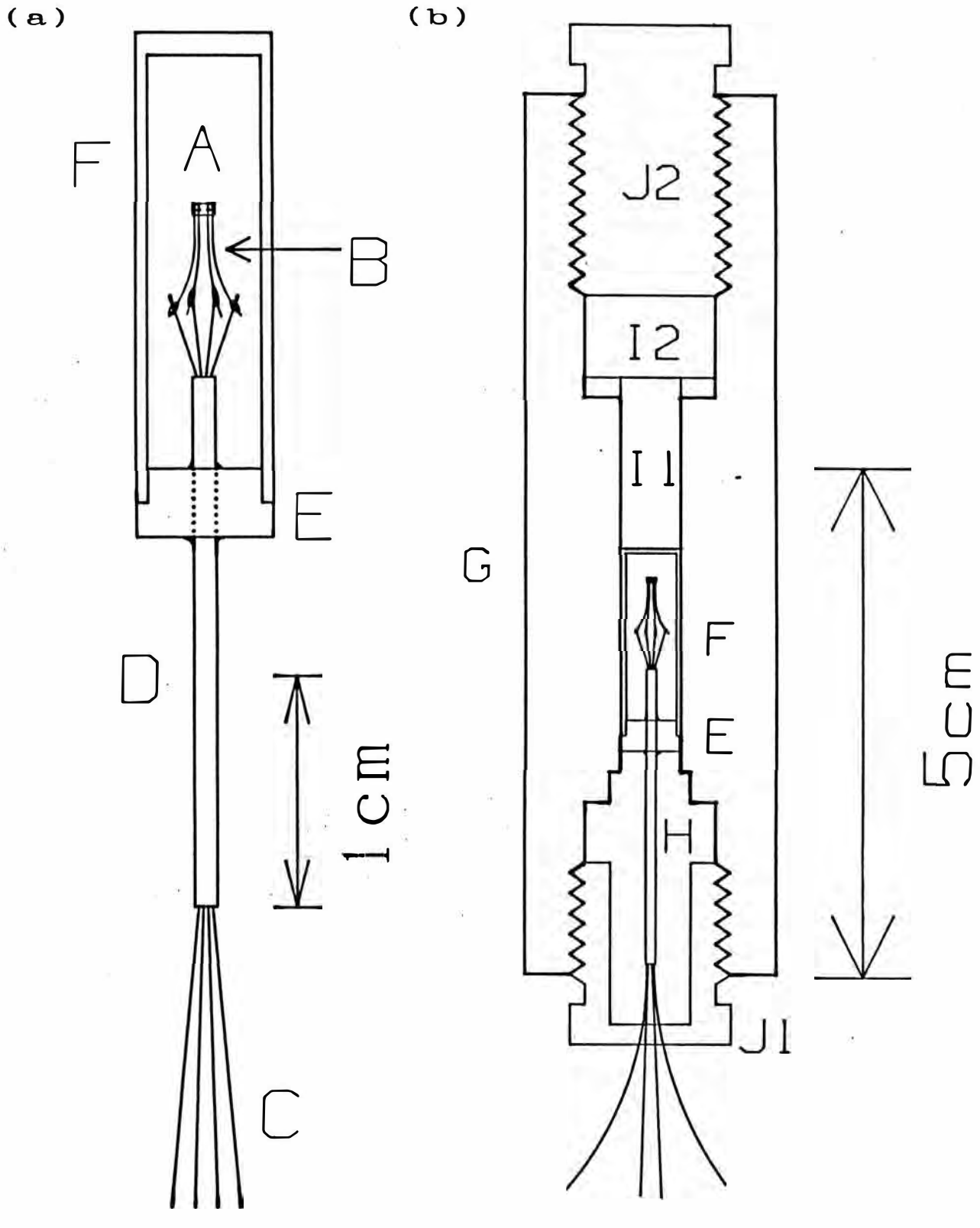

Fig. 2.4. (a) Sample holder for the resistivity measurement under pressures. (b) Pressure cell for the resistivity measurement under pressures.

2.2 Measurement of thermopower

2.2.1 Principle

Two kinds of materials, A and B are electrically connected as shown in Fig. 2.5. The temperature at one connection is kept T_1 and the temperature at the other connection T_2. The temperature at open ends of the connecting wire is kept T_0. In this case, the thermoelectric power E arises between the ends. If the two materials are given, the thermoelectric power E depends only on T_1 and T_2. This phenomenon is known as the Seebeck effect. The measurement of temperature with a thermocouple is using this phenomenon.

The thermopower (or Seebeck coefficient) S is the derivative of E with temperature T. S is a function of T in general. If $S(T)$ of the A-B thermocouple and T_1 and T_2 are given, E can be calculated by integrating $S(T)$ between T_1 and T_2. The S is divided into contribution of A and B.

$$S(T)=S_A(T)-S_B(T). \tag{2.12}$$

Here, S_A and S_B are the absolute thermopower of A and B. The absolute value of a material is intrinsic to the material.

The sign of S brings the information about the dominant carrier of the material as derived from the Boltzmann equation. If the sign is positive, the dominant carrier is hole. If the sign is negative, the dominant carrier is electron.

It is known that the temperature dependence of S of metals is proportional and that of semiconductors is inversely proportional. Namely S of metals proportionally decreases with decreasing temperature and S of semiconductors increases with decreasing temperature, though that in real case is much more complicated.

The expression of S of a kind of material is derived from the Boltzmann equation under some assumptions. Taking the tight-binding approximation for a 1D metal with single band, the next expression is derived.[4)]

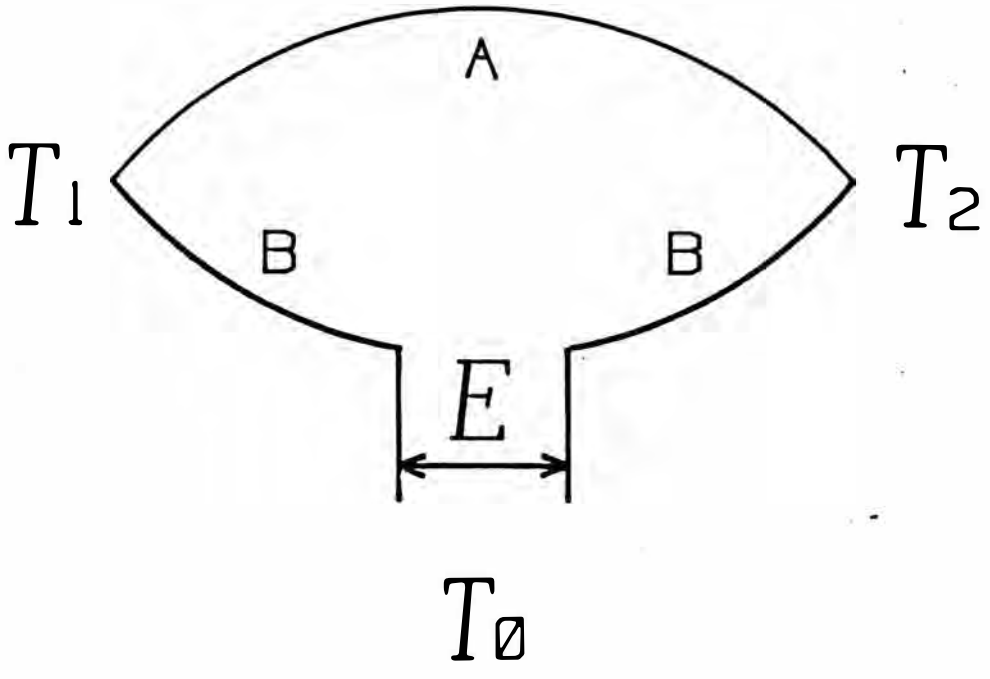

Fig. 2.5. Seebeck effect.

$$S=\frac{-\pi^2 k_B^2 T}{6|e||t|}\quad\frac{\cos\frac{1}{2}\pi\rho}{1-\cos^2\frac{1}{2}\pi\rho}\ , \tag{2.13}$$

Here, k_B is the Boltzmann constant; e is the electron charge; t is the transfer integral ($4t$ is the bandwidth) and ρ is the electron density in the band. Under the assumption, if ρ is known, one can estimate the bandwidth of a 1D metal from the slope of the T–S plot. In this study, ρ is regarded as 1.5 per site, because one electron is considered to be transferred from two HOMO's of two donor molecules.

The thermopower for a semiconductor can be approximated in Boltzmann theory by

$$S=\frac{-k_B}{|e|}\left(\frac{b-1}{b+1}\quad\frac{E_a}{k_B T}+\ln\frac{m_h}{m_e}\right), \tag{2.14}$$

where b is the ratio of electron-to-hole mobility ($b=\mu_e/\mu_h$), and m_h and m_e are the effective masses of hole and electron, respectively.[4] E_a is the activation energy of the semiconductor. For a semiconductor, one can estimate the effective activation energy $E_{eff}=-E_a(b-1)/(b+1)$ from the slope of the S vs. $1/T$ plot using Eq.(2.14).

As seen in the two example, one can get the information about the band structure from the thermopower measurement. Furthermore thermopower is, in general, more insensitive to sample quality than resistivity. This is an advantage of the thermopower measurement. The most important reason for the fact is that the thermopower measurement is performed under the current-less condition. The extrinsic characters such as the contact resistance or the resistance jump are not detected.

In short speaking, the thermopower measurement is effective method to get some intrinsic information about the band structure.

2.2.2 Instruments and methods

The sample-holder used for the thermopower measurement in this

study is an improved type of that used by Kamio,[5] and is shown in Fig. 2.6. The holder is set in the cryostat as same as the measurement of resistivity. The measurement of thermopower is made in vacuum in this study. The sample A is mounted on the Cu blocks B1 and B2. They are electrically and thermally contacted with the carbon paste. The temperature difference between the blocks (assumed to equal to that between the ends of the sample A) is measured with a thermocouple C1. The temperature difference between the Cu block B2 and another Cu block B3 is measured with another thermocouple C2. These thermocouples are made of Au-0.07 at% Fe and chromel. The thermocouples C1 and C2 are connected with pairs of Cu lead wires E1 and E2 at the block B3. Each EMF of the thermocouples is transmitted through each pair of the lead wires respectively. The connections between the thermocouples and the pairs of the lead wires are thermally contacted on the block B3. The Pt and Ge resistance thermometers D1 and D2 are used for the measurement of the temperature of the block B3. The temperature of the sample is determined with the thermocouples and the thermometers. A heater F (about 40 Ω in resistance) is non-inductively wounded around the block B1 to control the temperature difference between the blocks B1 and B2. Current running through F is supplied with lead wires E3. Each of Cu lead wires of E4 is electrically connected with the blocks B1 and B2, and thermoelectric power generated on the sample and Cu (blocks and wires) are measured through the lead wires E4. The blocks B1 and B3 are fixed on the epoxy plate H with screws. The block B2 is movable along the slit G to adjust the distance between B1 and B2 to fit the length of the sample. Covers I1, I2 and I3 made of Cu plates, are on the blocks B1, B2 and B3 to prevent influence of the thermal radiation.

To control the temperature difference between the blocks B1 and B2 with the heater F, a PID controller (laboratory made) is used. The PID controller receives the input signal from a micro-volt meter (AM-1001, Ohkura Electric Co.) that measures the difference of voltage of the thermocouple C1 and the reference voltage generated by a voltage-generator (R6142, ADVANTEST Corp.). The reference

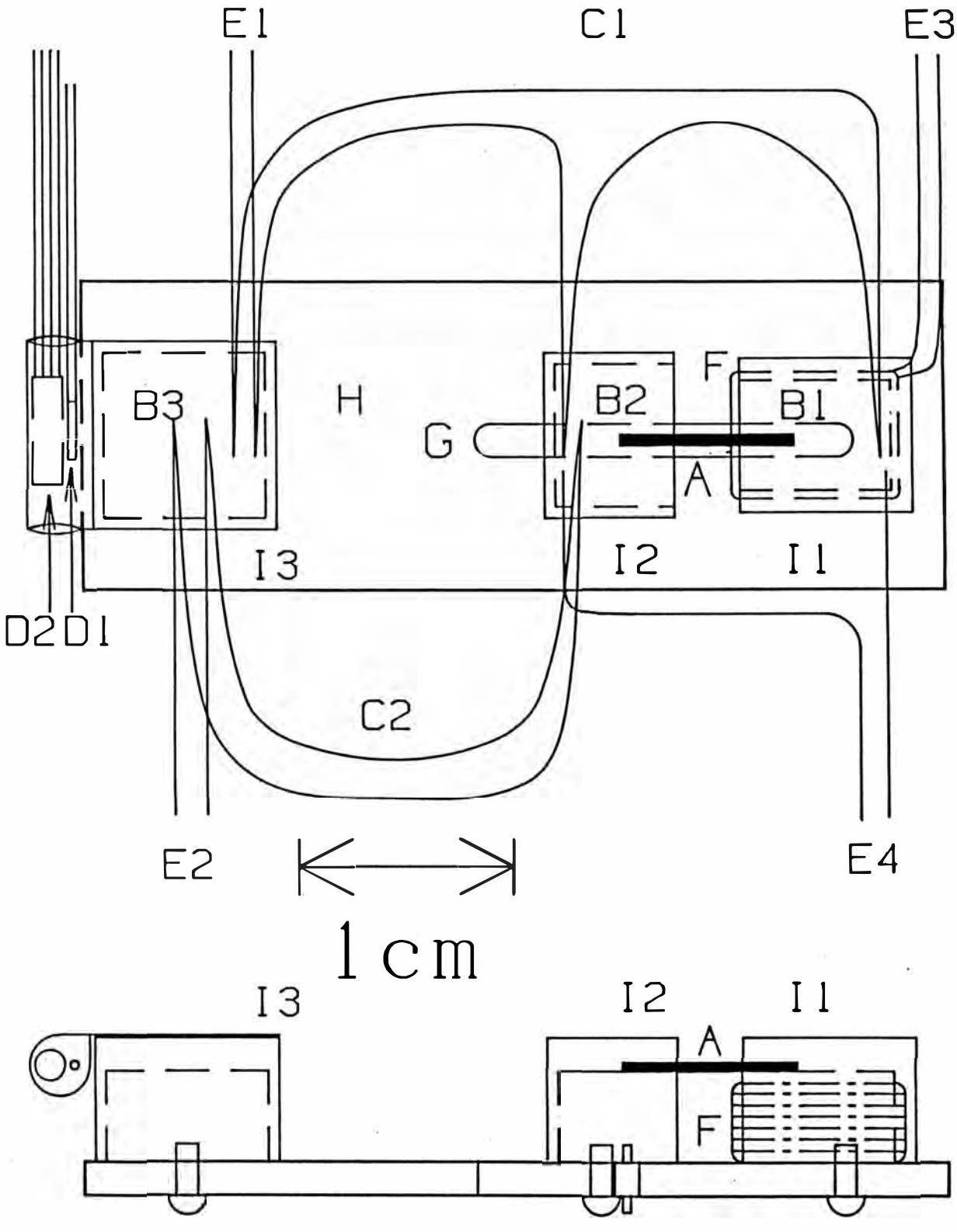

Fig. 2.6. Sample holder for the thermopower measurement.

voltage is determined as it is the same voltage arised from the thermocouple C1 when the temperature difference between the blocks B1 and B2 becomes a set value. The temperature difference is stepwise varied from 0.2 to 1.5 K at each temperature in this study. Since thermopower (Seebeck coefficient) is a derivative of thermoelectric power vs. temperature, the temperature difference must be suppressed as small as possible. For example, the temperature difference is stepwise increased from 0.5 K to 1.5 K by 0.1 K, after that it is decreased in the same manner and thermoelectric power is measured on each temperature difference.

The thermopower (Seebeck coefficient) is determined as the inclination of the fitted line for the data of thermoelectric power vs. temperature difference. The fitting is performed with the least-squares calculation. In this step, the influence of stray EMF of is canceled. The influence arises as a base voltage of measured thermoelectric power of the sample and Cu, and it tends to become larger as the resistance of the sample becomes larger. When the resistance is beyond about 10^6 Ω, the measurement of the thermoelectric power was impossible, because the data points largely diverges and no straight line could be determined. "Temperature" of the sample is determined as the average of the intermediate temperature between the blocks B1 and B2 on each temperature difference.

In reality, the sample breaks on decreasing temperature due to the difference in thermal contradiction of the sample and materials used for the sample-holder. To prevent this difficulty, each center of two Au wires is connected with each end of the sample with carbon paste. Using the carbon paste again, then the ends of each Au wire are connected with each of Cu blocks B1 and B2 on which the sample is mounted. The electrical contact between the sample and Cu blocks are held through the Au wires. At the same time, these Au wires put the sample on the Cu blocks and the thermal contact between the sample and the Cu blocks are realized. In the temperature region from RT down to the liquid He temperature, the measurement is made in this manner. However, the absolute value of thermopower measured

with this method is often smaller than the true value, because the temperature difference in this manner tends to be smaller than that in the case of the direct contact due to the imperfection of the thermal contact. The ratio of the value with Au wires to that with the direct contact is almost constant in most cases. The value measured with the direct contact at around RT, in this temperature region the sample does not break, is used for the correction of data using Au wires.

Even though the thermopower of a material corrected with measurements for the direct contact, the resulting magnitude is larger than the true value of the material. This is confirmed by the experiment using a constantan wire as a sample. The ratio of results of measurements to the true values can also be regarded as constant in the whole temperature range in this study. (The typical value of the ratio is 1.05 in this study.)

The measurements obtained using Au wires are multiplied by the two factors described above. This value is S in the left hand side of Eq.(2.12). Subtracting the thermopower of copper from the S, the absolute value of the sample is obtained.

References to Chapter 2

1 H. C. Montgomery, J. Appl. Phys., 42, 2971(1971).

2 B. F. Logan, S. O. Rice and R. F. Wick, J. Appl. Phys., 42, 2975(1971).

3 M. Ishibashi, M. Sc. Thesis, Department of Chemistry, Faculty of Sc., Tokyo Metropolitan University(1991).

4 P. M. Chaikin, R. L. Greene, S. Etmand and E. Engler, Phys. Rev., B13, 1627(1976).

5 K. Kamio, M. Sc. Thesis, Department of Chemistry, Faculty of Sc., Tokyo Metropolitan University(1989).

Chapter 3. Results

3.1 Thermopower of DMET salts

3.1.1 $(DMET)_2PF_6$ (Group 1)

This material is classified into the Group 1 of DMET salts.[1,3] The crystal structure of $(DMET)_2PF_6$ is shown in Fig. 3.1.1.[2-4] S is measured along the direction of the donor stacking, namely the most conducting direction. The temperature dependence of S of $(DMET)_2PF_6$ is shown in Fig. 3.1.2(a). The sign of S is positive. It shows that the dominant carrier is hole. With decreasing T, S increases from 45 μV/K at 273 K to 320 μV/K at 110 K. This semiconducting behavior of S is consistent with that of resistivity reported.[1] The plot of S vs. $1/T$ is also shown in Fig. 3.1.2(b). The curve becomes almost linear below about 130 K. Using Eq.(2.14) with the slope of the temperature region, the estimated effective activation energy E_{eff} is 0.11 eV. This is comparable with that estimated from the measurement of resistivity and reflectance spectra, though the slope in Fig. 3.1.2(b) is fairly small around RT. This is possibly due to the quality of the sample.

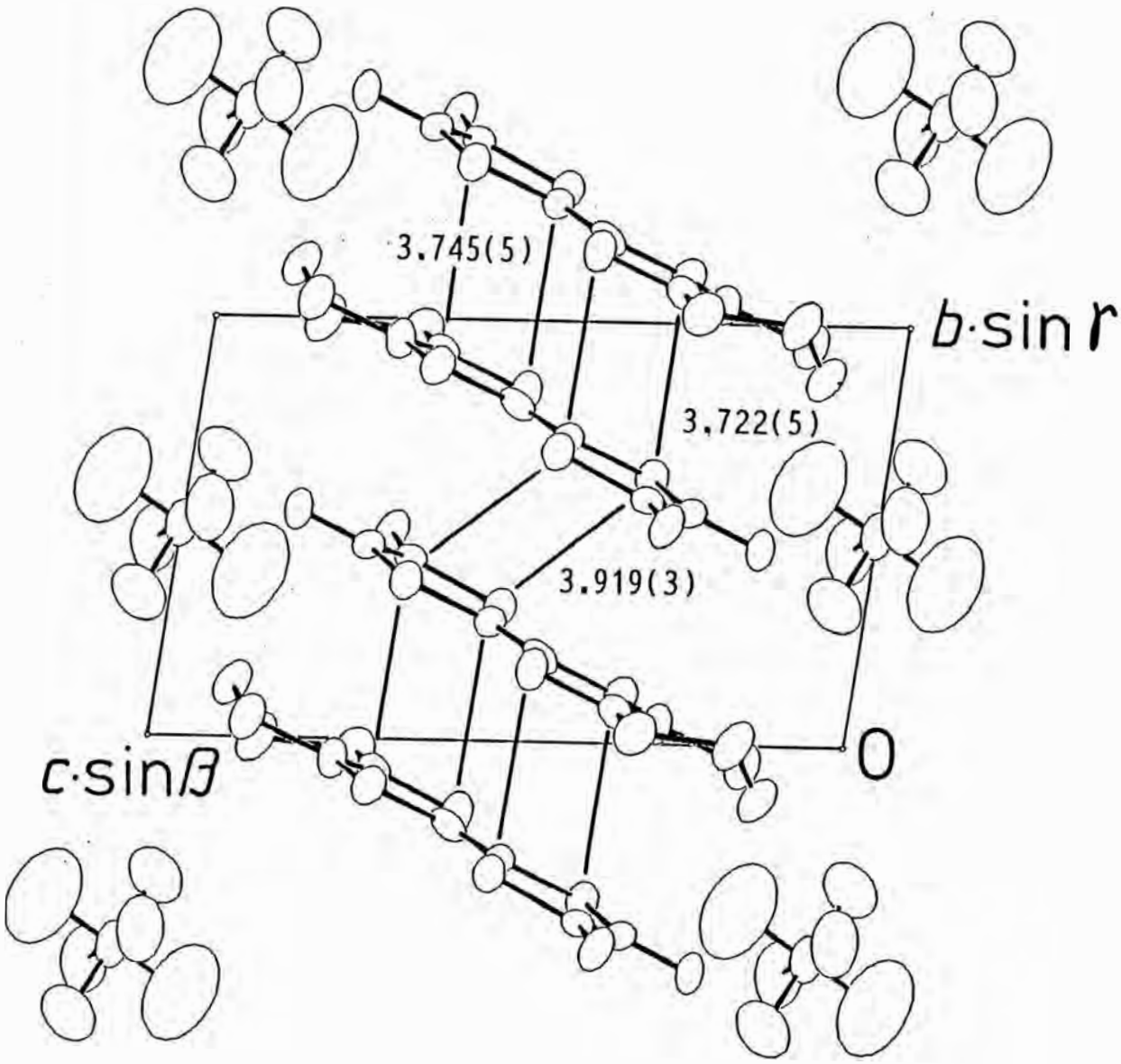

Fig. 3.1.1. Crystal structure of $(DMET)_2PF_6$ viewed along the a-axis.

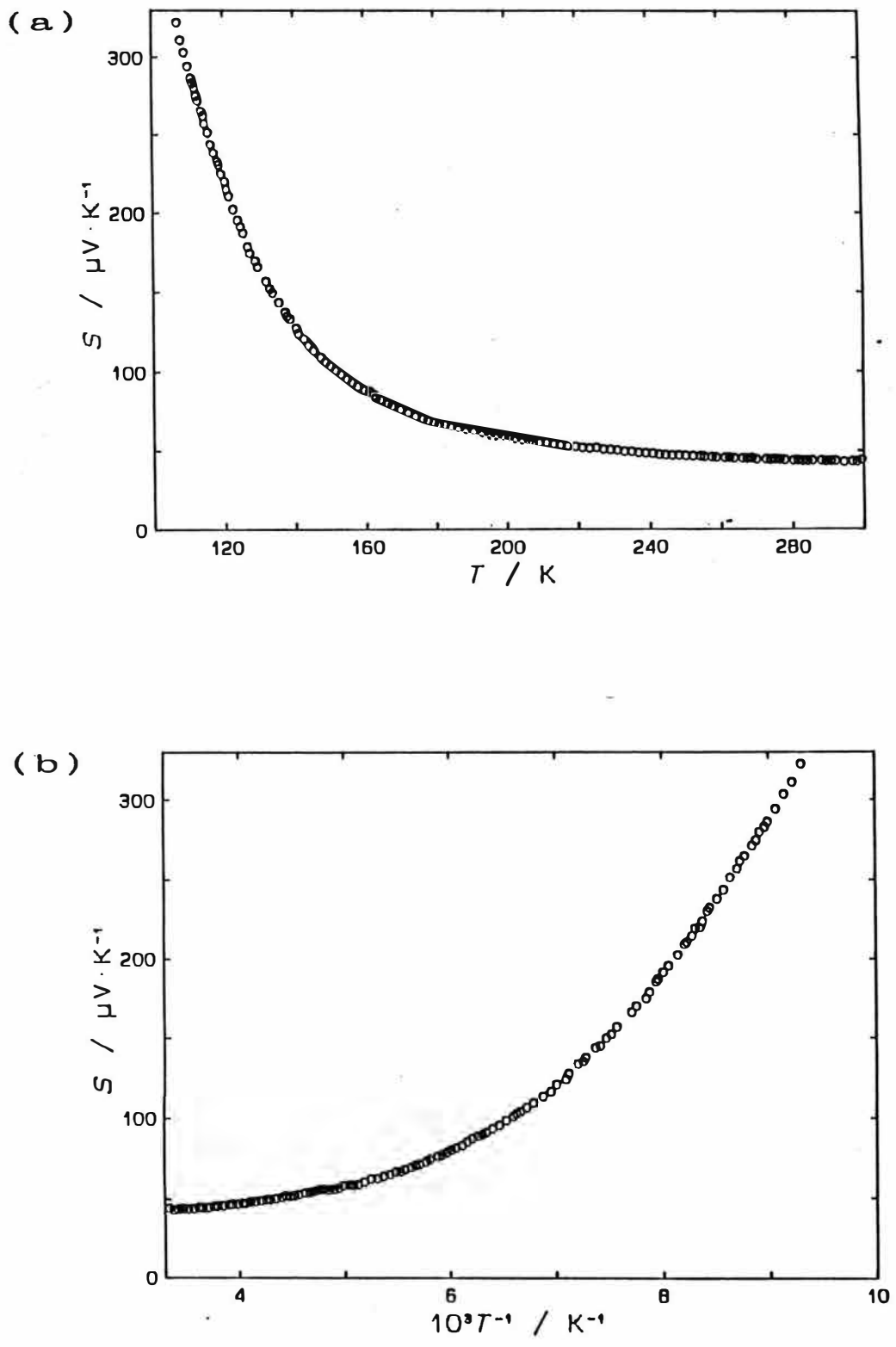

Fig. 3.1.2. (a) Thermopower of $(DMET)_2PF_6$. (b) Plot of the thermopower of $(DMET)_2PF_6$ versus $1/T$.

3.1.2 $(DMET)_2AsF_6$ (Group 1)

This salt is classified into the Group 1 as same as PF_6 salt.[1,3] The temperature dependence of S along the most conducting direction of AsF_6 salt is shown in Fig. 3.1.3(a). The sign of S is positive and it means that the dominant carrier is hole. The value of S is 48 μV/K at 273 K and increases with decreasing T like a semiconductor. This is consistent with the behavior of the resistivity.[1] The S more rapidly increases than PF_6 salt. The plot vs. $1/T$ is shown in Fig. 3.1.3(b). Only in the temperature range from 90 to 120 K, the curve seems almost linear. E_{eff} estimated for the region is 0.18 eV, it is larger than that of PF_6 salt. The crystal structure of AsF_6 salt has not been solved up to now and only the lattice constants are known. The lattice constant along the stacking direction is larger in AsF_6 salt than in PF_6 salt. This is probably attributed to the larger volume of the counter anion AsF_6. The overlap of MO of donors along the stacking direction is probably smaller for AsF_6 salt than for PF_6 salt. The difference in magnitudes of E_{eff} of these salts is consistent with this fact.

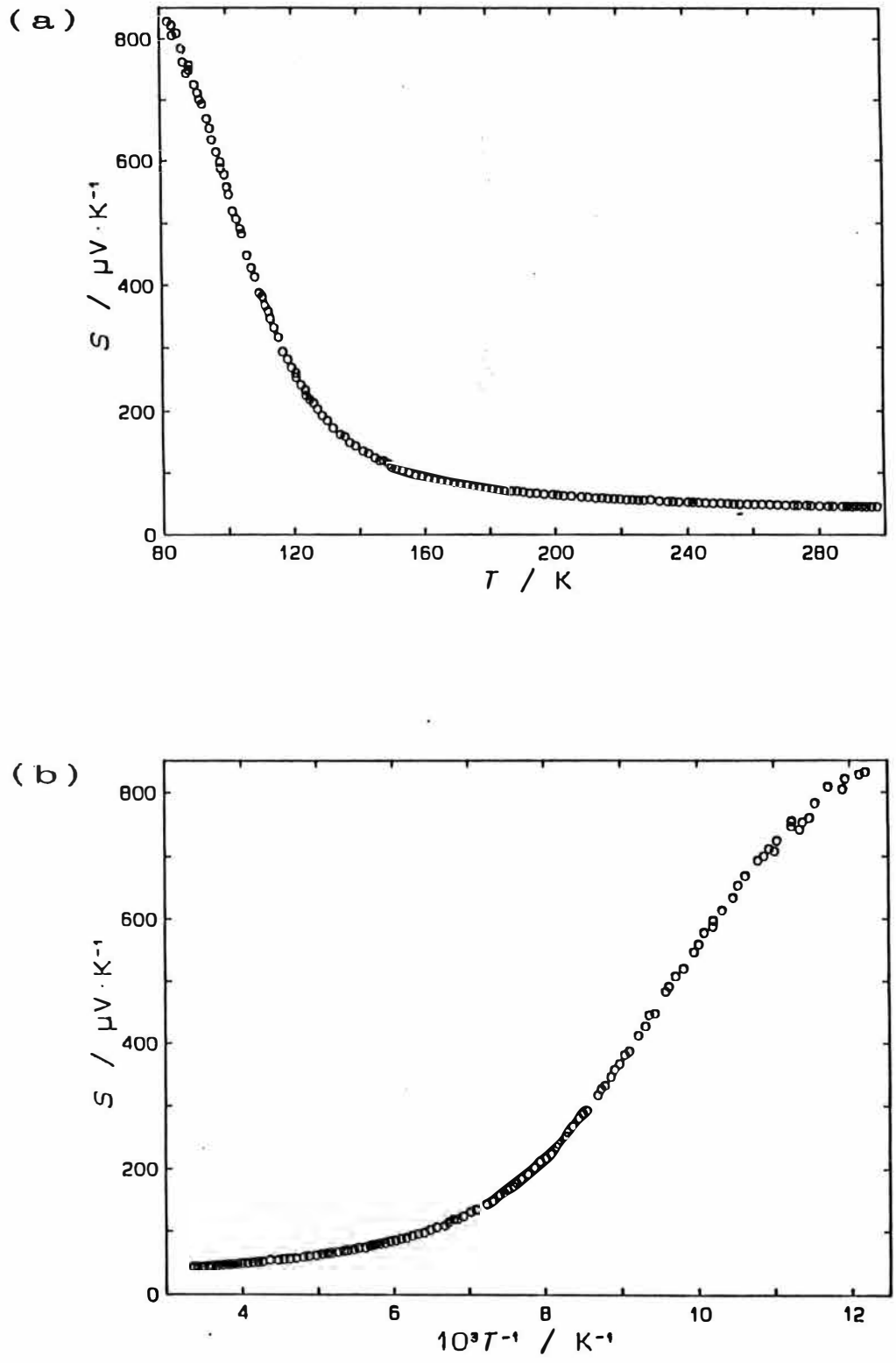

Fig. 3.1.3. (a) Thermopower of $(DMET)_2AsF_6$. (b) Plot of the thermopower of $(DMET)_2AsF_6$ versus $1/T$.

3.1.3 $(DMET)_2BF_4$ (Group 2)

$(DMET)_2BF_4$ is classified into the Group 2.[1,3] The interesting character of the crystal structure of this salt is the existence of two kinds of donor stack as shown in Fig. 3.1.4.[3,4] The stacking mode along the a-axis is different from that in other groups of DMET salts. As seen in Fig 3.3(a), the molecular plane in the donor stack along the a-axis is almost normal to the direction. The molecular plane in the stack along the b-axis is tilted from the direction like in the cases of Groups 1, 3 and 4. In order to investigate electronic state along each direction, S is measured along the a- and the b-axes. The temperature dependence of S is shown in Fig. 3.1.5(a) and (b). In Fig. 3.1.5(a), the results on three samples for each direction is shown. The measurements at low temperatures were made only for the sample 1 and the results are shown in Fig. 3.1.5(b).

The temperature dependence of resistivity of the material has never been measured along both of the directions down to the liquid He temperature. To compare with the result of the thermopower measurement, the resistivity measurement was also made and the result is shown in Fig. 3.1.6 in the form of the Arrhenius plot. The temperature dependence of the thermopower is metallic down to about 40 K. This is consistent with the behavior of the resistivity, in which the M-I transition occurs at around 35 K. In the metallic region, the sample dependence of the value of S was observed for $(DMET)_2BF_4$ as shown in Fig. 3.1.5(a). The sample dependence of the absolute value of S is larger for the measurement along the a-axis than along the b-axis. However $dS(T)/dT$ for each direction is very similar to each other for three samples. The similar phenomenon has been reported for the thermopower of β-$(BEDT\text{-}TTF)_2I_3$ by Mortensene *et al.*[5] They explained the same $dS(T)/dT$ and the different absolute value of S assuming the next equation.

$$S(T)=S_1(T)+S_0 \qquad (3.1)$$

In Eq.(3.1), S_1 represents the temperature dependent term and S_0 the

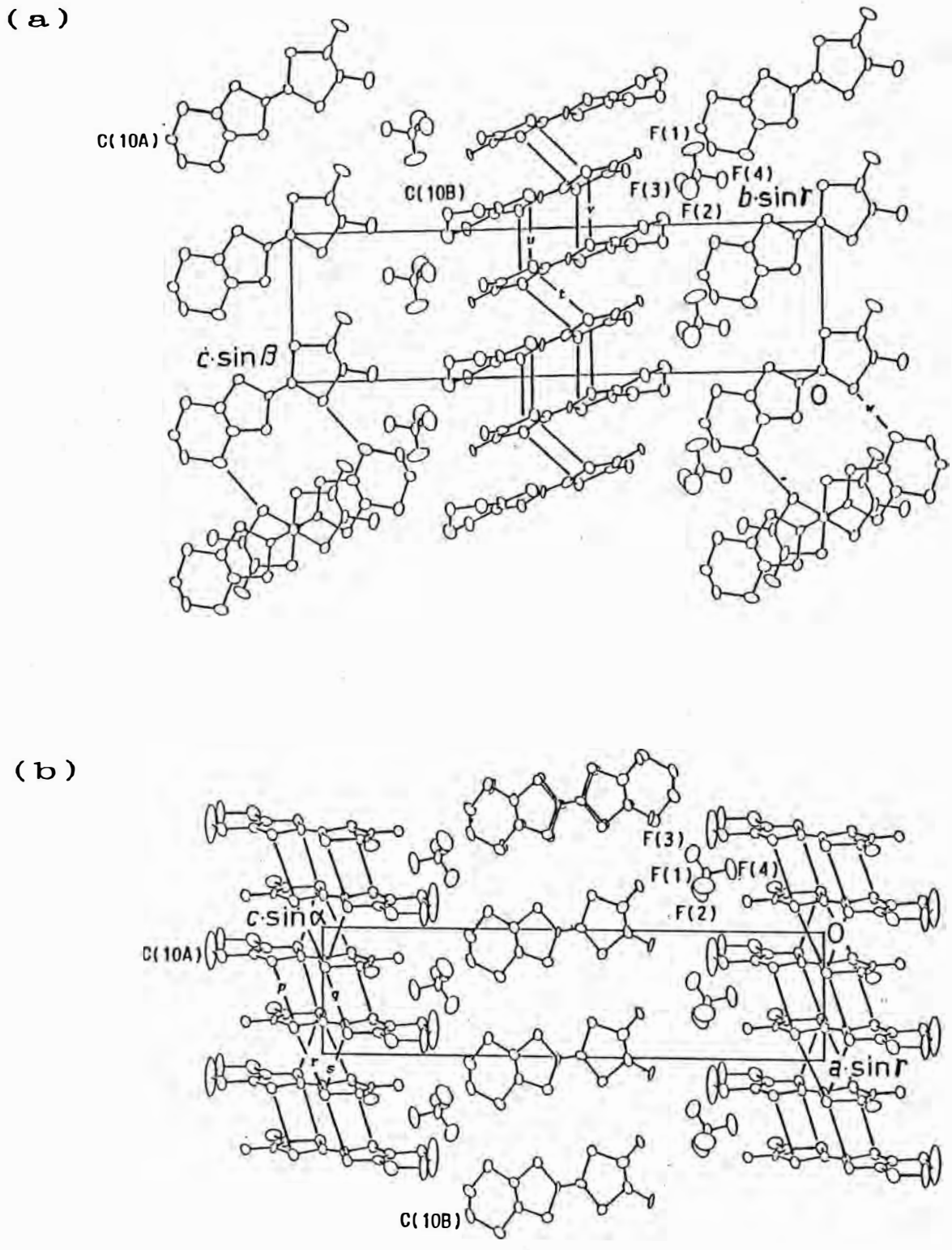

Fig. 3.1.4. Crystal structure of $(DMET)_2BF_4$ viewed along the b-axis (a) and viewed along the a-axis (b).

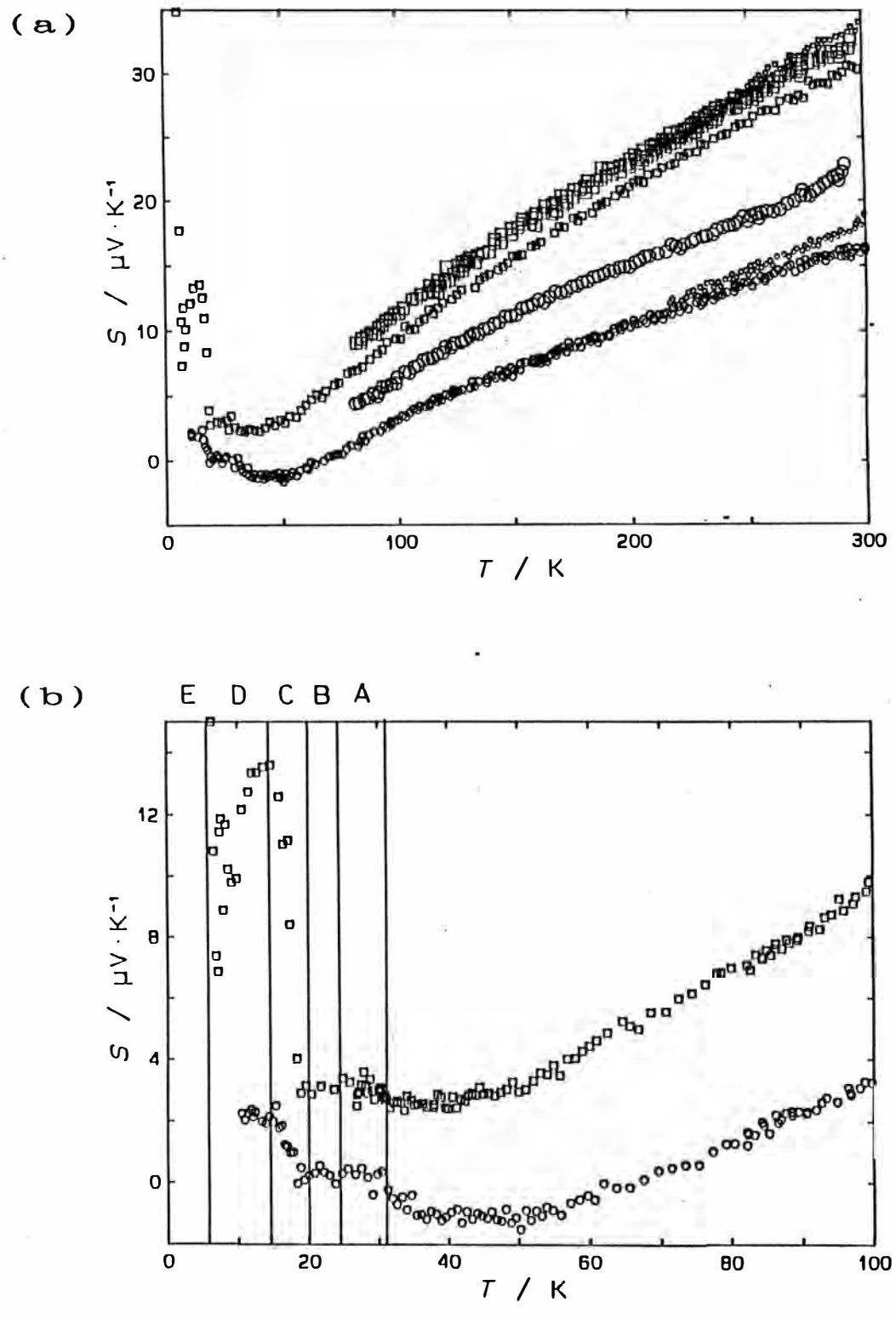

Fig. 3.1.5. Results of the thermopower measurements on three samples of $(DMET)_2BF_4$. Circles are for the a-axis and squares are for the b-axis (#1(middle), #2(large), #3(small)). (a) Temperature range below 300 K. (b) Temperature range below 100 K.

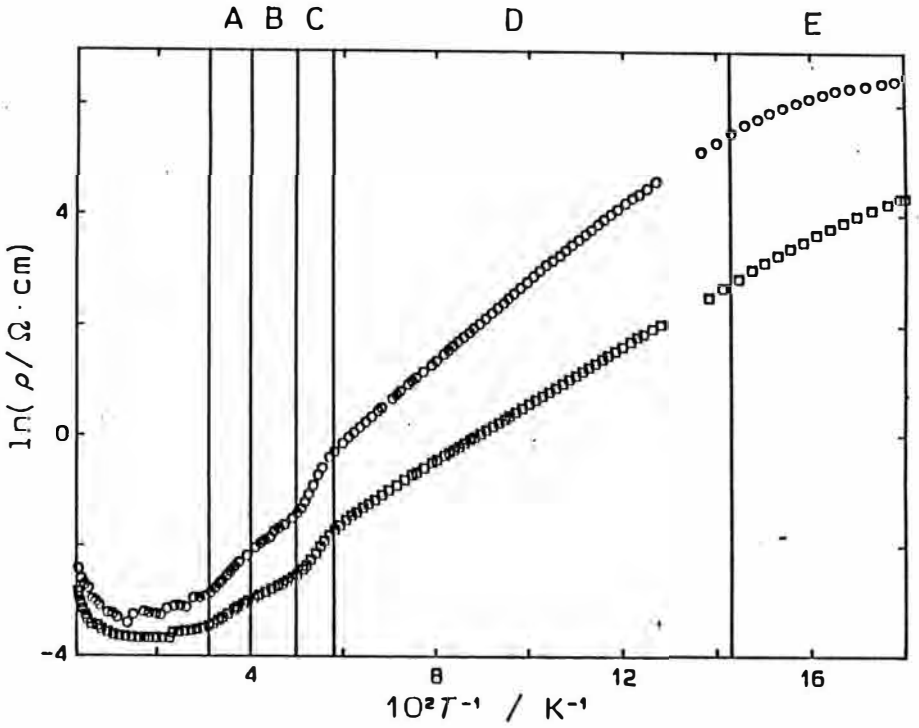

Fig. 3.1.6. Arrhenius plot of resistivity of $(DMET)_2BF_4$. Circles are for the a-axis and squares are for the b-axis.

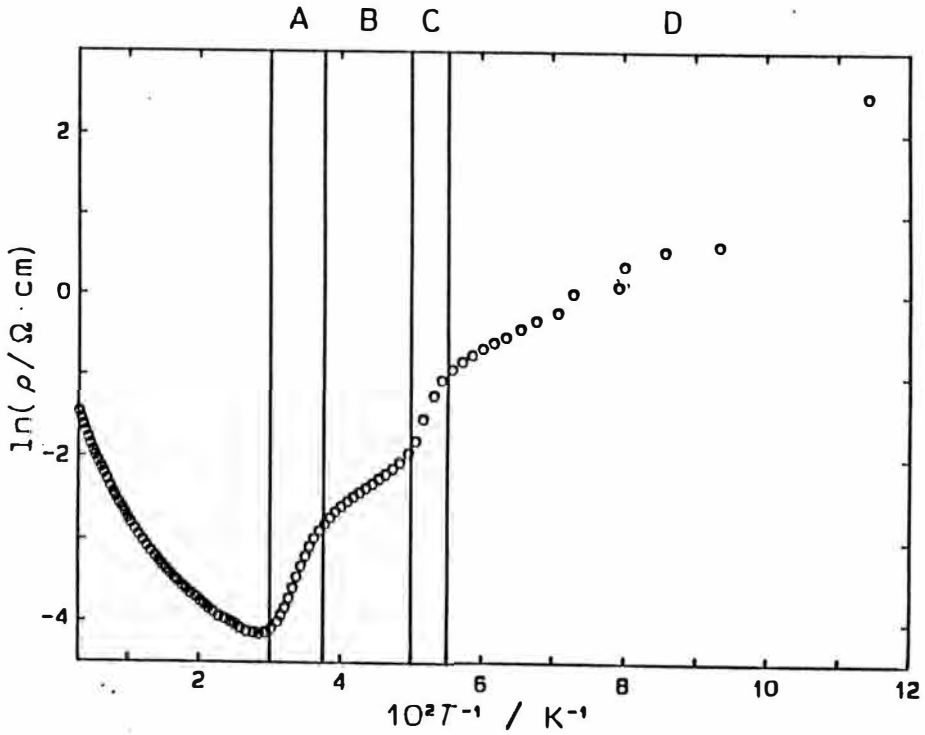

Fig. 3.1.7. Arrhenius plot of resistivity of $(DMET)_2ClO_4$.

temperature independent one. The term S_1 expresses the intrinsic character for the conducting direction and S_0 depends on the orientation of the sample crystal. It is considered that the weak interstack (intercolumn) interaction is responsible for the orientation dependence under the assumption that the weak interaction between 1D stacks does not vary when temperature is varied. Because the thermopower is a tensor, it can be influenced by the sample orientation especially for the plate-like crystal of $(DMET)_2BF_4$.

Assuming the contribution of S_0 to the present results, the slope of the linear part of S is used to estimate the transfer integral t for the both directions. The slopes are 0.072 $\mu V/K^2$ for the a-axis and 0.10 $\mu V/K^2$ for the b-axis, respectively. On the other hand, there is another problem to determine t's of $(DMET)_2BF_4$ with two kinds of stack. That is the electron density ρ in the each quasi-1D band. For other single column DMET salts, ρ can be determined as 1.5 (per site) at the request of the stoichiometry and the crystal structure. However, there exist two different columns in $(DMET)_2BF_4$ and two columns, consequently, can possess different ρ's. In fact, the Raman spectra of neutral DMET crystal and a monovalent DMET salt and DMET radical salts containing $(DMET)_2BF_4$ suggest the different ρ's for the two kinds of column of $(DMET)_2BF_4$.[6] From the Raman spectra measurement, ρ for the a-axis column is 1.43 (ρ_a) and therefore for the b-axis 1.57 (ρ_b). In addition, from the reflectance spectra of $(DMET)_2BF_4$, assuming 1D column with ρ=1.5 under the tight-binding approximation, t's have been determined as 0.27 eV for the a-axis and 0.26 eV for the b-axis.[6] If one takes smaller ρ for the a-axis, about 1.43, than for the b-axis, the smaller t for the a-axis (t_a) than for the b-axis (t_b) is reasonably obtained from both the reflectance spectra and the thermopower present, though the magnitude of t's from the thermopower is not the same as that from the reflectance spectra. For trial, if one calculates ρ_a, so as to make t_a/t_b's from the thermopower and the reflectance spectra the same, ρ_a=1.45, therefore ρ_b=1.55, is obtained. These values are favorably composed with those determined from the Raman spectra. Thus the second problem to determine t's of $(DMET)_2BF_4$ from the

thermopower has been solved. Using ρ_a=1.45 and ρ_b=1.55, the transfer integrals are determined t_a=0.19 eV and t_b=0.22 eV from the present result of the thermopower measurement (t_a=0.25 eV and t_b=0.28 eV from the reflectance spectra). The result suggests the bandwidth of the b-axis column is larger than that of the a-axis column.

For the metallic region, an evidence of the crossover of the dimensionality in $(DMET)_2BF_4$ has reported by Kanoda *et al.*[7] They observed the temperature dependence of the EPR linewidth of DMET salts. The linewidth of $(DMET)_2BF_4$ decreases linearly with decreasing temperature and seems to shift to a steeper linearity below 130 K. They refereed the consideration, by Pedersen *et al.*,[8] that such a characteristic temperature corresponds to the interchain transverse integral and therefore the transverse electron motion is coherent below that temperature but is diffusive above that. If so, the dimensionality of each stack in $(DMET)_2BF_4$ turns out to be similar to that of $(TMTSF)_2PF_6$. Below 130 K, the thermopower also shifts to a steeper linearity for each direction. This is possibly related to the crossover of the dimensionality. The resistivity measurement, with the Montgomery method, has performed for $(DMET)_2BF_4$ by Ishibashi[9] at this laboratory. No anomalous behavior has detected at around 130 K by the measurement. In the measurement, the anisotropy in the a-b plane was measured. The change in the intercolumn interaction will appear in the temperature dependence of the resistivity along the c-axis. However, owing to the small thickness of the sample crystals (<0.1 mm), it is impossible to measure the c-axis resistivity up to now.

In the semiconducting regime, the complicated temperature dependence was observed both for the thermopower and the resistivity along both directions. Due to the large resistance of the sample, the values of S are scattered in the low temperature regime as shown in Fig. 3.1.5(b). The semiconducting region is divided into four smaller regions from A to E in Fig. 3.1.6. The division is based on the change of the slope in the Arrhenius plot of the resistivity. The region from about 32 K to about 25 K is symbolized as A. Also from about 25 K to about 20 K as B, from about 20 K to about 17 K as

C, from about 17 K to about 7 K as D, then below about 7 K as E, respectively. At about 32 K the abrupt increase of the resistivity due to the M-I transition occurs. Kanoda *et al.*[7] have reported that the abrupt decrease and disappearance of the spin susceptibility and the abrupt increase of the EPR linewidth below about 20 K. They claimed that the occurrence of an antiferromagnetic order is responsible for it. Namely the antiferromagnetic transition, probably an SDW transition, occurs below the minimum in resistivity. The similar behavior of the resistivity of $(DMET)_2ClO_4$, which is in Group 2 as same as $(DMET)_2BF_4$, has been detected as shown in Fig. 3.1.7. Although the change at the boundary between the regime A and B in the slope of the Arrhenius plot of the resistivity of $(DMET)_2BF_4$ in Fig. 3.1.6. is small, the corresponding change in the resistivity of $(DMET)_2ClO_4$ is rather clear. The division into the areas A to E is, therefore, reliable. The regime corresponding to E for $(DMET)_2BF_4$ in Fig. 3.1.6 has not been detected in the resistivity of $(DMET)_2ClO_4$ in the temperature region studied.

In good accordance with the division in the resistivity in Fig. 3.1.6, the change of the variation of S is observed as shown in Fig. 3.1.5(b). For both along the a- and the b-axes, S decreases from RT to about 35 K. Below 35 K, for both directions, S becomes almost independent of temperature after slight increase. At around 20 K, S increases especially for the b-axis direction. Again S becomes constant below about 15 K, and impossible to measure below 10 K due to the large resistivity for the a-axis direction. For the b-axis direction, the abrupt decrease is seen below 15 K, and the variation changes at around 7 K again. Below 7 K, S becomes to increase very rapidly, and amounts to a few 100 μV/K at 5 K. These complicated behavior of the resistivity and thermopower suggests the existence of certain changes in the electronic state below the SDW transition temperature about 20 K.

3.1.4 $(DMET)_2ReO_4$

$(DMET)_2ReO_4$ has not classified into any group of DMET salts. By the previous measurement of resistivity of $(DMET)_2ReO_4$, the minimum of the resistivity was found at around 293 K at ambient pressure. It seems to be the M-I transition. On the other hand, the X-ray diffraction analysis revealed that the salt contains the tetramer of donors even at 297 K as shown in Fig. 3.1.8. Since the period of four DMET molecules corresponds to the $2k_F$ distortion, $(DMET)_2ReO_4$ should be insulating at 297 K. Seemingly there exists the discrepancy between the results of the resistivity measurement and the crystal structure. To understand the character of $(DMET)_2ReO_4$ deeper, the thermopower measurement was performed.

The temperature dependence of the thermopower along the most conducting direction is shown in Fig. 3.1.9. The thermopower at RT is about 33 μV/K and almost independent of temperature down to about 200 K. The positive value of S suggests that the dominant carrier is hole in this region. No anomalous behavior is observed at around 293 K. The change of the band structure is not considered to exist around the temperature of the resistance minimum, namely it is not due to a phase transition. To account for the minimum, the consideration using Eq.(2.11) is performed by Saito *et al.*[10] In conclusion, $(DMET)_2ReO_4$ is intrinsically semiconducting and the apparent metallic behavior is due to the temperature dependence in the mobility of the carriers.

It is well known that the thermopower becomes independent of temperature when the on-site Coulomb energy U is large, $U \gg 4t$. The almost constant thermopower observed for $(DMET)_2ReO_4$ is probably explained in this manner.[10]

Below about 200 K, thermopower starts to decrease with decreasing temperature and changes its sign to minus at about 110 K. On lowering temperature, the slope of S vs. T becomes larger. In these temperature region, no anomalous behavior of the resistivity has not observed for $(DMET)_2ReO_4$. It might be attributed for the influence of defects and so on.[10] Another possible explanation is the gradual change of the relative superiorities of electrons and

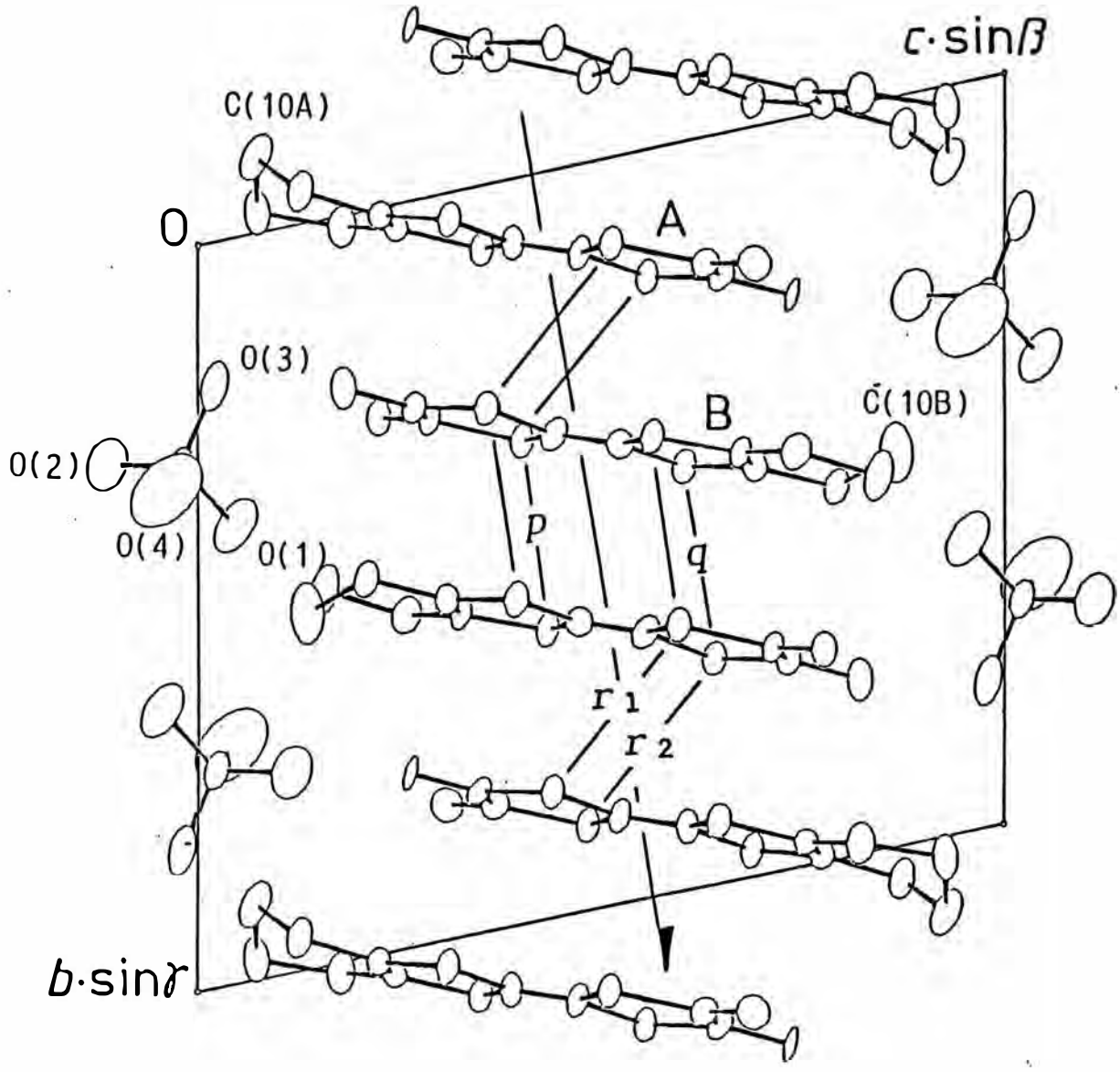

Fig. 3.1.8. Crystal structure of $(DMET)_2ReO_4$ viewed along the a-axis.

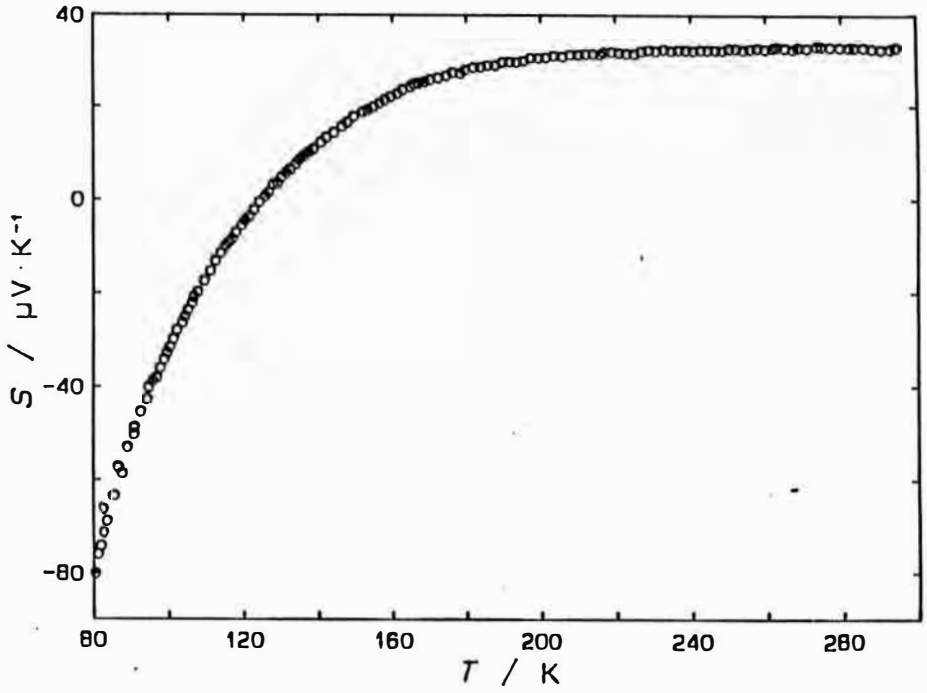

Fig. 3.1.9. Thermopower of $(DMET)_2ReO_4$.

holes. In principle, both electron and hole contribute to the electrical conduction in an intrinsic semiconductor. However, owing to the difference of shapes of the electron band and the hole band, either of them is dominant in the semiconductor. If the balance is sensitive to temperature, the dominance may be given either of them by the other. To confirm this hypothesis, measurements and/or calculations to determine the shape of the bands is necessary.

3.1.5 $(DMET)_2Au(CN)_2$ (Group 3)

$(DMET)_2Au(CN)_2$ is classified into the Group 3 of DMET salts.[1,3] The crystal structure of $(DMET)_2Au(CN)_2$ is shown in Fig. 3.1.10.[4] This type of the crystal structure is generally seen in DMET radical salts. The temperature dependence of resistivity of $Au(CN)_2$ salt is metallic down to 28 K, and semiconducting below the temperature. The temperature dependence of thermopower along the donor-stacking direction is shown in Fig. 3.1.11(a) and (b). The range of S in (b) is a part of that in (a). S is 20 μV/K at 300 K. The positive sign suggests the dominant carrier is hole. This is consistent with the 1/4-filled hole band of this salt. S is metallic down to about 50 K, though there is an anomaly due to the phase transition at about 180 K as seen in Fig. 3.1.11(b). The phase transition is previously found by the measurement of the resistivity.[11] The slope of S vs. T is larger below the transition temperature than above the temperature. From these slopes, using Eq.(2.13), the transfer integral t can be estimated. In Fig. 3.1.11(b), each solid line is a fit to each linear part of S. Above 180 K, t is 0.25 eV, and 0.21 eV from 60 to 170 K, respectively. In the previous study by Kamio et al,[4,12,13] S from RT down to about 100 K has been measured for another sample crystal. There is a good agreement of the absolute value of S between by the previous measurement and by this study. The transfer integrals estimated with the previous result are 0.25 eV above 180 K and 0.20 eV below the temperature. For the estimation of t in the lower temperature region, the extrapolating value of the slope of S vs. T to 0 K was used.

As shown in Fig. 3.1.11(a), below 100 K, somewhat complicated behavior was found in this study. With decreasing temperature from 100 K, the broad minimum of S is observed at around 50 K, then S starts to increase up to 15 μV/K at about 25 K. The way to increase between 25 K and 50 K is exponential to $1/T$ rather than linear to $1/T$. After showing the maximum at about 25 K, S abruptly decreases with decreasing T. Then the sign of S changes from plus to minus at about 21 K. At about 11 K, again, S shows another sharp minimum and turns to increase.

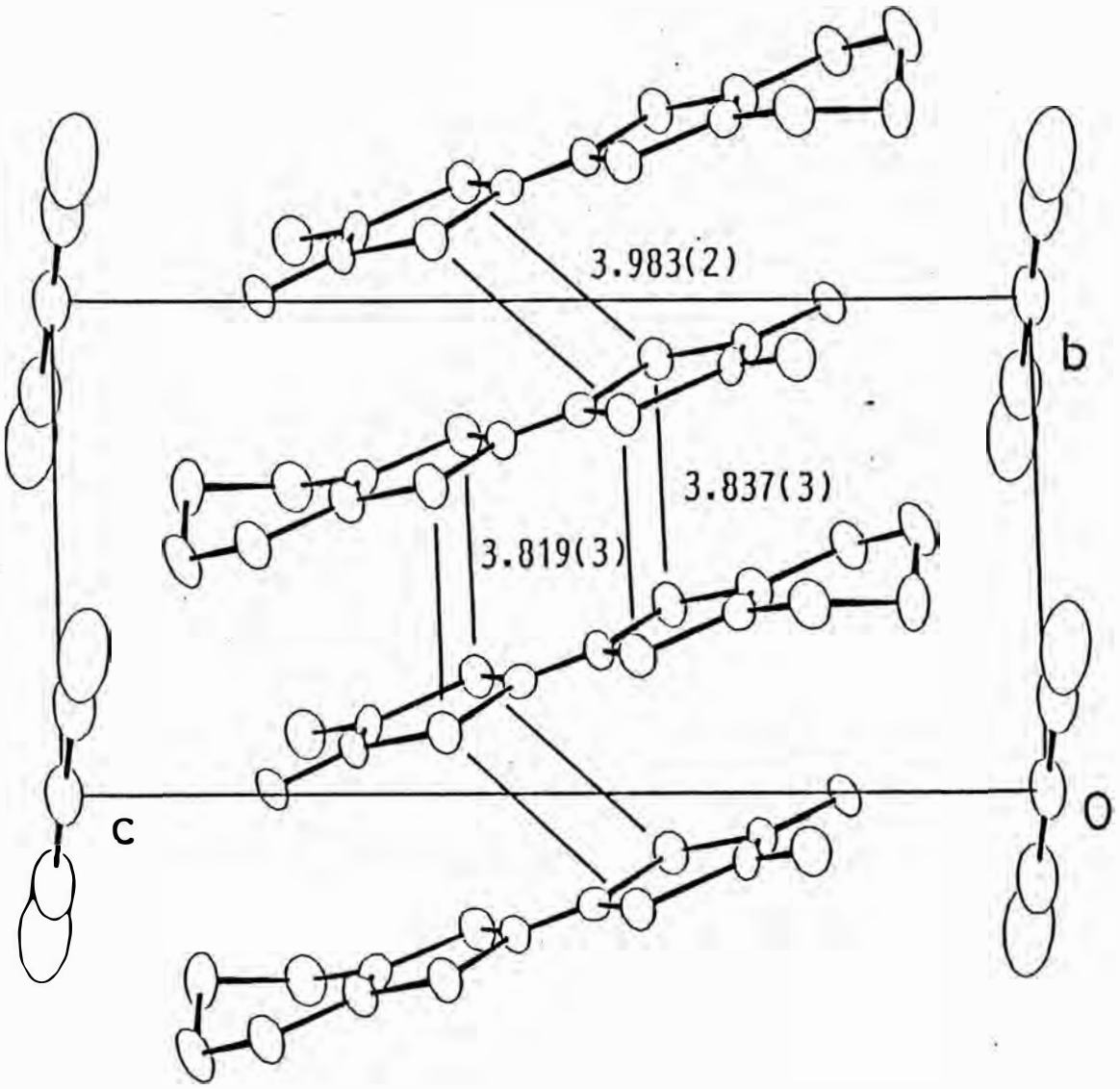

Fig. 3.1.10. Crystal structure of $(DMET)_2Au(CN)_2$ viewed along the a-axis.

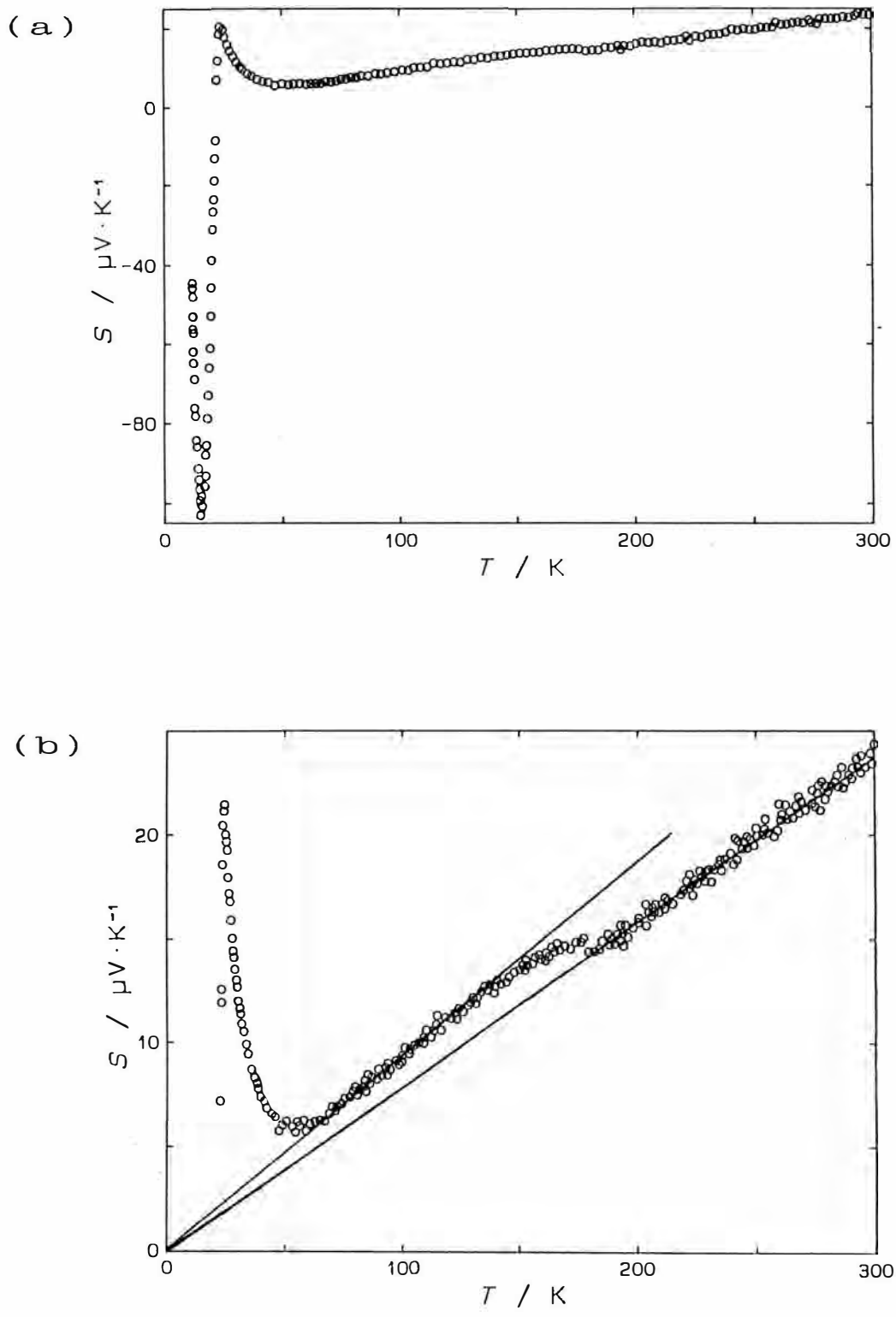

Fig. 3.1.11. (a) Thermopower of $(DMET)_2Au(CN)_2$. (b) A part of (a). Solid lines are fitted for metallic regions above and below the phase transition at 180 K.

The abrupt decrease at 25 K corresponds to the M-I transition found in the resistance measurement. The M-I transition is an SDW transition confirmed with EPR and NMR measurements.[4,7,14] Then the gradual increase of S between 25 K and 50 K is considered to be a precursor of the transition,[15] though the exponential temperature dependence can not be explained. There is no anomaly of the resistivity in this temperature region. However it is not inconsistent with the interpretation.

The sharp minimum at about 11 K is probably corresponding to an anomaly of the resistivity. Below T_{M-I} the resistivity of $(DMET)_2Au(CN)_2$ increases rapidly with decreasing temperature, however the increase of the resistivity is suppressed below about 15 K. The start of the variation can be seen in Fig. 1.3.

The abrupt decrease, corresponding to the M-I transition, and the sharp minimum at a lower temperature than T_{M-I} of the thermopower are also observed for $(DIMET)_2I_3$, $(DIMET)_2IBr_2$ and $(DIMET)_xCu(NCS)_2$. The mechanism that explains these phenomena is not known up to now. However, the consideration about these salts is made together in the later chapter.

3.1.6 $(DMET)_2I_3$ (Group 4)

$(DMET)_2I_3$ is classified into Group 4.[1-4] The crystal structure of $(DMET)_2I_3$ is shown in Fig. 3.1.12. It is the general type of crystal structure in DMET radical salts. The temperature dependence of thermopower measured along the most conducting direction of $(DMET)_2I_3$ is shown in Fig. 3.1.13. S at 300 K is 27 μV/K. The positive value suggests the dominant carrier is hole. The metallic behavior was observed from RT down to 5 K. This is consistent with the metallic temperature dependence of the resistivity above 0.5 K. (I_3 salt becomes superconducting below 0.5 K.) However, below about 200 K the thermopower separates from the linear temperature dependence as seen in Fig. 3.1.13. Furthermore thermopower seems to become on the straight line again below about 20 K, though the data points are somewhat scattered. The deviation from the proportional line to T possibly corresponds to the increase of the dimensionality suggested from the EPR measurement.[7] The transfer integral estimated with the slope of the solid line in Fig. 3.1.13 is 0.19 eV. The transfer integral is smaller than that of $Au(CN)_2$ salt in the metallic region below 180 K.

At about 50 K, S becomes independent of T and starts to decrease at about 20 K as mentioned above. However, no anomaly is observed in the results of the resistivity measurement. The result of EPR has not been obtained below 30 K.[7] One interpretation for the low temperature anomaly of S is due to the phonon drag. Another is the existence of a new electronic state which has not been observed at ambient pressure before. In fact, the Hall constant of $(DMET)_2I_3$ shows anomalous behavior around this temperature region, though that is observed under some pressures.[9,16]

3.1.7 $(DMET)_2SCN$ (Group 4)

This salt is classified into Group 4 of DMET salts as same as I_3 salt.[1-4] Though the superconductivity has not been observed for SCN salt, the crystal structure and temperature dependence is similar to $(DMET)_2I_3$. The temperature dependence of the thermopower of $(DMET)_2SCN$ along the most conducting direction is shown in Fig.

3.1.14. The S at 300 K is 29 μ/K and the positive sign shows holes are dominant in $(DMET)_2SCN$. The reliable data is obtained only above 80 K. In this temperature region, the thermopower seems to be proportional to temperature as same as that of $(DMET)_2I_3$. This metallic behavior is consistent with the temperature dependence of the resistivity.[1)] The transfer integral t estimated from the slope of S vs. T is 0.15 eV. This is smaller than that of $Au(CN)_2$ salt in Group 3.

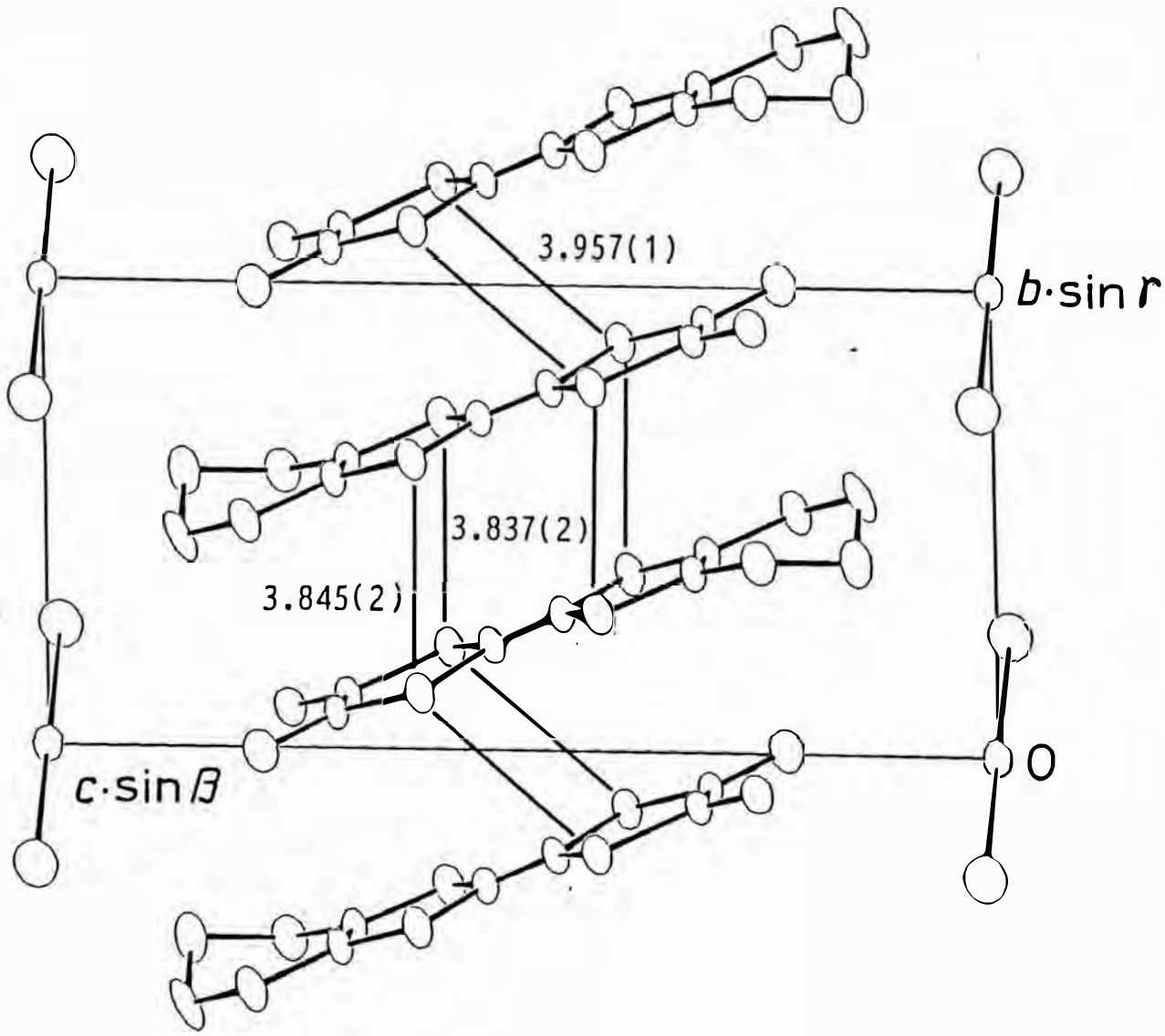

Fig. 3.1.12. Crystal structure of $(DMET)_2I_3$ viewed along the a-axis.

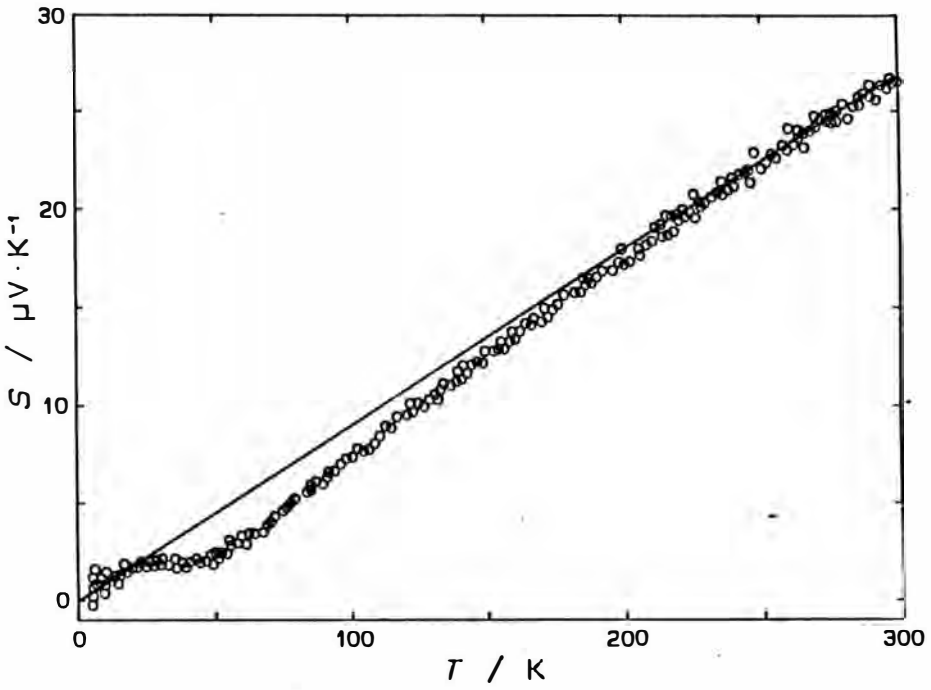

Fig. 3.1.13. Thermopower of $(DMET)_2I_3$. The solid line is fitted for the proportional region.

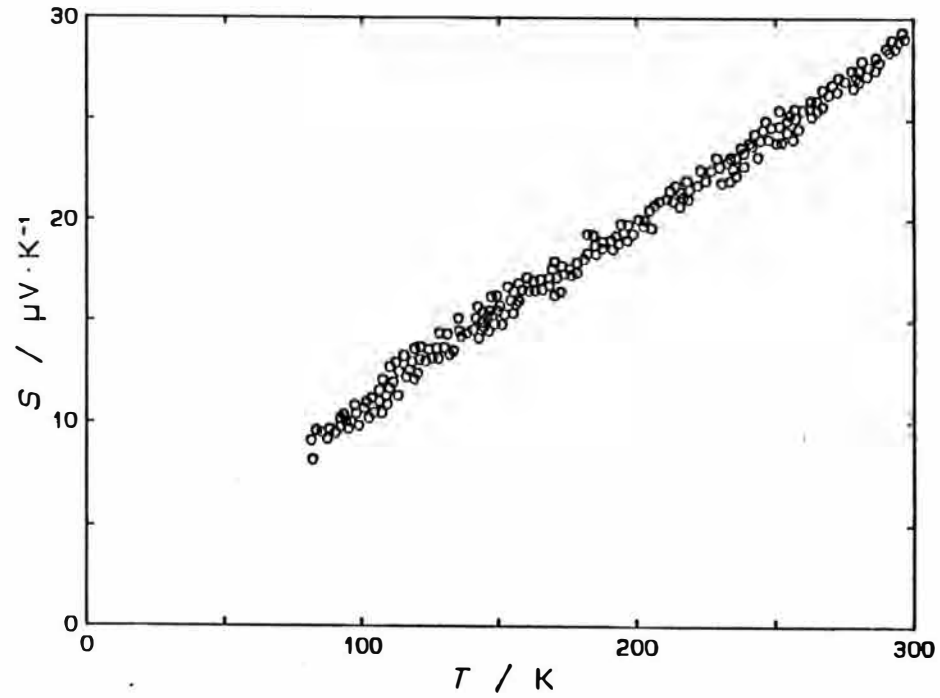

Fig. 3.1.14. Thermopower of $(DMET)_2SCN$.

3.1.8 $(DMET)_2AuBr_2$ (Group 5)

$(DMET)_2AuBr_2$ classified into Group 5 has the κ-type structure as seen in Fig. 3.1.15.[1-4] As mentioned in the introduction, on cooling, the resistivity of $(DMET)_2AuBr_2$ slightly increases down to around 150 K and turns to decrease below the temperature. The superconducting transition occurs at 1.9 K at ambient pressure. The dimer of DMET molecule constructs donor sheets. Each of the sheets are separated by an anion sheet. Since the quasi-2D electrical properties can be expected from the crystal structure, the thermopower measurements are performed along two kinds of the crystal-growth axis, namely along the edges of the sample crystal as shown in the inset in Fig. 3.1.16. However, the correspondence between the orientations and the crystal axes is not clear at present. The temperature dependence of S along the two directions is shown in Fig. 3.1.16. At RT S is 21 μV/K for the first direction and about 23 μV/K for the second though it is an extrapolating value. For each direction, S gradually decreases with decreasing temperature from RT. On decreasing temperature, S passes through zero at about 240 K for the first direction and at about 130 K for the second. Around 130 K, S along the first direction turns to increase. This temperature is reasonably close to the temperature of the broad maximum in the resistivity. S along the second direction also turns to increase at around 100 K. The increase is suppressed at around 50 K for the both directions. Below the temperature, S along the both directions rapidly increases with decreasing temperature. Around the temperature, the change in variation of the resistivity has been observed as shown in Fig. 1.3.

Because $(DMET)_2AuBr_2$ is a quasi-2D conductor, the analysis using Eq.(2.13) is not appropriate. Furthermore, the thermopower of this salt does not show the simple proportional behavior expected for general metals. The complicated behavior like this is also observed for κ-$(BEDT\text{-}TTF)_2Cu(NCS)_2$ as shown in Fig. 3.1.17.[17] The crystal structure of $(DMET)_2AuBr_2$ is the same type of that of κ-$(BEDT\text{-}TTF)_2Cu(NCS)_2$. Though the sign of the thermopower of κ-$(BEDT\text{-}TTF)_2Cu(NCS)_2$ changes with the direction along which the measurement

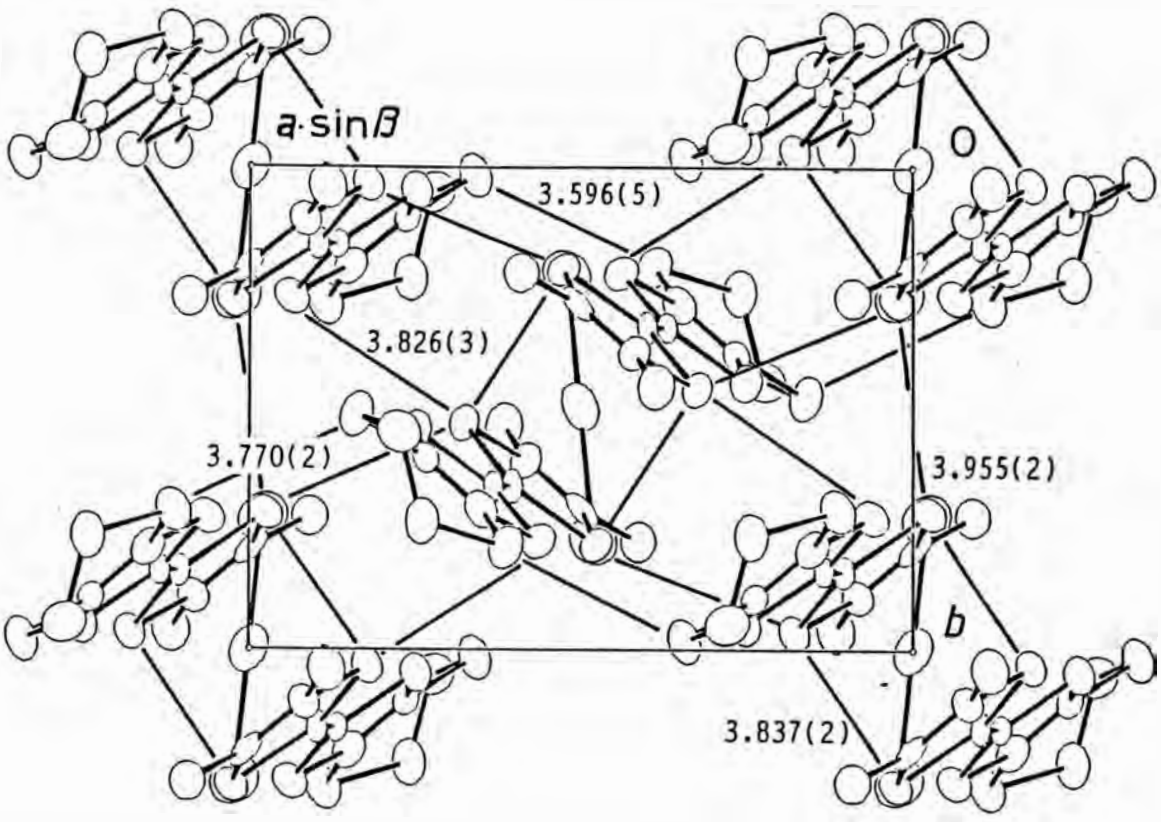

Fig. 3.1.15. Crystal structure of $(DMET)_2AuBr_2$ (Z=2) viewed along the c-axis.

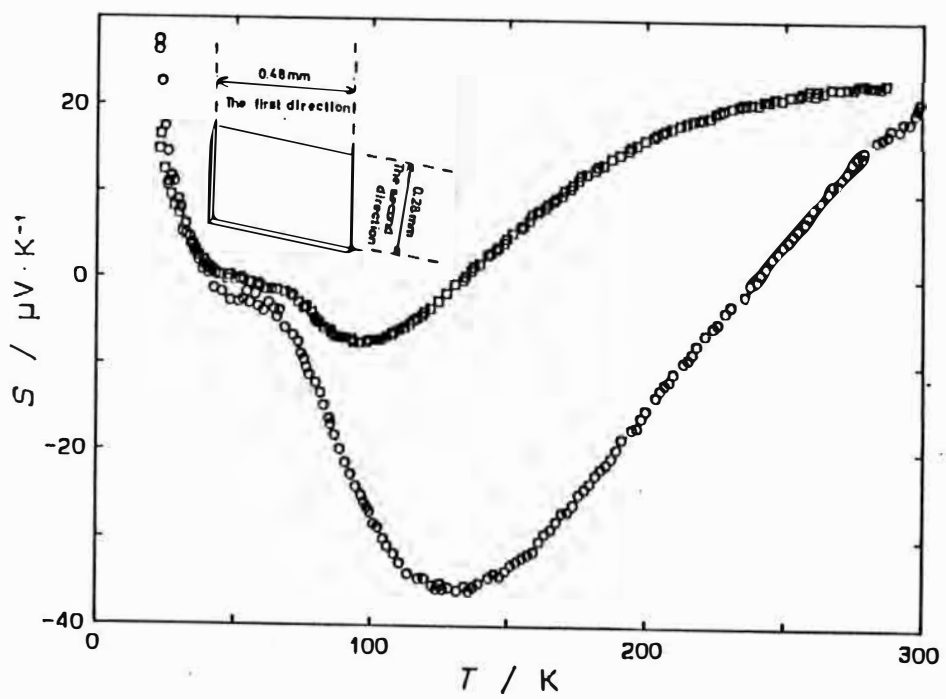

Fig. 3.1.16. Thermopower of $(DMET)_2AuBr_2$ (Z=2). Inset shows the shape of the sample.

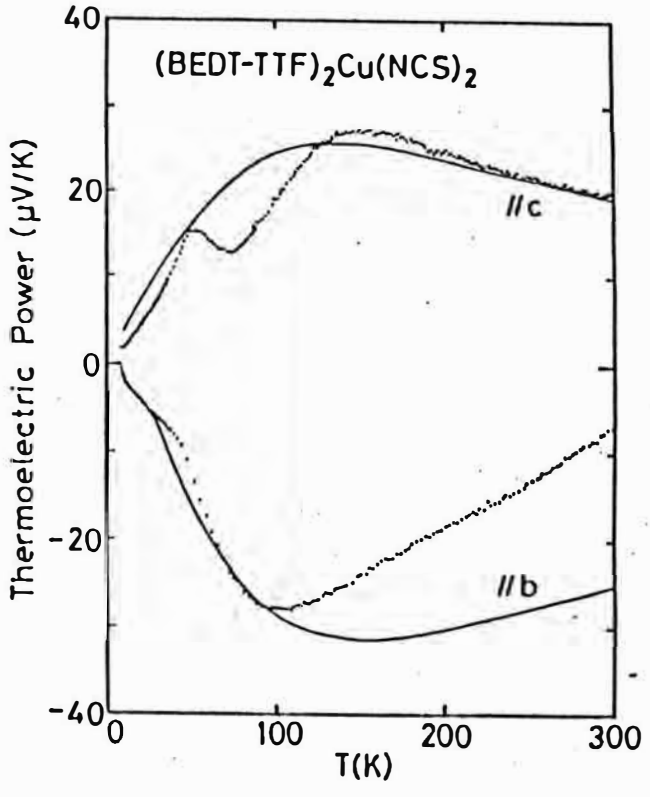

Fig. 3.1.17. Thermopower of $(BEDT-TTF)_2Cu(NCS)_2$. Solid lines are results of theoretical calculations.

is performed, the shape of the curve of S vs. T is similar to S of $(DMET)_2AuBr_2$. For κ-$(BEDT\text{-}TTF)_2Cu(NCS)_2$, the theoretical estimation based on the band calculation of the thermopower was performed as shown in Fig. 3.1.17. With the method described in Ref.17, the similar calculation was performed for the thermopower of $(DMET)_2AuBr_2$. As a result, the temperature dependence of S along the a- and the b-axes is obtained. That is similar to the calculated temperature dependence of κ-$(BEDT\text{-}TTF)_2Cu(NCS)_2$. Therefore if the measurements of S of $(DMET)_2AuBr_2$ along the crystal axes are made, the more similar temperature dependence of S will be obtained. The reason why the sign of S changes is probably explained by the mixing of elements of the tensor of S.

3.2 Resistivity of DIMET salts

3.2.1 $(DIMET)_2I_3$

The crystal structure of $(DIMET)_2I_3$ is shown in Fig. 3.2.1.[18] This is isostructural to $(DMET)_2I_3$. The electrical resistance was measured along the stacking direction with the four-probe method both at ambient pressure and under some pressures. The pressure dependence of the electrical resistance of $(DIMET)_2I_3$ at RT is shown in Fig. 3.2.2. The resistance decreases with increasing pressure. The slope of the p–R plot becomes more gradual when the pressure is increased. The pressures, under which the temperature dependence of the resistance was studied and the reliable results were obtained, are 3.8, 4.5, 6.0 and 14.5 kbar at RT. Due to the solidification of the oil used for pressuring, pressure in the cell is reduced about 1.5 kbar below about 200 K. The temperature dependence of electrical resistance normalized at 300 K is shown in Fig. 3.2.3(a). In Fig. 3.2.3(b), the plot of the resistance versus $1/T$ is also shown. These results are for the pressure of 0.0 (ambient pressure), 3.8, 4.5, 6.0 and 14.5 kbar at RT.

At ambient pressure, the temperature dependence of the electrical resistance is metallic from RT to about 42 K with decreasing temperature, though resistance jumps are observed at about 100 K and 200 K. The resistance jump tends to be suppressed under pressure in general. This tendency is also seen in $(DIMET)_2I_3$. The M–I transition temperature $T_{M\text{-}I}$ is about 40 K at ambient pressure. Below $T_{M\text{-}I}$, the electrical resistance rapidly increases with decreasing temperature. The transition is due to the formation of SDW, as confirmed with the ESR experiments by Kanoda *et al*. It is interesting that the change in the slope of $1/T$–R plot is observed around a specific temperature T^* as shown in Fig. 3.2.2(b). At ambient pressure, T^* is about 33 K. The temperature dependence of $(DIMET)_2I_3$ is similar to $(DMET)_2Au(CN)_2$ below $T_{M\text{-}I}$. The activation energies estimated using Eq.(2.10) are 46 meV above T^* and 6.0 meV below T^* at ambient pressure. This anomaly is discussed in the next chapter combined with other results.

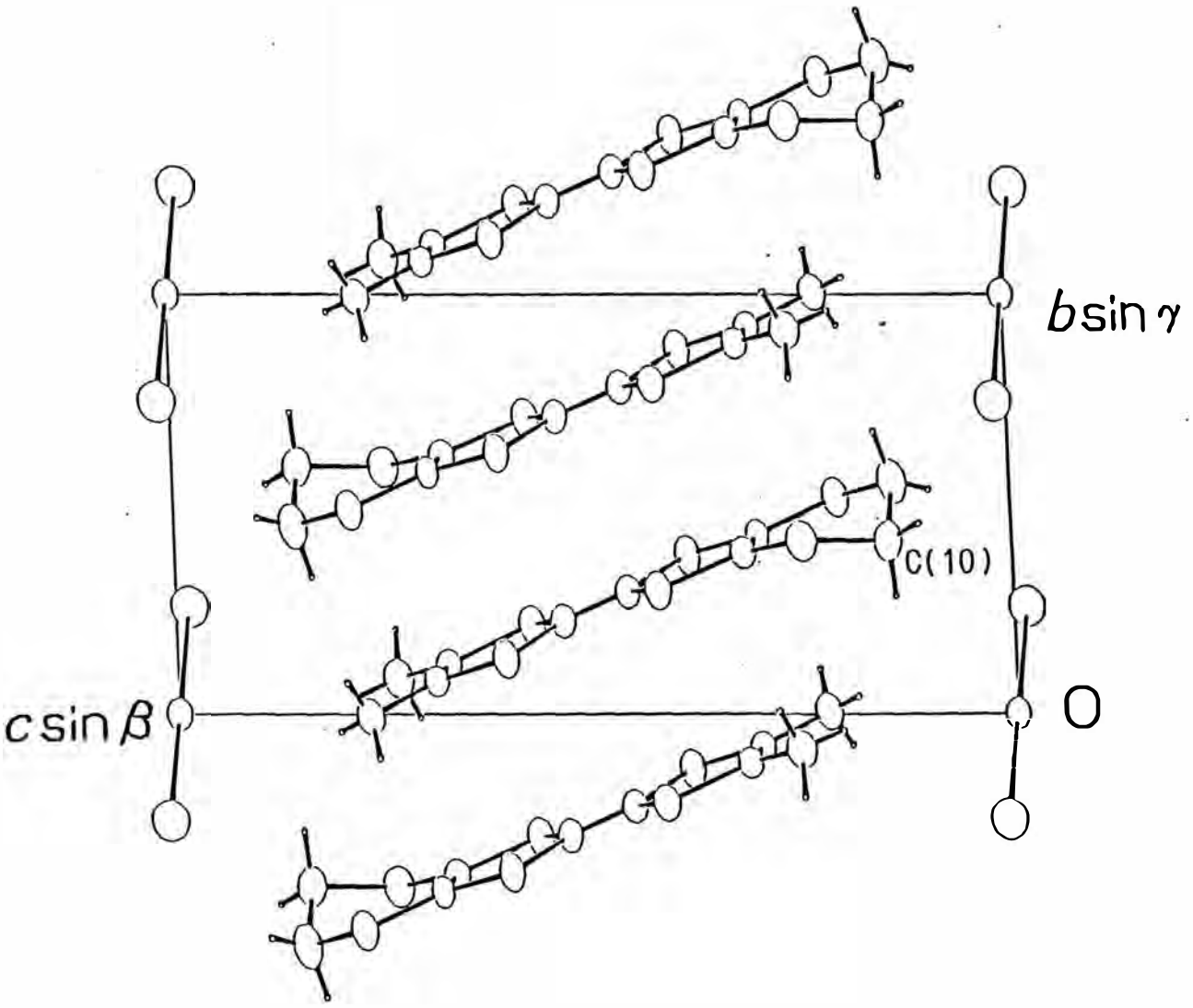

Fig. 3.2.1. Crystal structure of $(DIMET)_2I_3$ viewed along the a-axis.

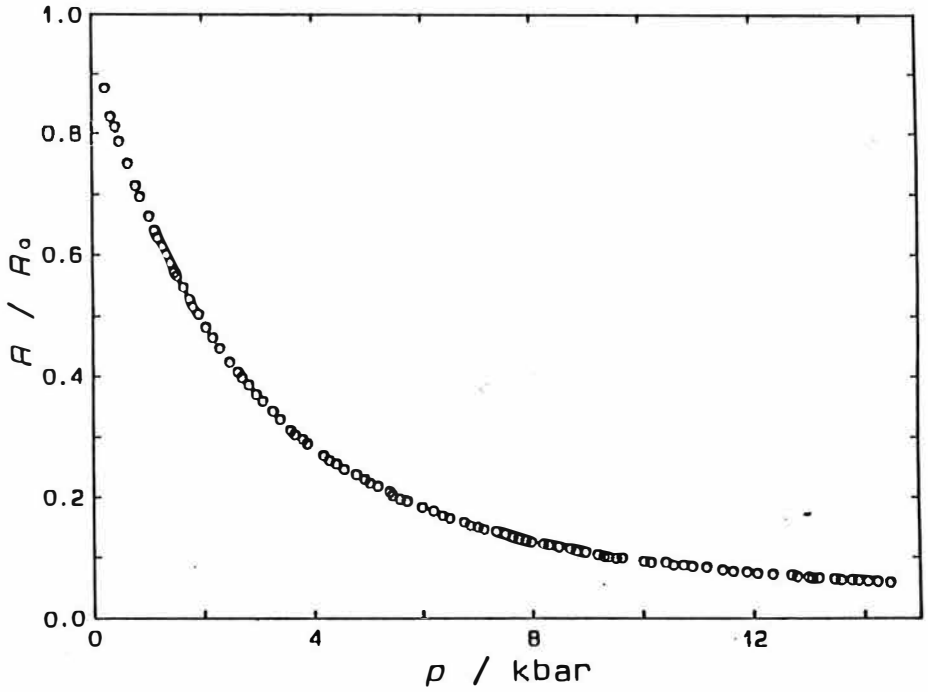

Fig. 3.2.2. Pressure dependence of electrical resistance of $(DIMET)_2I_3$ at room temperature normalized at 0 kbar.

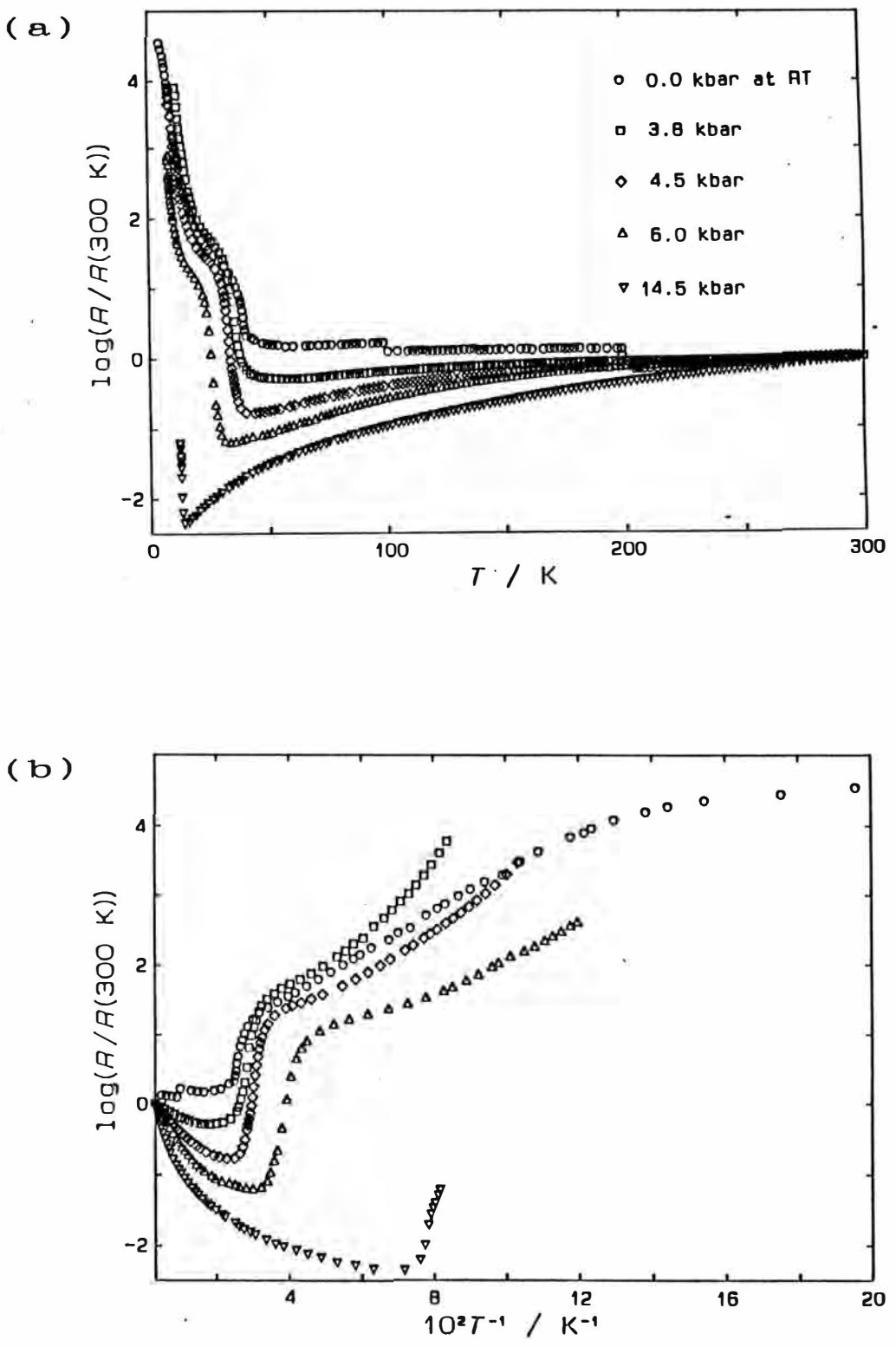

Fig. 3.2.3. (a) Electrical resistance of $(DIMET)_2I_3$ under pressures normalized at 300 K. (b) Plot of electrical resistance of $(DIMET)_2I_3$ versus $1/T$ under pressures.

Under pressure, T_{M-I} and T^* decrease with increasing pressure as seen in Fig. 3.2.2(b). (The anomaly at T^* under 13.0 kbar is slightly observed in the figure.) The pressure dependence of T_{M-I} and T^* is shown in Fig. 3.2.4. It seems that the pressure dependence is large around the intermediate pressures in the shown pressure range studied. The activation energy in the semiconducting region is almost independent of pressure. Up to 13.0 kbar (below 200 K), the superconductivity has not been observed. It can not be said, however, that the superconducting transition does not occur under higher pressures than 13.0 Kbar.

The measurement of the resistivity was also made with Montgomery method. The size of the plate-like sample crystal was 0.25 x 0.14 x 0.08 mm^3. The temperature dependence of the resistivity, along the most conducting direction and another direction perpendicular to the former in the plate-like surface, is shown in Fig. 3.2.5(a). The first direction is probably the donor-stacking direction (the b-axis in Fig. 3.2.1). The second direction also corresponds to the direction normal to the b-axis in the a-b plane in Fig. 3.2.1. The resistivity along the second direction is strongly influenced by the magnitude of the side-by-side interaction between neighboring DIMET molecules. The consistent behavior with the result of the four-probe method is observed for the first direction corresponding to the donor stack. It is interesting that the similar behavior is also observed for the second direction. If this behavior is intrinsic to the second direction, it can be considered that the band is formed along the second direction by the side-by-side interaction of HOMO's of DIMET molecules. In reality, the face-to-face interaction is considered to be much larger than the side-by-side interaction, because the π-orbital of DIMET molecule contributes to the face-to-face interaction. The apparent metallic behavior is possibly extrinsic to the second direction.

Though the above consideration is possible, the ratio of the resistivity along the second direction to that along the first direction must contain the information about the anisotropy of the material. The temperature dependence of the ratio is shown in Fig.

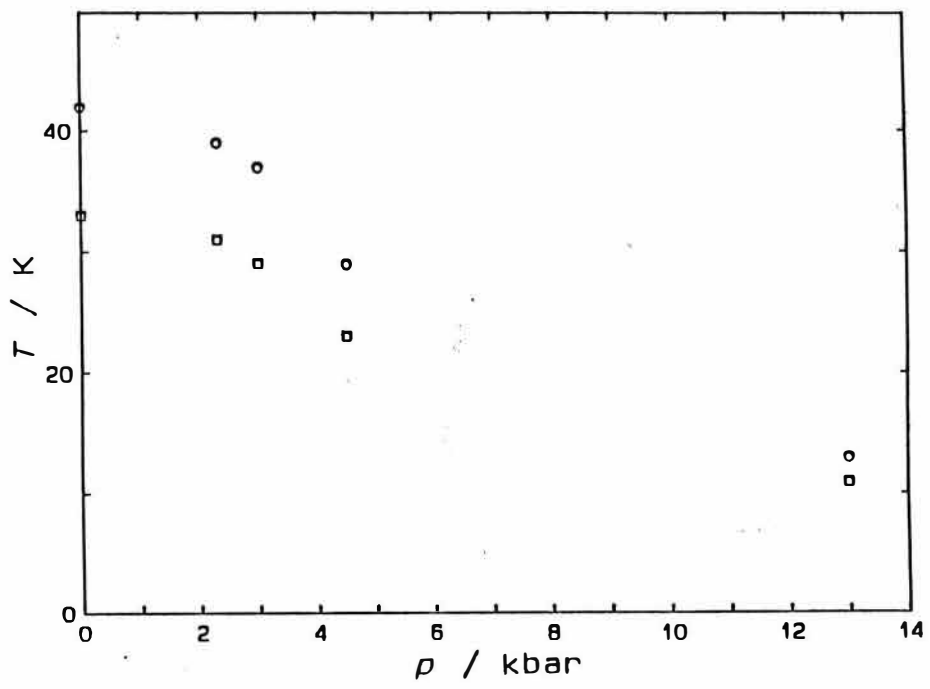

Fig. 3.2.4. Pressure dependence of T_{M-I} (circles) and T^* (squares) of $(DIMET)_2I_3$.

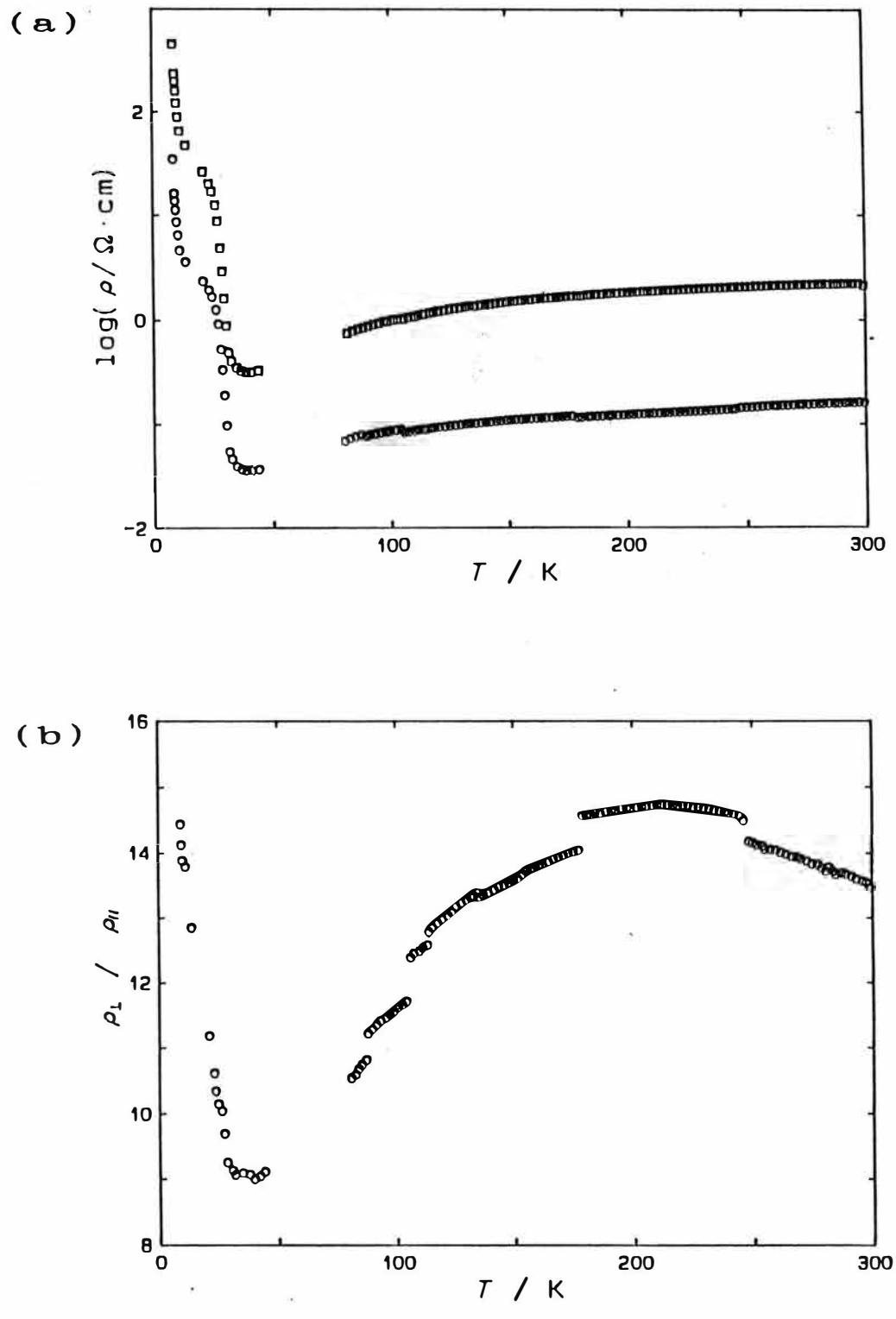

Fig. 3.2.5. (a) Resistivity of $(DIMET)_2I_3$ along the directions parallel (circles) and perpendicular (squares) to the most growing edge of the sample crystal measured with the Montgomery method. (b) Temperature dependence of the anisotropy in resistivity of $(DIMET)_2I_3$.

3.2.5(b). The jumps seen in the metallic region is not an intrinsic character of the material. It is interesting that no large resistance jump is seen in Fig. 3.2.5(a), in spite of the somewhat large jumps in Fig. 3.2.5(b), though the reason for this is not known. The anisotropy determined with the Montgomery method is strongly depends on the assumed distances between the terminals. Due to the very small size of the sample crystal, the error on measuring the distances possibly makes the ratio from 8 to 20. This is nevertheless small for the quasi-1D material. For example, the ratio reaches about 25 for $(TMTSF)_2ClO_4$ and 200 for $(TMTSF)_2PF_6$ at RT, both of them is known as quasi-1D material.[19-21] Because the absolute value of the ratio has a large error, the relative variation of the ratio should be reliable. The anisotropy, namely the one-dimensionality, gradually increases with decreasing temperature from RT to about 210 K. After the broad maximum around 210 K, the anisotropy decreases with decreasing temperature down to T_{M-I}, namely becomes more 2D. Below T_{M-I}, the anisotropy rapidly increases with decreasing temperature. In the low temperature region, below about 40 K, the data points are scattered due to the abrupt cooling and the large resistivity of the sample. The interesting fact is the existence of the maximum of the anisotropy in the metallic regime. This result is referred in the subsection for the thermopower of $(DIMET)_2I_3$.

3.2.2 $(DIMET)_2IBr_2$

The crystal structure of $(DIMET)_2IBr_2$ has not been solved up to now. By comparing the lattice constants of $(DIMET)_2IBr_2$ with those of $(DIMET)_2I_3$, it is considered that the structure of $(DIMET)_2IBr_2$ is similar to that of $(DIMET)_2I_3$. The temperature dependence of the resistivity of $(DIMET)_2IBr_2$, measured with the four-probe method at ambient pressure, is shown in Fig. 3.2.6(a). The plot of the resistivity versus $1/T$ is also shown in Fig. 3.2.6(b). The result is very similar to that of $(DIMET)_2I_3$. (Comparing with $(DIMET)_2I_3$, the resistance jump is less observed for $(DIMET)_2IBr_2$.) The temperature dependence is metallic down to about 40 K. At the temperature, the M-I transition occurs. Below T_{M-I}, the resistivity rapidly increases with decreasing temperature. The anomaly in the resistivity at T^* is also observed for $(DIMET)_2IBr_2$. T^* is about 30 K. The activation energies above and below T^* are 80 meV and 7.6 meV respectively. The apparent decrease of the activation energy is observed.

The measurement with the Montgomery method is also performed for $(DIMET)_2IBr_2$. The size of the sample crystal is 0.20 x 0.15 x 0.03 mm^3. The temperature dependence of the resistivity, both along the stacking direction and the other direction perpendicular to the former, is shown in Fig. 3.2.7(a). The temperature dependence of the ratio of the resistivity along the most conducting direction versus the resistivity along the other direction is also shown in Fig. 3.2.7(b). The anisotropy at RT is about 6 in this result, though the large error is also expected. The behavior of the resistivity along the both directions are very similar to each other as seen in the results for $(DIMET)_2I_3$. The ratio shows the very broad maximum around 260 K, though the extrinsic jumps are also seen in the metallic region. This temperature is higher than the temperature at which the anisotropy of $(DIMET)_2I_3$ becomes the maximum. This result is also referred in the subsection for the thermopower of $(DIMET)_2IBr_2$. The anisotropy becomes the minimum at T_{M-I} and then rapidly increases with decreasing temperature. Though it must be confirmed by another measurement whether the anomaly around 30 K, slightly below T_{M-I}, is

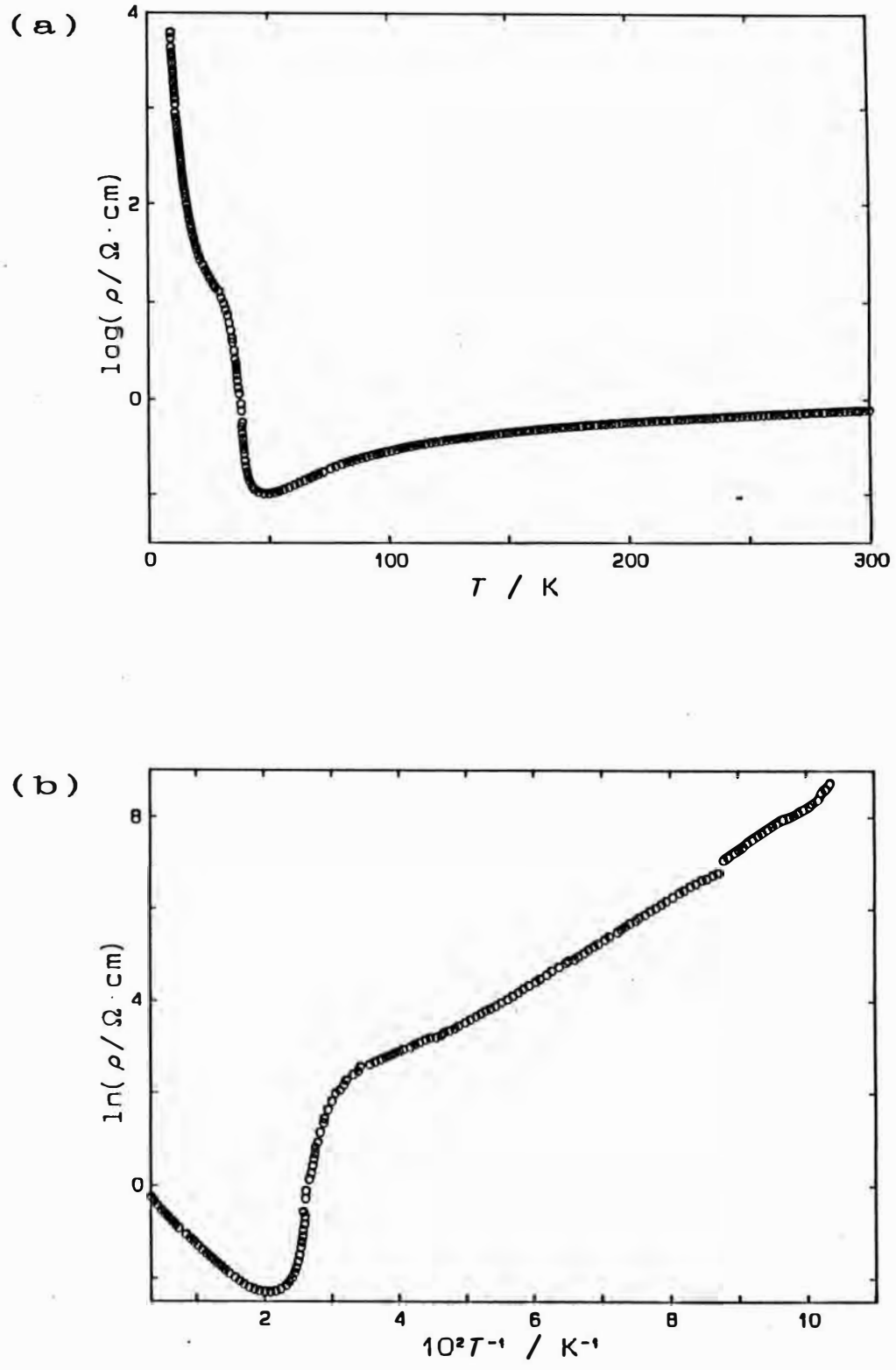

Fig. 3.2.6. (a) Resistivity of $(DIMET)_2IBr_2$. (b) Arrhenius plot of resistivity of $(DIMET)_2IBr_2$.

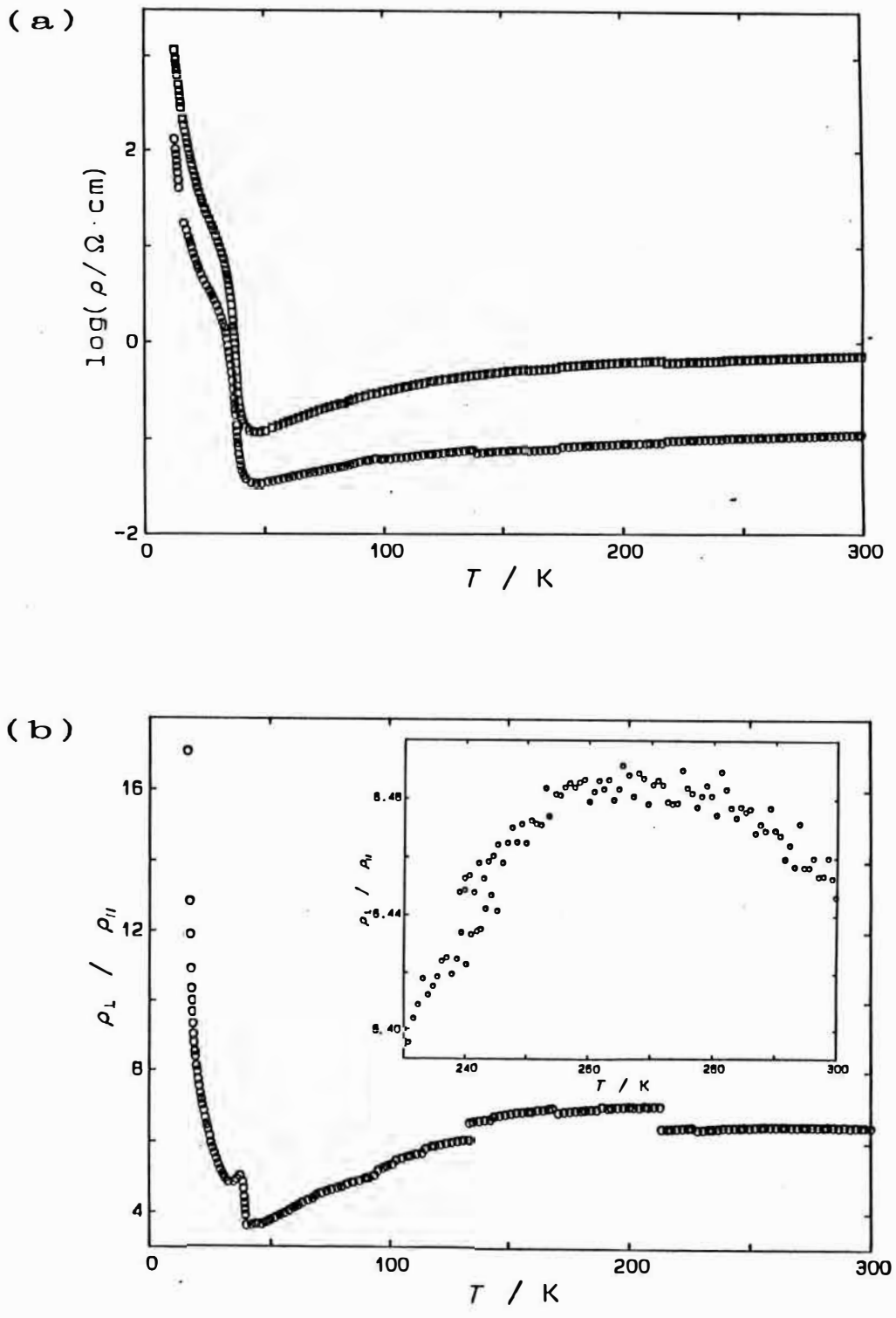

Fig. 3.2.7. (a) Resistivity of $(DIMET)_2IBr_2$ along the directions parallel (circles) and perpendicular (squares) to the most growing edge of the sample crystal measured with the Montgomery method. (b) Temperature dependence of the anisotropy in resistivity of $(DIMET)_2IBr_2$. Inset shows the high temperature region.

intrinsic or extrinsic, the anomaly seems to correspond to the anomaly of the resistivity at T_{M-I} measured with the four-probe method.

3.2.3 $(DIMET)_xCu(NCS)_2$

The crystal structure of $(DIMET)_xCu(NCS)_2$ has not been solved up to now. The composition of the DIMET molecule and the counter anion is, therefore, unknown. The temperature dependence of the resistivity along the most growing direction of the sample crystal is shown in Fig. 3.2.8(a). The result is obtained with the four-probe method at ambient pressure. In Fig. 3.2.8(b), the plot of the resistivity versus $1/T$ is also shown. The resistivity is apparently metallic down to about 50 K, though some resistance jumps are observed. The resistivity increases with decreasing temperature. The temperature dependence is somewhat weak in the whole temperature range studied. Though the quality of the sample crystal used is not so good, the similar results has been obtained for other some samples. The weak temperature dependence is possibly intrinsic to $(DIMET)_xCu(NCS)_2$. To obtain the result without resistance jumps, the measurement with the Montgomery method is perhaps effective as mentioned in the subsection 3.2.1. The activation energy from 14 K to 50 K is about 14 meV and less than 14 meV below 14 K. These small activation energy in the semiconducting region is general in DIMET salts in this study. The anomaly observed for $(DIMET)_2I_3$ and $(DIMET)_2IBr_2$ at T^* is not detected in this result in Fig. 3.2.8(b).

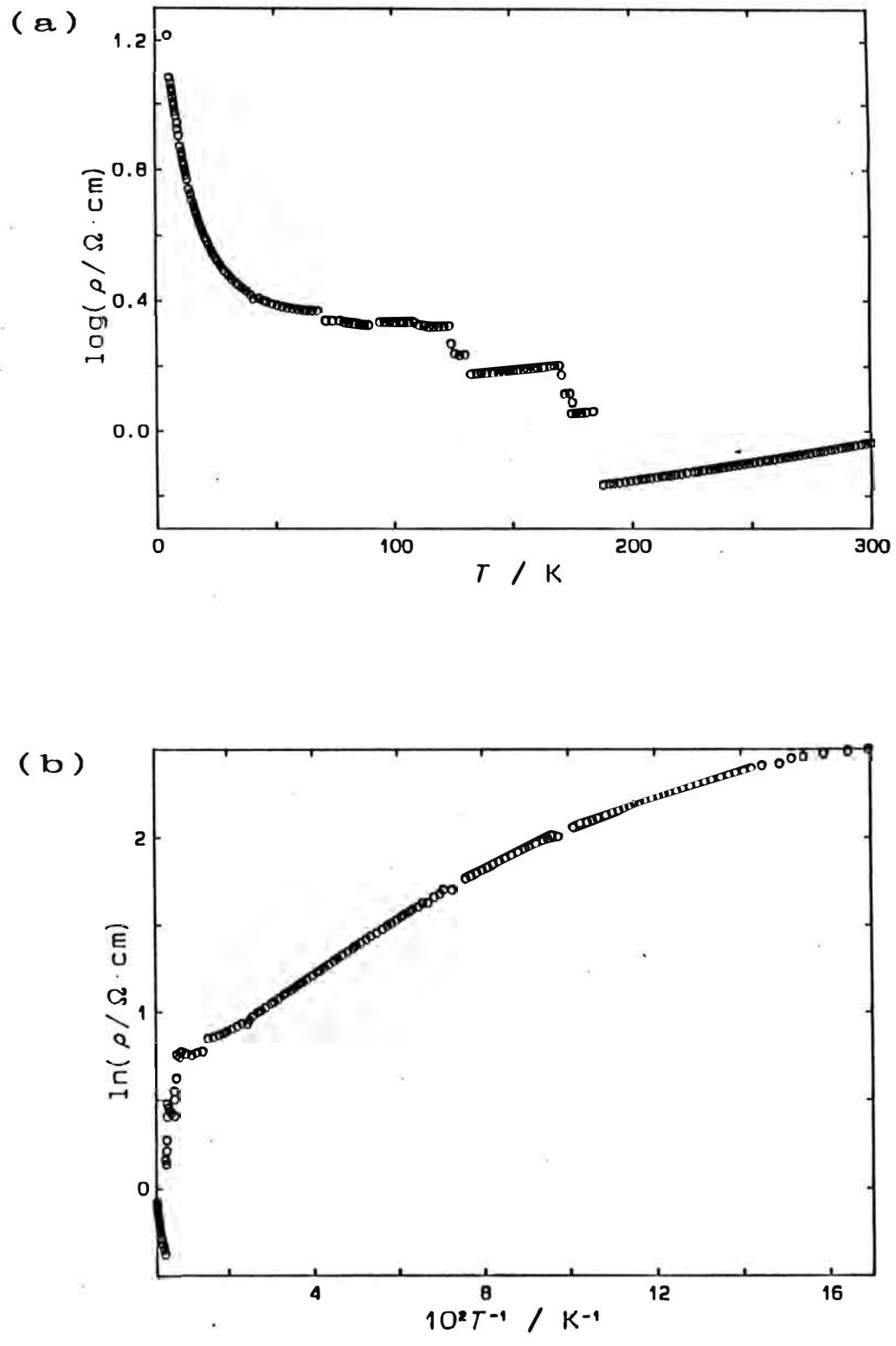

Fig. 3.2.8. (a) Resistivity of $(DIMET)_xCu(NCS)_2$. (b) Arrhenius plot of resistivity of $(DIMET)_xCu(NCS)_2$.

3.2.4 $(DIMET)_2BF_4$

The crystal structure of $(DIMET)_2BF_4$ is shown in Fig. 3.2.9.[17] This structure is the same type of $(DIMET)_2ClO_4$ and $(DMET)_2BF_4$.[2-4,22] There are two types of the donor-stack which are almost perpendicular to each other as shown in Fig. 3.2.9. The donor stack along the a-axis of $(DIMET)_2BF_4$ corresponds to the stack along the a-axis of $(DMET)_2BF_4$ as shown in Fig. 3.1.4. There is the same correspondence between the stacks along the b-axis of $(DIMET)_2BF_4$ and along the b-axis of $(DMET)_2BF_4$. Because there are the two types of stacks in $(DIMET)_2BF_4$, the temperature dependence of the resistivity along each of the crystal axes was measured. The results are shown in Fig. 3.2.10(a). The temperature dependence is metallic for both of the directions down to T_{M-I}, about 40 K, and semiconducting below T_{M-I}. The temperature dependence is somewhat weak, namely R(40 K)/R(300 K) is 0.30 for the a-axis and 0.24 for the b-axis.

The plot of the resistivity versus $1/T$ is also shown in Fig. 3.2.10(b). The temperature dependence of the resistivity is very complicated below T_{M-I} for both of the directions. Because the slope below T_{M-I} in Fig. 3.2.10(b) changes stepwise with temperature, the semiconducting region can be divided into some temperature regions. These regions are symbolized from A to D as shown in Fig. 3.2.10(b). The similar complicated behavior has been also observed for the resistivity of $(DMET)_2BF_4$ and $(DMET)_2ClO_4$ as described in the subsection 3.1.3. It is possibly the specific phenomenon for these salts with the characteristic structure.

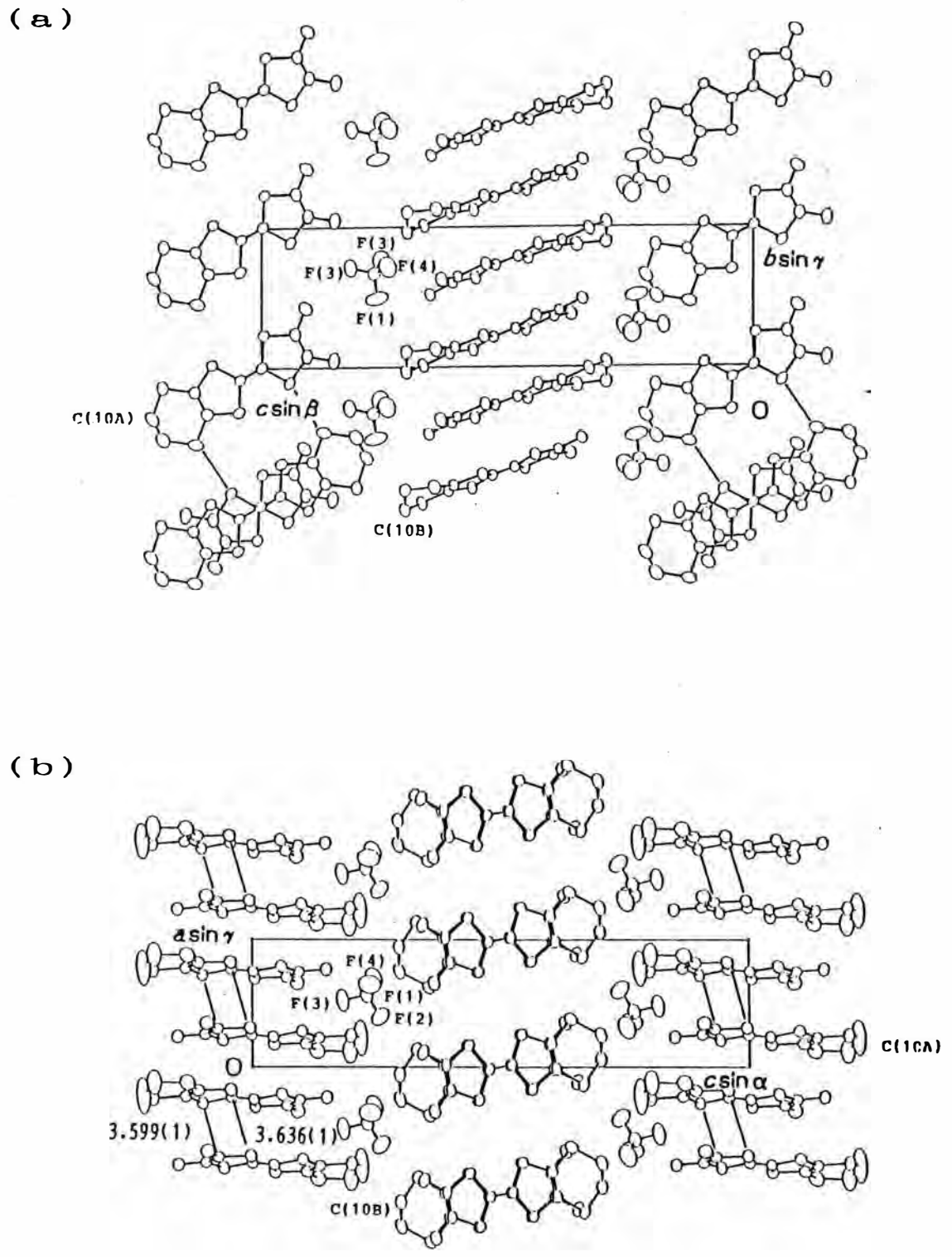

Fig. 3.2.9. Crystal structure of $(DIMET)_2BF_4$ viewed along the b-axis (a) and along the a-axis.

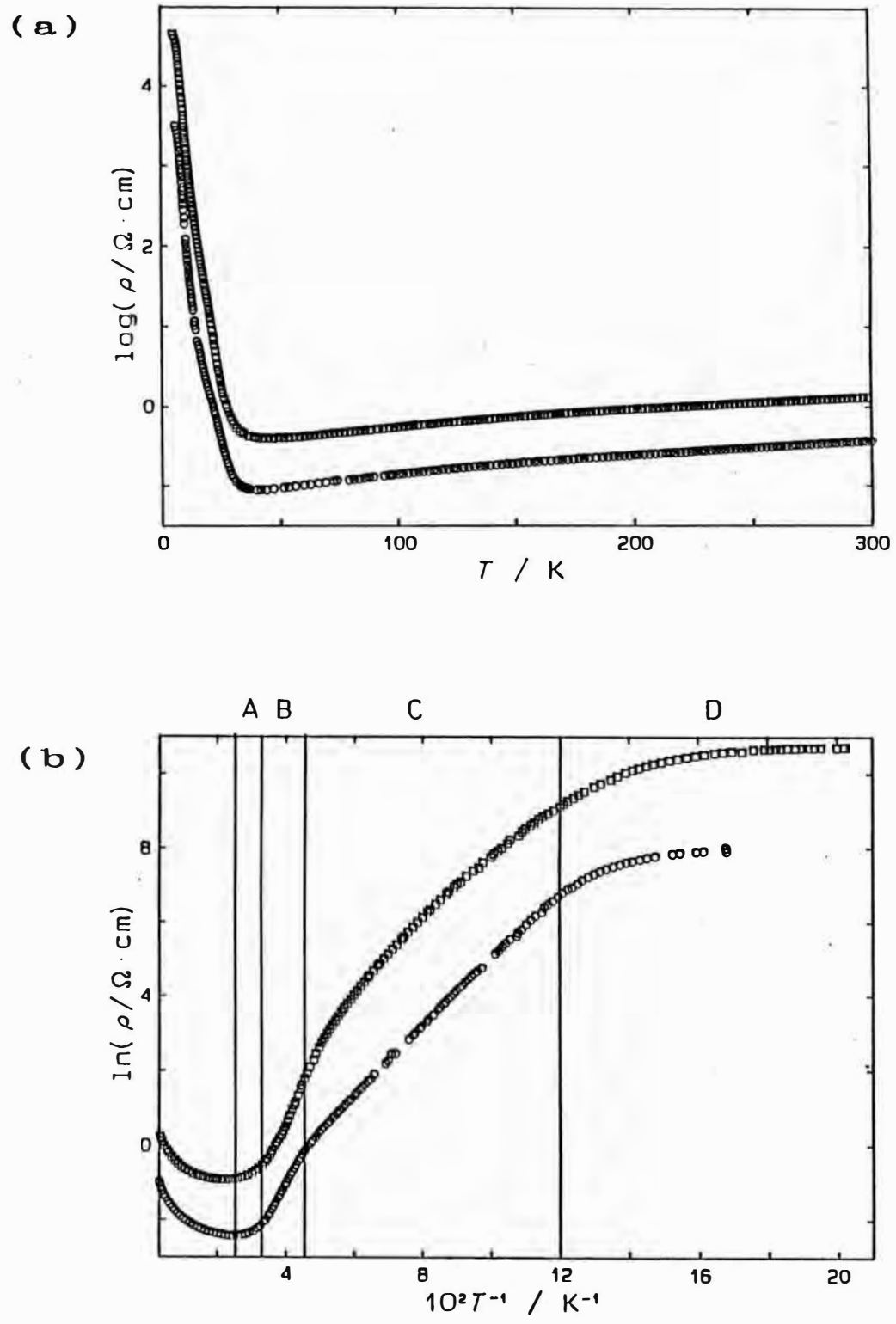

Fig. 3.2.10. (a) Resistivity of $(DIMET)_2BF_4$. (b) Arrhenius plot of resistivity of $(DIMET)_2BF_4$. Squares are for a-axis and circles are for the b-axis.

3.2.5 $(DIMET)_2AuCl_2$

The crystal structure of $(DIMET)_2AuCl_2$ is shown in Fig. 3.2.11, and the structure is the same type of the crystal structure of $(DIMET)_2I_3$.[18] The resistivity was measured along the most growing axis of the needle-like sample crystal. The behavior of the resistivity is semiconducting below about 240 K and metallic above the temperature. The temperature dependence of the resistivity above 220 K is shown in Fig. 3.2.12(a). The very broad minimum of the resistivity can be seen around 240 K. In Fig. 3.2.12(b), the plot of the resistivity versus $1/T$ is shown. Though the resistance jumps are seen, the slope of the Arrhenius plot in Fig. 3.2.12(b) seems to be constant between 70 K and 170 K. The activation energy E_a in this temperature region is 29 meV and E_a seems to decrease slightly below about 70 K.

It is very strange that $(DIMET)_2AuCl_2$ is semiconducting below the relatively high temperature 240 K, in spite of the similar crystal structure to $(DIMET)_2I_3$ which is metallic down to about 40 K. This point is discussed in the later chapter.

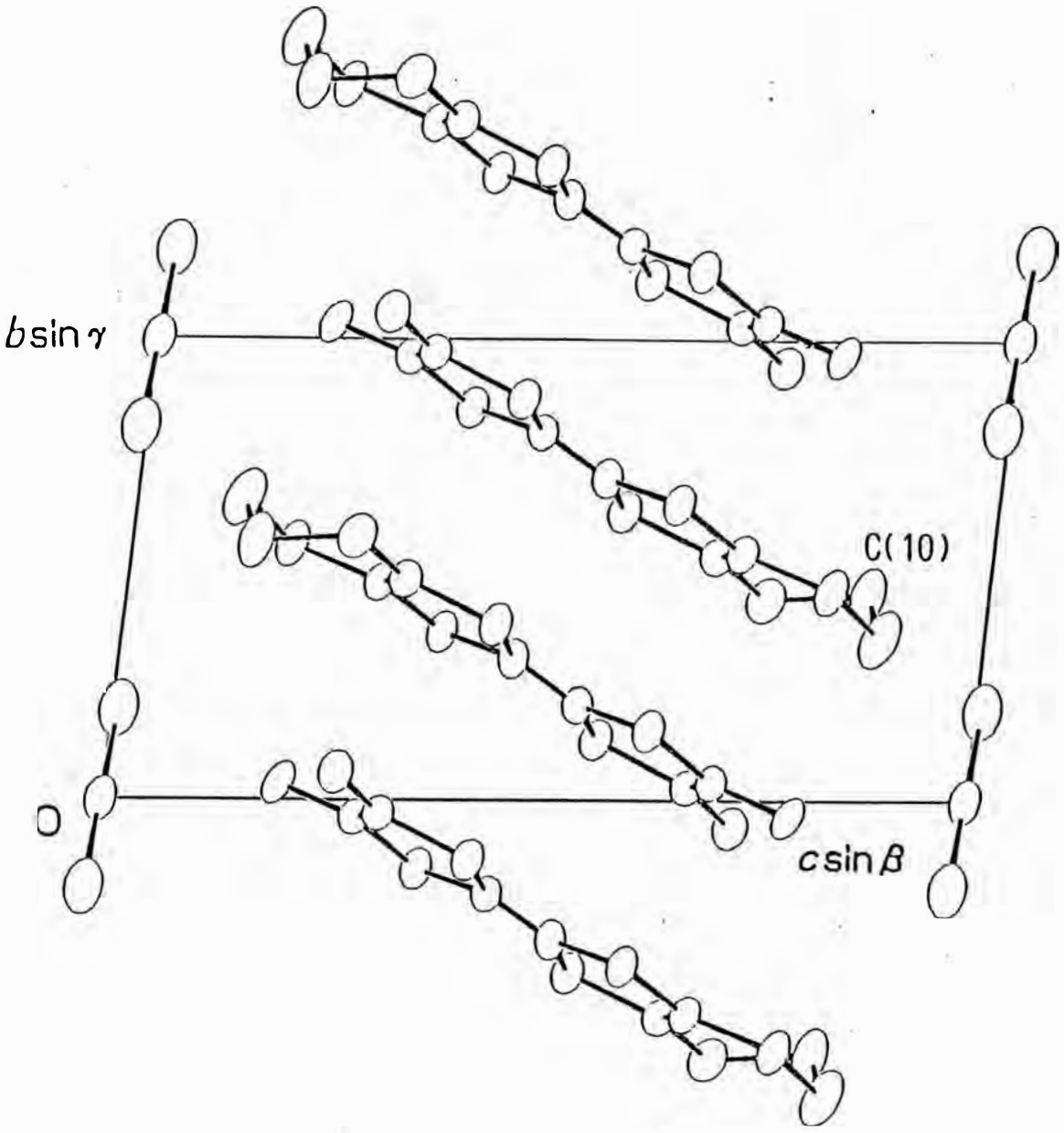

Fig. 3.2.11 Crystal structure of $(DIMET)_2AuCl_2$ viewed along the b-axis.

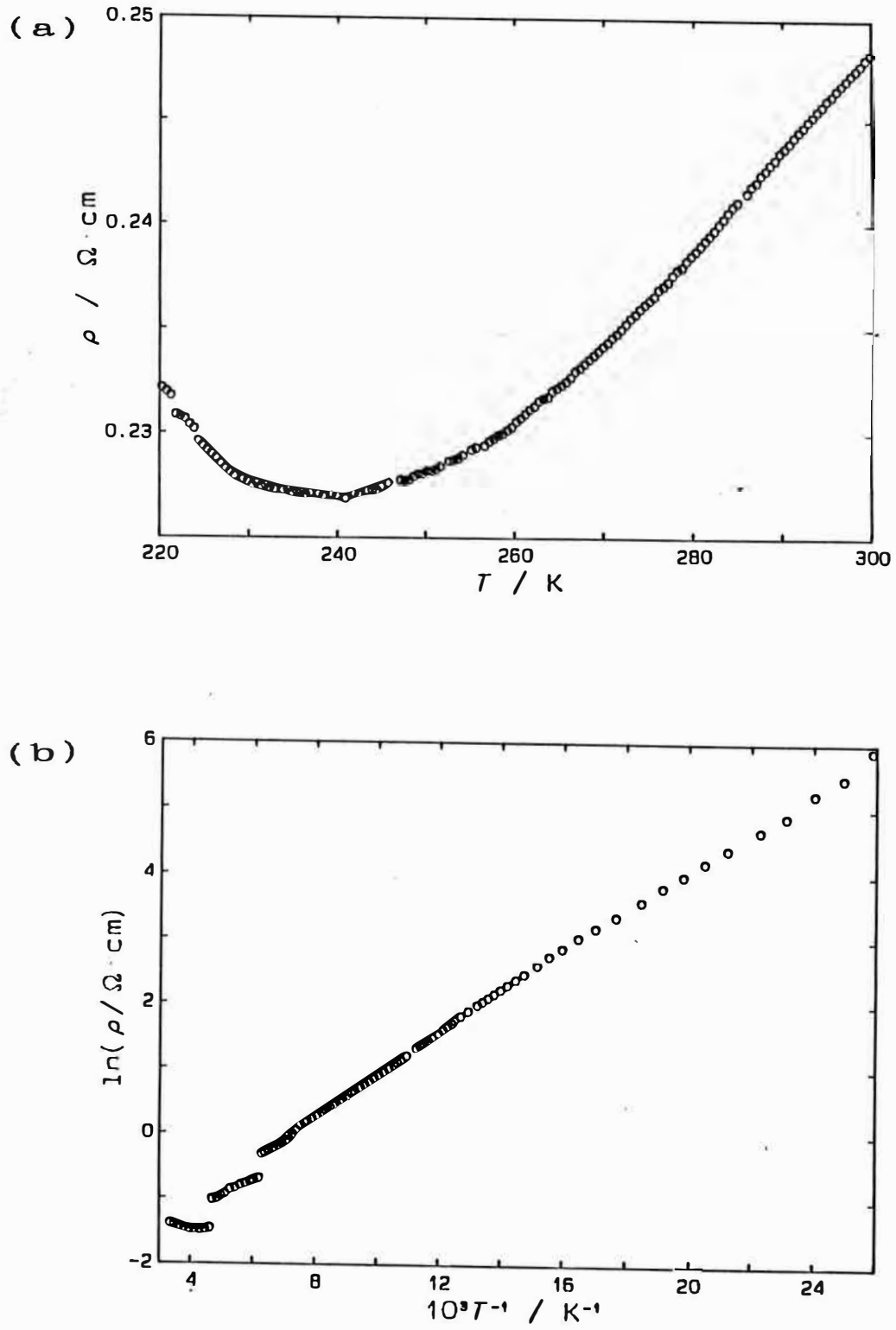

Fig. 3.2.12. (a) Resistivity of $(DIMET)_2AuCl_2$ in the high temperature region. (b) Arrhenius plot of resistivity of $(DIMET)_2AuCl_2$.

3.2.6 $(DIMET)_2AuI_2$

The crystal structure of $(DIMET)_2AuI_2$ is very similar to those of $(DIMET)_2I_3$ and $(DIMET)_2AuCl_2$.[18] The resistivity was measured along the most growing axis of the sample crystal. The temperature dependence of the resistivity of $(DIMET)_2AuI_2$ is similar to that of $(DIMET)_2AuCl_2$. The broad minimum of the resistivity was observed around 310 K as shown in Fig. 3.2.13(a). This temperature is higher than the corresponding temperature of $(DIMET)_2AuCl_2$. Below 310 K, the resistivity increases with decreasing temperature. The Arrhenius plot of the resistivity of $(DIMET)_2AuI_2$ is shown in Fig. 3.2.13(b). The slope in the Arrhenius plot seems to increase from RT down to about 100 K.

There is the similarity to $(DIMET)_2AuCl_2$ in the case of $(DIMET)_2AuI_2$. The temperature dependence of $(DIMET)_2AuI_2$ is semiconducting below RT, in spite of the similar crystal structure to $(DIMET)_2I_3$. This point is also discussed together with $(DIMET)_2AuCl_2$ in the later chapter.

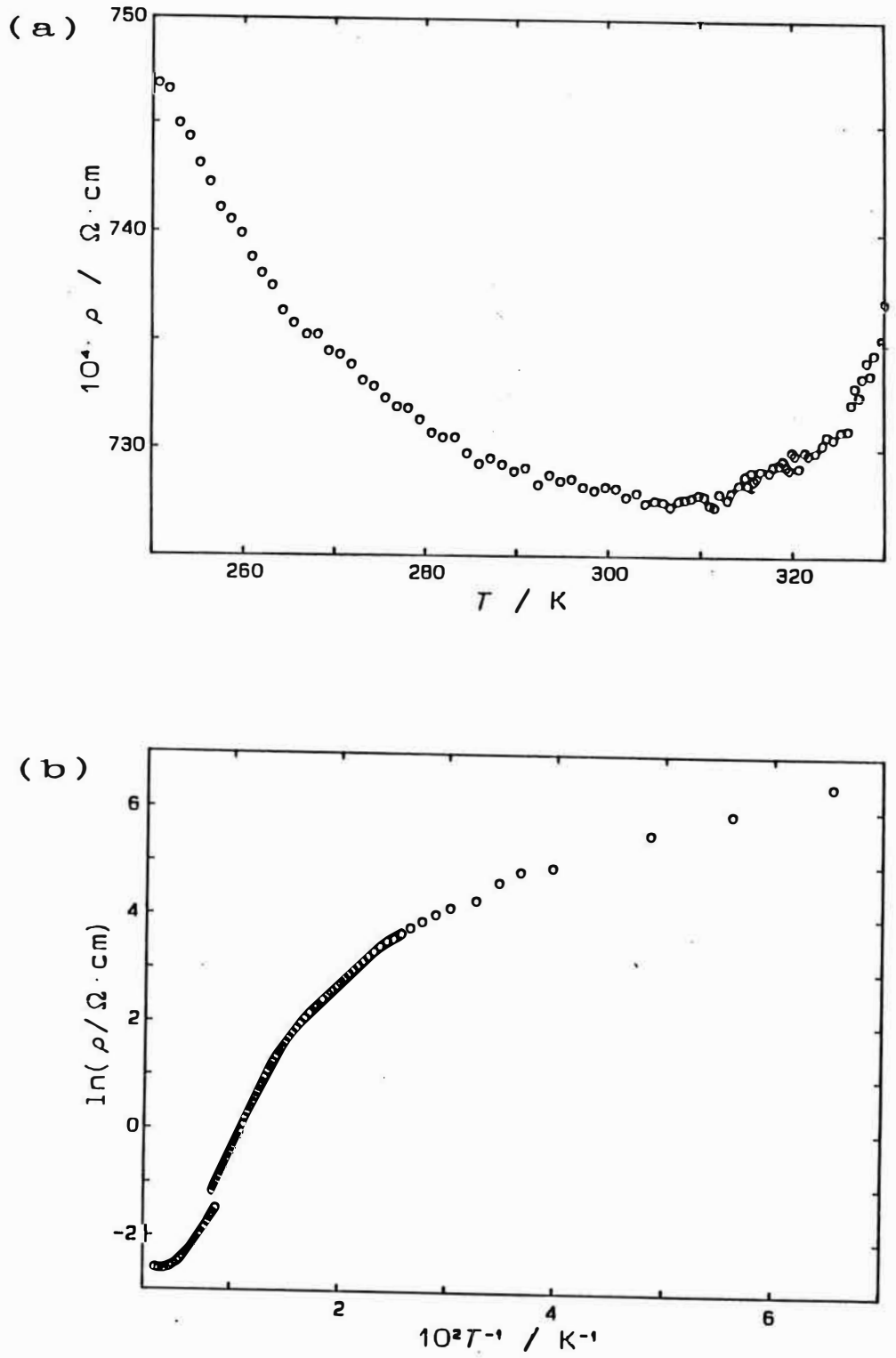

Fig. 3.2.13. (a) Resistivity of $(DIMET)_2AuI_2$ in the high temperature region. (b) Arrhnius plot of resistivity of $(DIMET)_2AuI_2$.

3.2.7 $(DIMET)_xBr_3$

The crystal structure of $(DIMET)_xBr_3$ has not been solved, due to the bad quality of the sample crystal. The composition of the donor and the anion is, therefore, unknown. However the measurement of the resistivity was possible. The temperature dependence of the resistivity is shown in Fig. 3.2.14 in the form of Arrhenius plot. $(DIMET)_xBr_3$ shows semiconducting behavior below RT, though the I_3 and IBr_2 salts of DIMET is metallic down to about 40 K. The activation energy E_a is about 80 meV above about 130 K. The magnitude of E_a is somewhat large in DIMET salts. On cooling E_a gradually decreases. This behavior is similar to $(DIMET)_2AuI_2$.

3.2.8 $(DIMET)_xAg(CN)_2$

The crystal structure of $(DIMET)_xAg(CN)_2$ has not been solved due to the bad quality of the sample crystal. The composition of the donor and the counter anion is also not known. The sample crystal is a very thin plate-like crystal. The plot of the resistivity versus $1/T$ is shown in Fig. 3.2.15. Due to the small thickness, the absolute magnitude of the resistivity calculated is the lower limit. The temperature dependence of the resistivity is semiconducting below RT. The activation energy above about 130 K is about 30 meV. On cooling E_a gradually decreases, though the reason for the decrease is unknown.

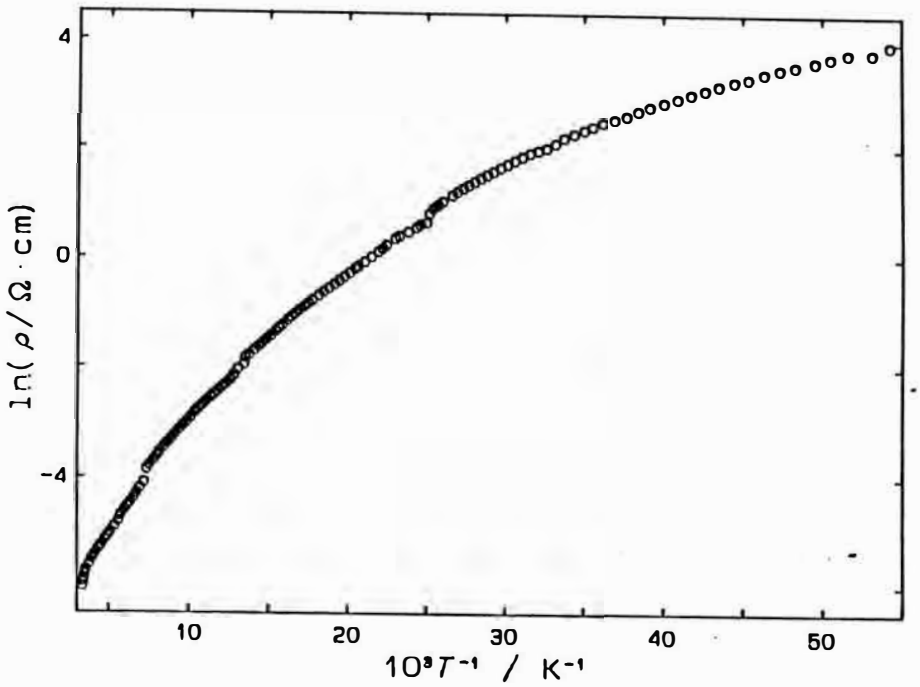

Fig. 3.2.14. Arrhuius plot of resistivity of $(DIMET)_xBr_3$.

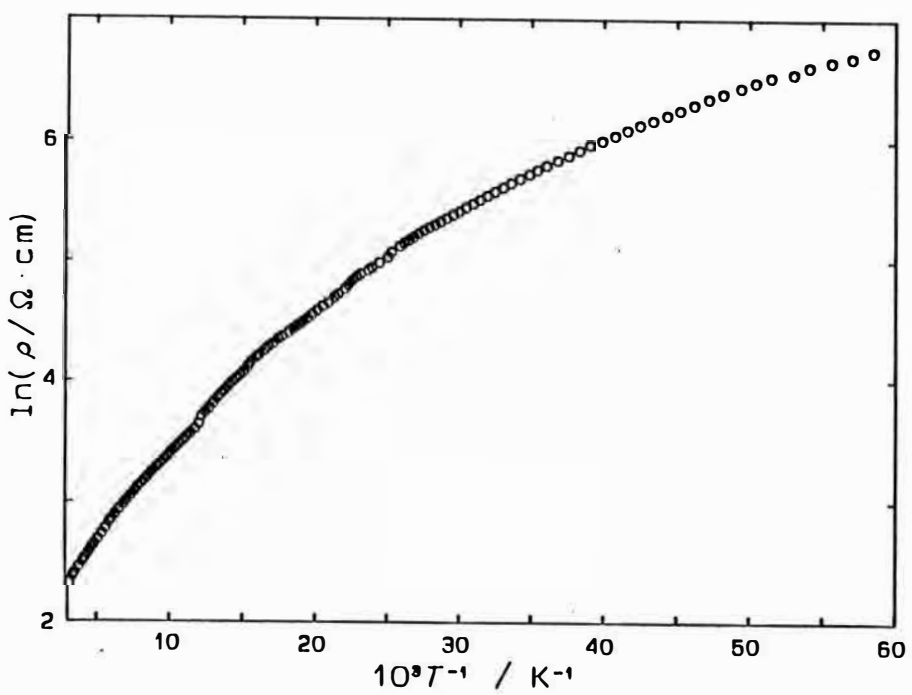

Fig. 3.2.15. Arrhuius plot of resistivity of $(DIMET)_xAg(CN)_2$.

3.3 Thermopower of DIMET salts

3.3.1 $(DIMET)_2I_3$

The thermopower of $(DIMET)_2I_3$ along the longest edges of the plate-like sample crystals was measured on a few samples. The typical size of the sample crystal was 0.68 x 0.18 x 0.08 mm^3. The crystal structure of $(DIMET)_2I_3$ has already been shown in Fig.3.2.1. The temperature dependence of the thermopower is shown for the one sample in Fig. 3.3.1(a). The same temperature dependence is seen in the results on the other samples. The temperature dependence of the thermopower is metallic down to about 40 K. This metallic behavior is consistent with the result of the resistivity measurement. In the metallic region, the sign of the thermopower is positive. It suggests the dominant carrier is hole above 40 K.

The interesting behavior of the thermopower of $(DIMET)_2I_3$ was observed in the metallic temperature region as seen in Fig. 3.3.1(b). The fitted line for the high temperature region of the thermopower is also shown in the figure. Below about 210 K, the thermopower deviates from the linearity and decreases rather rapidly with decreasing temperature, though the thermopower seems proportional to temperature above 210 K. The deviation of the thermopower from the linear temperature dependence is also observed for DMET salts, *e.g.* $(DMET)_2I_3$. For $(DMET)_2I_3$, the deviation perhaps corresponds to the increase in the dimensionality. The same thing can be said on $(DIMET)_2I_3$, because the anomaly in the temperature dependence of the anisotropy of the resistivity of $(DIMET)_2I_3$ has been also observed as mentioned in the subsection 3.2.1. The anomaly in the anisotropy suggests the apparent dimensionality of $(DIMET)_2I_3$ gradually decreases, namely becomes more 1D, with decreasing temperature down to about 210 K, and increases below 210 K (becomes more 2D). The region where the proportional temperature dependence of the thermopower was observed seems to correspond to the region where the dimensionality becomes more 1D with decreasing temperature.

Using Eq.(2.13) for 1D materials, one can estimate the transfer integral above 210 K. On estimating the transfer integral, it is

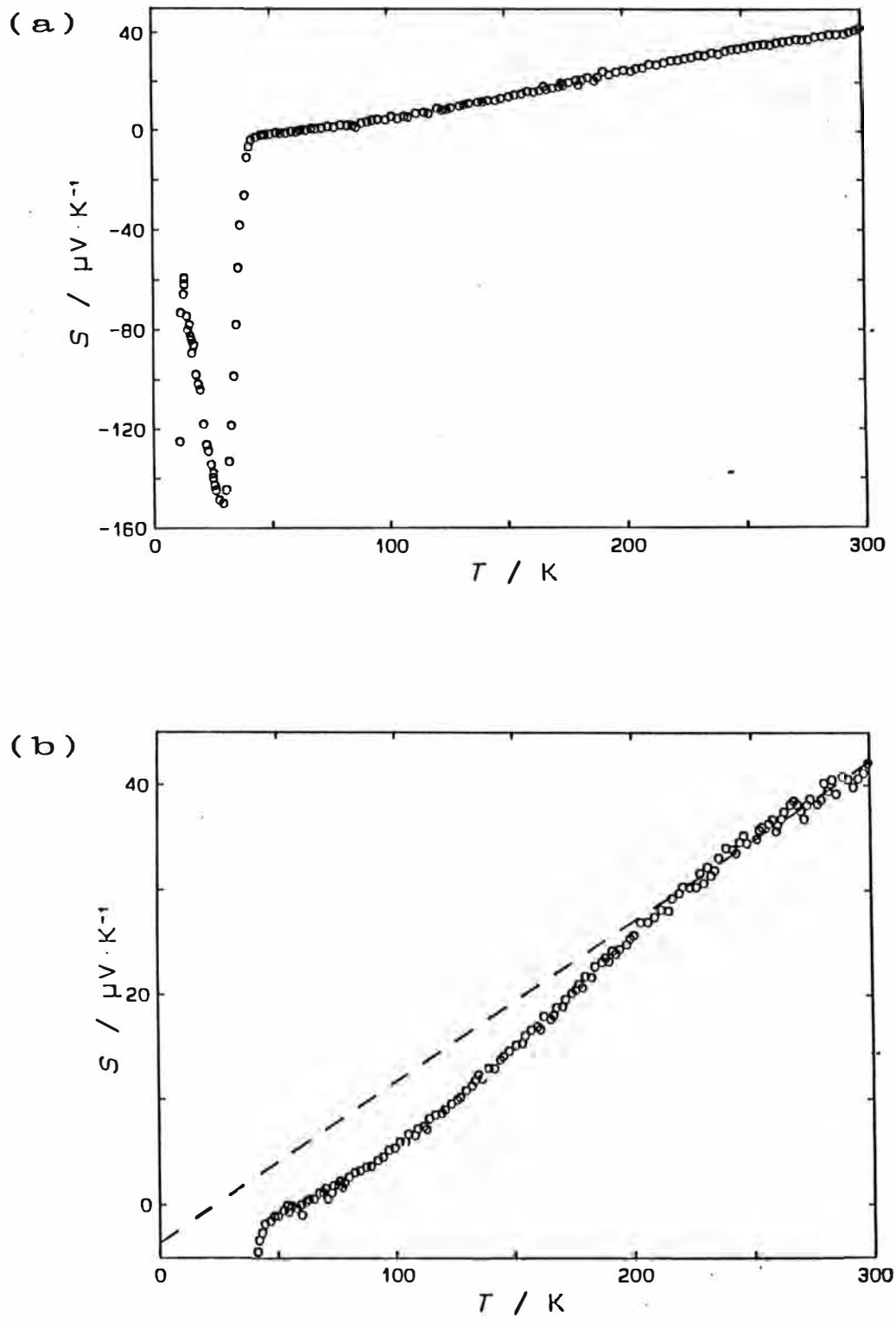

Fig. 3.3.1. (a) Thermopower of $(DIMET)_2I_3$. (b) A part of (a) with a fitted line to the high temperature region.

assumed that the "base" thermopower is contained in the observed thermopower of $(DIMET)_2I_3$ in Fig. 3.3.1(a) and (b). Namely the Eq.(3.1) in the subsection 3.1.3 in this chapter is again used. The reason for adopting the assumption is the minus sign of the thermopower between 40 and 65 K. Below about 65 K, the sign of the thermopower has already become minus, though the material is metallic above 40 K. Then it is considered that the transverse element of the thermopower tensor, assuming that it is independent of temperature as S_0 in Eq.(3.1), contributes to the observed thermopower of $(DIMET)_2I_3$.

$$S(T)=S_1(T)+S_0 \qquad (3.1)$$

Because the sample crystal of $(DIMET)_2I_3$ is small and plate-like, it is plausible that the transverse element of the thermopower tensor contributes to the magnitude of the measurement as a base. Here assuming that S_0 is -3 μV/K, the transfer integral of $(DIMET)_2I_3$ is estimated as 0.12 eV from the slope of the fitted line in Fig. 3.3.1(b). The transfer integral estimated for $(DMET)_2I_3$ with the result of the thermopower measurement is 0.19 eV. The transfer integral corresponds to the overlap integral of adjacent HOMO's of donors in a column for the DMET and DIMET salts. Because the two S atoms in the TMTTF side of the DIMET molecule are substituted with two Se atoms in the DMET molecule and the distance between adjacent molecules in the donor stack is not so different, it is expected that the overlap integral is larger in $(DMET)_2I_3$ than in $(DIMET)_2I_3$. The transfer integral of $(DIMET)_2I_3$ obtained from the thermopower measurement, using the result of the high temperature region, is consistent with the expectation. It seems likely that the dimensionality of $(DIMET)_2I_3$ is more 2D than that of $(DMET)_2I_3$.

Below 40 K, the thermopower rapidly decreases with decreasing temperature and changes its sign from plus to minus. After the rapid decrease, the thermopower turns to increase at about 30 K. Then the thermopower shows a sharp minimum, about -150 μV/K. The increase below 30 K is also rapid and continues down to about 13 K at least.

The rapid decrease at 40 K corresponds to the M-I transition observed in the resistivity. Furthermore, the temperature, 30 K, at which the minimum of the thermopower is observed, corresponds to the change in the slope seen in Fig. 3.2.3(b), the Arrhenius plot of the ambient pressure resistivity. These temperature dependence of the thermopower and the resistivity observed below T_{M-I} for $(DIMET)_2I_3$ is very similar to that observed for $(DMET)_2Au(CN)_2$ as described before, though an apparent precursor of the transition, observed above T_{M-I} in the thermopower of $(DMET)_2Au(CN)_2$, is not seen in the thermopower of $(DIMET)_2I_3$. This fact suggests the anomalies in the resistivity and thermopower in these results are corresponding phenomena to each other, and that if one of the anomalies like these results is observed for the resistivity or the thermopower, the another is probably observed.

The plot of the thermopower versus $1/T$ is shown in Fig. 3.3.2. In the semiconducting regime, the apparent linear dependence of S on $1/T$ was observed both above and below 30 K. The change in the sign of thermopower around 40 K suggests the dominant carrier changes from hole to electron. The changes of the slope of S around 30 K also suggests the relative contribution of electron to the electrical conduction becomes less below 30 K. The change in the ratio of the electron-to-hole mobility b in Eq.(2.14) determines the relative contribution of electron to hole. Under the assumption that b is almost constant between 30 K and 40 K, the estimated effective activation energy E_{eff} is obtained as about -20 meV in this temperature region, though the sign of the gradient is minus. Under the same assumption, E_{eff} is estimated as about 2.9 meV below 30 K. The activation energy E_a obtained from the resistivity measurement of $(DIMET)_2I_3$ is about 46 meV above 30 K and about 6.0 meV below 30 K respectively. By using the next relation,

$$E_{eff}=-E_a(b-1)/(b+1) \qquad (3.2)$$

b can be estimated for each temperature region. Then b=2.5 between 30 K and 40 K, and b=1.0 below 30 K respectively. These values

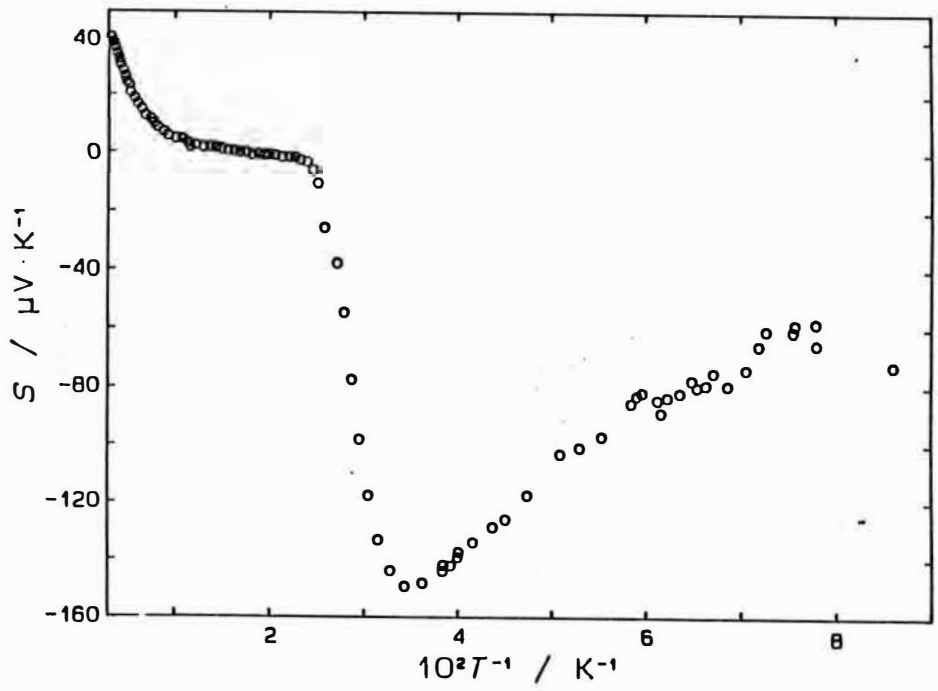

Fig. 3.3.2. Plot of thermopower of $(DIMET)_2I_3$ versus $1/T$.

suggest the change of the relative contribution of electron and hole to the conduction around 30 K. Though the reason why the change occurs is unknown, the characters of the anomaly in the semiconducting regime of $(DIMET)_2I_3$ is discussed with some other salts in the later chapter.

In addition, the characteristic behavior of the thermopower of $(DIMET)_2I_3$ was observed. Below about 13 K, the thermopower suddenly decreases with decreasing temperature after the rapid increase between 13 K and 30 K. Though, due to the large resistivity of the sample, the magnitude of the thermopower is somewhat scattered, the thermopower decreases down to about -5 mV/K around 8 K at least. It implies the possibility of the change of the band structure below about 13 K.

3.3.2 $(DIMET)_2IBr_2$

The crystal structure of $(DIMET)_2IBr_2$ is considered to be isostructural to that of $(DIMET)_2I_3$ as mentioned in the subsection 3.2.2. The sample used for the measurement of the thermopower is plate-like crystal whose size is 0.79 x 0.25 x 0.13 mm^3. The thermopower was measured along the longest edges of the sample crystal and the direction is considered as the most conducting direction. The temperature dependence of the thermopower of $(DIMET)_2IBr_2$ is shown in Fig. 3.3.3(a). The thermopower at 300 K is about 37 μV/K. It suggests the dominant carrier is hole. The thermopower decreases with decreasing temperature down to about 40 K. This metallic behavior is consistent with the result of the resistivity measurement.

In the metallic region, the deviation of the thermopower from the linearity was also observed for $(DIMET)_2IBr_2$ above about 250 K as shown in Fig. 3.3.3(b) with the fitted line. $(DIMET)_2IBr_2$ is probably more 1D above about 250 K than below 250 K. It is supported by the measurement of the anisotropy with the Montgomery method described in the subsection 3.2.2 in this chapter. The broad maximum of the apparent anisotropy was observed around 260 K. The "base" thermopower S_0, assumed to interpret the result of $(DIMET)_2I_3$, seems to be zero for $(DIMET)_2IBr_2$. From the slope of the fitted line, one obtains the transfer integral of $(DIMET)_2IBr_2$ as 0.14 eV. The magnitude of the transfer integral is not inconsistent with those of $(DIMET)_2I_3$ (0.12 eV) and $(DMET)_2I_3$ (0.19 eV).

Below about 40 K, the rapid decrease of the thermopower was observed for $(DIMET)_2IBr_2$. It corresponds to the M-I transition observed in the resistivity measurement. In addition, a sharp minimum of the thermopower is also observed at about 27 K as seen in Fig. 3.3.3(a). This minimum also corresponds to the anomaly in the resistivity around 30 K as mentioned in the subsection 3.2.2. Below the temperature of the minimum, the thermopower increases with decreasing temperature down to 13 K at least. These behavior from RT down to 13 K is very similar to that of $(DIMET)_2I_3$. The treatment of the data, as made on $(DIMET)_2I_3$, below T_{M-I} is also possible for

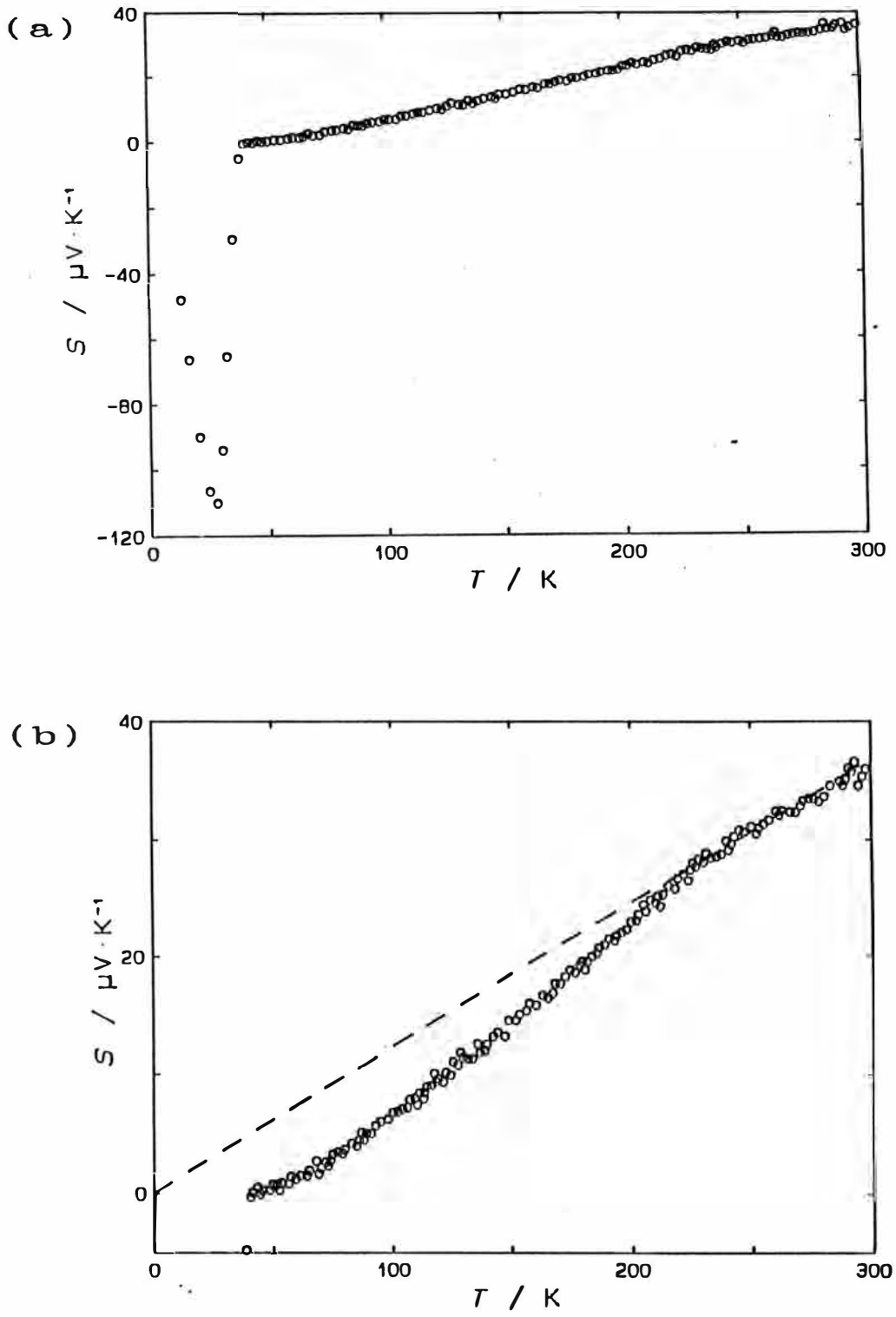

Fig. 3.3.3. (a) Thermopower of $(DIMET)_2IBr_2$. (b) A part of (a) with a fitted line to high temperature region.

$(DIMET)_2IBr_2$. In the semiconducting regime, the E_a estimated from the resistivity is 80 meV above about 30 K and 7.6 meV below about 30 K. E_{eff} estimated from the plot of the thermopower versus $1/T$ as shown in Fig. 3.3.4 is -12 meV above 30 K and 1.8 meV below 30 K respectively. Using Eq.(3.2), the ratio of electron-to-hole mobility b can be calculated for each temperature region. As a result, b is 1.4 above 30 K and 0.61 below 30 K respectively. The relative contribution of electron to the conduction in the semiconducting region seems to decrease below about 30 K. Comparing with b of $(DIMET)_2I_3$ (2.5 (T > 30 K), 1.0(T < 30 K)), the relative contribution of electron is less in $(DIMET)_2IBr_2$ than in $(DIMET)_2I_3$ in the semiconducting region. This difference is probably attributed to the difference of the band structures of these materials.

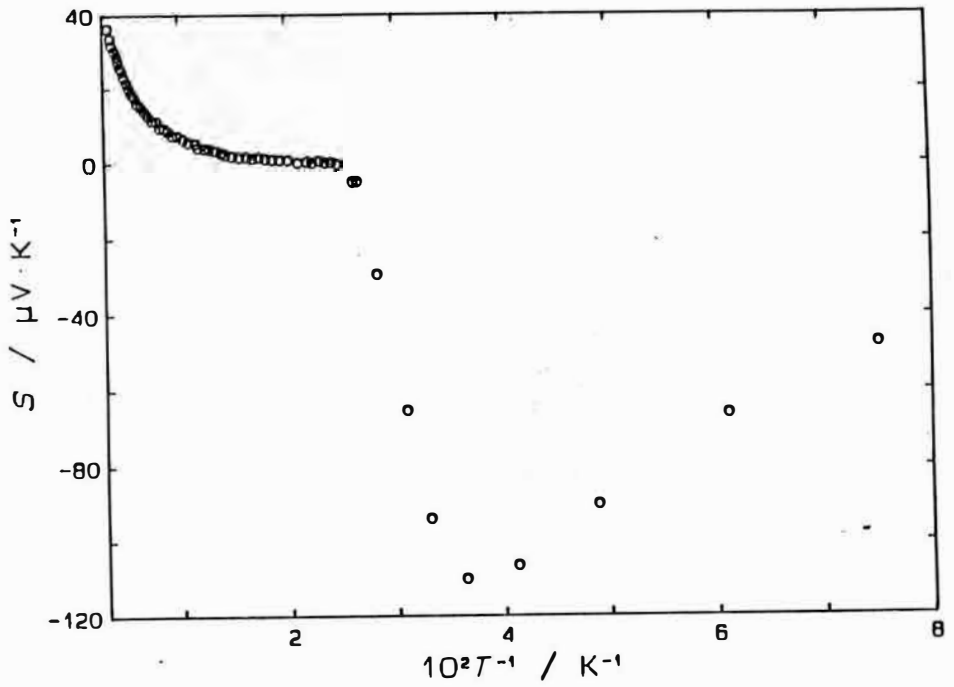

Fig. 3.3.4. Plot of thermopower of $(DIMET)_2IBr_2$ versus $1/T$.

3.3.3 $(DIMET)_xCu(NCS)_2$

The thermopower of $(DIMET)_xCu(NCS)_2$ was measured with the sample crystal whose size was 0.40 x 0.13 x 0.04 mm^3. The measurement was made along the most growing edge of the sample crystal. The temperature dependence of the thermopower of $(DIMET)_xCu(NCS)_2$ is shown in Fig. 3.3.5(a) for the whole temperature range. The temperature dependence of the thermopower of $(DIMET)_xCu(NCS)_2$ is very similar to those of $(DIMET)_2I_3$ and $(DIMET)_2IBr_2$. This result suggests the similar structure of these three salts, though the crystal structure of $(DIMET)_xCu(NCS)_2$ has not been resolved.

Above about 50 K, the metallic behavior was observed as shown in Fig. 3.3.5(b). The apparent linearity is also seen above about 210 K. The fitted line in Fig. 3.3.5(b) is drawn under the assumption that the "base" thermopower S_0 is -5 μV/K. From the slope of the fitted line, the transfer integral t is obtained as 0.15 eV. This is somewhat larger than the transfer integral of $(DIMET)_2I_3$ (t= 0.12 eV) and comparable with that of $(DIMET)_2IBr_2$ (t= 0.14 eV). The magnitude of t of $(DIMET)_xCu(NCS)_2$ is the largest in DIMET salts in this study. The larger t means the larger overlap of HOMO's of adjacent donors, namely the better packing of donor molecules.

Below about 50 K, the thermopower decreases with decreasing temperature as shown in Fig. 3.3.5(a). The rapid decrease corresponds to the M-I transition observed with the resistivity measurement as mentioned in the subsection 3.2.3. The change in the sign of the thermopower suggests the dominant carrier is electron in the semiconducting region. There is a minimum of the thermopower at about 28 K. The minimum is not so sharp as those of $(DIMET)_2I_3$ and $(DIMET)_2IBr_2$. Below 28 K, the thermopower increases with decreasing temperature down to 8 K at least. In Fig. 3.3.6, the plot of the thermopower versus $1/T$ is shown. For the apparent linear regions above and below about 28 K, applying Eq.(2.14) the effective activation energy is estimated. As a result, E_{eff} is -8.5 meV above 28 K and 0.8 meV below the temperature. The magnitude of E_{eff} of $(DIMET)_xCu(NCS)_2$ is smaller than those of $(DIMET)_2I_3$ and $(DIMET)_2IBr_2$. It is consistent with the weak temperature dependence of the

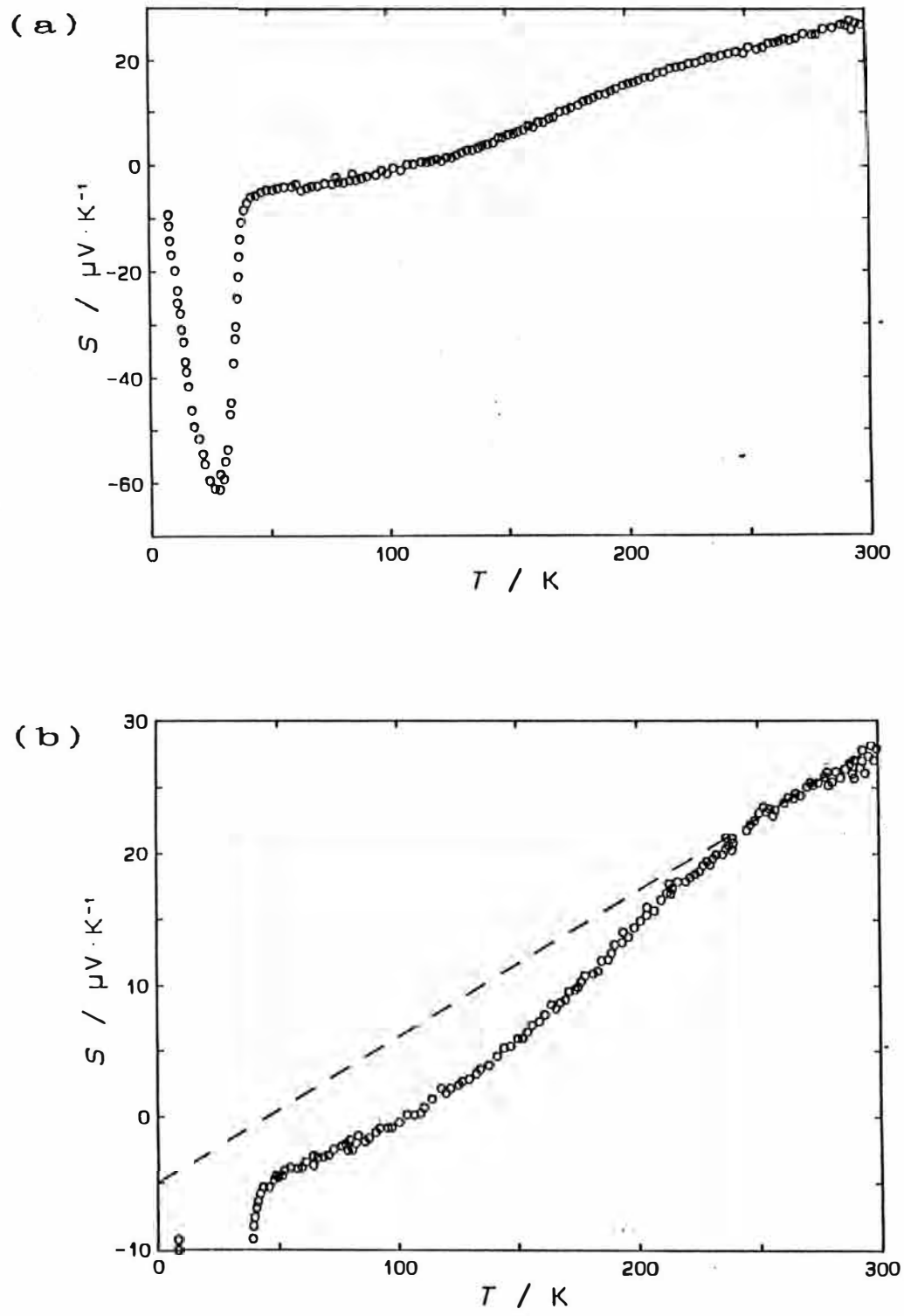

Fig. 3.3.5. (a) Thermopower of $(DIMET)_xCu(NCS)_2$. (b) A part of (a) with a fitted line to the high temperature region.

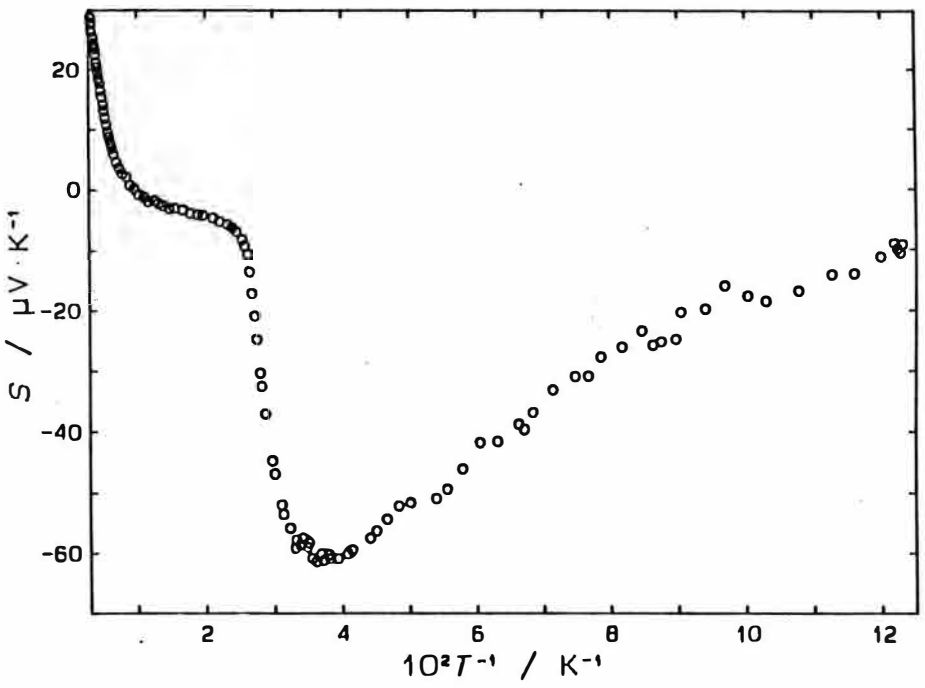

Fig. 3.3.6. Plot of thermopower of $(DIMET)_xCu(NCS)_2$ versus $1/T$.

resistivity of $(DIMET)_xCu(NCS)_2$. It is strange that the fine anomaly of the resistivity as observed for $(DIMET)_2I_3$, $(DIMET)_2IBr_2$ and $(DMET)_2Au(CN)_2$ below T_{M-I} are not recognized in spite of the minimum of the thermopower below T_{M-I}. This is the problem to be considered. Because the absence of the fine anomaly in the resistivity, the estimation of b as made for $(DIMET)_2I_3$ and $(DIMET)_2IBr_2$ is impossible for $(DIMET)_xCu(NCS)_2$.

3.3.4 $(DIMET)_2BF_4$

The crystal structure of $(DIMET)_2BF_4$ has already been shown in Fig. 3.2.9. To investigate the band structure along each donor-stack, the thermopower along the a-axis and the b-axis was measured. For along the a-axis, the result with one sample (symbolized as #1) was obtained. Two samples (#1 and #2) were used for the measurement along the b-axis to investigate about the sample dependence of the thermopower. The size of the sample crystal #1 was 0.41 x 0.34 x 0.15 mm^3, for example. The temperature dependence of the thermopower is shown in Fig. 3.3.7(a) and (b), Along the b-axis the sample dependence was observed above about 100 K. In contrast, below about 100 K, temperature dependence is similar to each other. From the appearance of the sample crystal #1, the quality of the sample is considered to be not so good. Contrary to this, the sample #2 has the good appearance. The result of the resistivity measurement described in the subsection 3.2.4 was obtained using #2. Through the resistivity measurement with #2, no resistance jump was observed. It suggests the sample #2 still retains good quality. The result along the b-axis using #2 is, therefore, considered to be more reliable and intrinsic than that using #1. If it is the case, the gradual change in the slope in the high temperature region above about 100 K is due to some defects for the sample #1. This situation should be in the result along the a-axis, though the result using #2 has not been obtained along the direction yet.

In contrast to the high temperature region, the sample dependence seems less in the middle region between 50 K and about 90 K. Between 50 K and 90 K, the linear temperature dependence of the thermopower is seen both along the a- and b-axes. The linear temperature dependence is probably intrinsic to $(DIMET)_2BF_4$. The M-I transition occurs about 40 K for $(DIMET)_2BF_4$. The linear temperature dependence of the thermopower above 40 K reflects, therefore, the metallic character of $(DIMET)_2BF_4$. The estimated transfer integral, from the slope of the thermopower versus temperature in the middle region, is 0.10 eV for the a-axis and 0.14 eV for the b-axis. The magnitude of the transfer integrals is

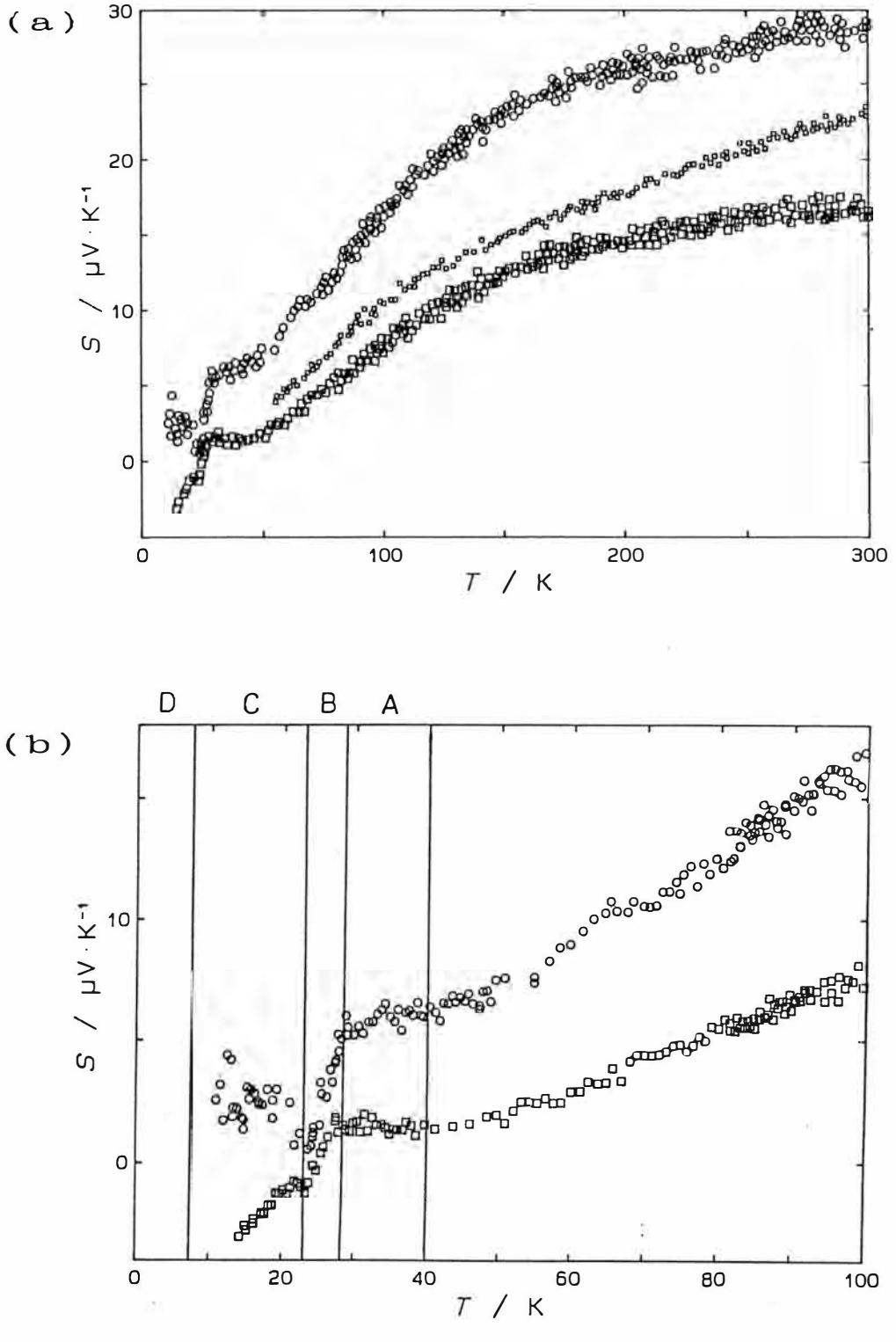

Fig. 3.3.7. (a) Thermopower of $(DIMET)_2BF_4$. (b) A part of (a) below 70 K. Circles are for the a-axis and squares are for the b-axis.

eV for the b-axis. The magnitude of the transfer integrals is comparable with those of other DIMET salts in this study. This fact supports the assumption that the linear parts are intrinsic for the material.

The crystal structures of $(DIMET)_2BF_4$ and $(DMET)_2BF_4$ have been shown in Figs. 3.2.9 and 3.1.4. Although these two BF_4 salts are isostructural to each other, the magnitude of the intra- and intercolumn interaction in one salt is probably different from that in the other. The solid lines in these figures show the shorter contacts between heteroatoms than the sum of corresponding van der Waals radii. (The van der Waals radius of S is assumed as 1.85 Å and that of Se 2.00 Å.[23]) $(DMET)_2BF_4$ has four kinds of short contact in the a-axis column and three kinds in the b-axis column as shown in Fig. 3.1.4. In contrast to this, in the case of $(DIMET)_2BF_4$, there are only two kinds of short contacts in the a-axis column and no short contacts in the b-axis column. Hence, the smaller magnitude of t's of $(DIMET)_2BF_4$ than that of $(DMET)_2BF_4$ is also reasonable in the viewpoint of the crystal structures.

However, the discussion is based on the assumption that the electron density ρ is 1.5 for each column of $(DIMET)_2BF_4$, although ρ=1.45 for the a-axis column and ρ=1.55 for the b-axis column in $(DMET)_2BF_4$ as described in the subsection 3.1.3. Since the optical measurements to determine the electron density of each column of $(DIMET)_2BF_4$ have not been carried out yet, more detailed discussion about the relation among the bandwidths, the electron densities and the crystal structures of these double-stack type of salts can not be made.

Below T_{M-I}, about 40 K, the temperature dependence of the thermopower of $(DIMET)_2BF_4$ shows somewhat complicated behavior for the both directions as seen in Fig. 3.3.7(b). From the temperature dependence of the resistivity, the observed semiconducting region is divided into the four small region A to D as described in the subsection 3.2.4. The division into the four temperature region on the plot of the thermopower in Fig. 3.3.7(b) is based on the division made on the resistivity. The obvious change in the slope of S vs.

are almost constant both along the a-axis and the b-axis in $(DIMET)_2BF_4$ (3.51 and 3.52 Å in the a-axis, 3.56 and 3.59 Å in the b-axis), the short contacts only seen in the dimer in the column along the a-axis possibly decrease the intracolumn interaction on the whole because of the influence of the stronger dimerization. If the explanation is valid, the result of the thermopower suggests that the equal alignment of donor molecules increases the bandwidth, although there is no short contact in the stack.

Below T_{M-I}, about 40 K, the temperature dependence of the thermopower of $(DIMET)_2BF_4$ shows somewhat complicated behavior for the both directions as seen in Fig. 3.3.7(b). From the temperature dependence of the resistivity, the observed semiconducting region is divided into the four small region A to D as described in the subsection 3.2.4. The division into the four temperature region on the plot of the thermopower in Fig. 3.3.7(b) is based on the division made on the resistivity. The obvious change in the slope of S vs. T can be seen at the boundaries of the adjacent temperature regions as seen in Fig. 3.3.7(b). Below 13 K, the thermopower could not be measured due to the large resistance of the sample (#1). Below about 8 K, the thermopower along the a-axis increases very rapidly with decreasing temperature. Though, due to the large resistance of the sample, the data points are scattered, the thermopower possibly reaches about 500 μV/K below 8 K at least. The complicated temperature dependence of the thermopower like this result has also been observed for $(DMET)_2BF_4$ as mentioned in the subsection 3.1.3. The complicated behavior has also found for $(DMET)_2ClO_4$ in the resistivity measurement. These three salts have the two types of donor-stacking almost perpendicular to each other. All these results seem to suggest that the ground state in the low temperature semiconducting region changes one after another in these salts.

3.3.5 $(DIMET)_2AuCl_2$

The crystal structure of $(DIMET)_2AuCl_2$ has already been shown in Fig. 3.2.11. That is isostructural to $(DIMET)_2I_3$. In contrast the temperature dependence of the resistivity is very different from that of $(DIMET)_2I_3$ described in the subsection 3.2.5. The apparent M-I transition occurs at around 240 K on $(DIMET)_2AuCl_2$ and the apparent T_{M-I} is too high as compared with T_{M-I} of $(DIMET)_2I_3$, about 40 K. To investigate whether the change in the band structure occurs at around 240 K, the thermopower measurement was made on $(DIMET)_2AuCl_2$. The thermopower of two different sample crystals was measured, then the sample dependence was observed in the middle temperature region from about 70 K to 200 K as shown in Fig. 3.3.8. The typical size of the sample crystal was 0.53 x 0.28 x 0.08 mm^3. The appearance of the crystals is not so good. The spoiling of the sample is possibly responsible for the sample dependence. Comparing with the temperature dependence of the thermopower of $(DIMET)_2AuI_2$ whose crystal structure and temperature dependence of the resistivity is very similar to those of $(DIMET)_2AuCl_2$, the temperature dependence of the thermopower obtained using the sample crystal #2 seems to be more intrinsic for $(DIMET)_2AuCl_2$. The additional positive contribution is perhaps due to some defects which supplies hole as carrier.

The temperature dependence of the thermopower of $(DIMET)_2AuCl_2$ is, therefore, discussed based on the result of #2. The thermopower gradually decreases from about 38 μV/K at 300 K to about 20 μV/K around 80 K with decreasing temperature. The positive sign of the thermopower suggests the dominant carrier is hole. Around 240 K at which the minimum of the resistivity was observed, no anomaly is seen in the thermopower. The band structure is, therefore, considered not to change around 240 K. Namely the minimum of the resistivity is not the result of the change in the band structure.

The gradual but non-proportional temperature dependence of the thermopower is possibly explained with the large correlation of electrons as same as $(DMET)_2ReO_4$ mentioned in the subsection 3.1.4. The abrupt decrease at about 70 K corresponds to the change in the slope of the Arrhenius plot of the resistivity in Fig.3.2.12(b).

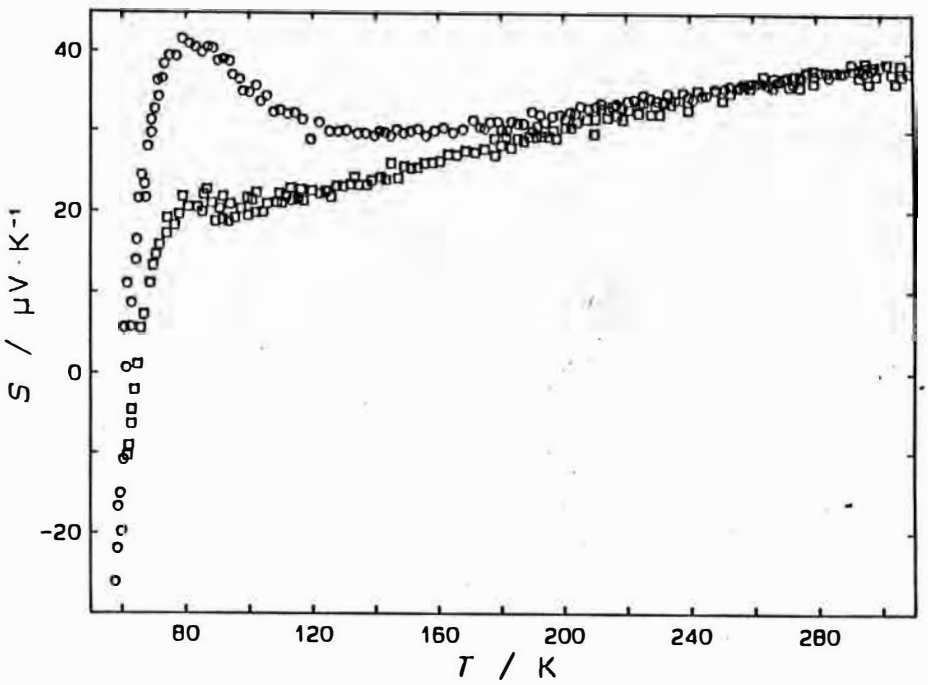

Fig. 3.3.8. Thermopower of $(DIMET)_2AuCl_2$. Circles are for #1 and squares are for #2.

Below about 70 K, the thermopower changes its sign from plus to minus, namely the dominant carrier becomes electron. The change implies a certain change occurs in the band structure of $(DIMET)_2AuCl_2$ around 70 K.

3.3.6 $(DIMET)_2AuI_2$

The crystal structure of $(DIMET)_2AuI_2$ is isostructural to $(DIMET)_2AuCl_2$ as mentioned previously. $(DIMET)_2AuI_2$ have a minimum of the resistivity around 310 K as mentioned in the subsection 3.2.6. The thermopower of the needle-like crystal along the most growing direction was measured. The temperature dependence of the thermopower of $(DIMET)_2AuI_2$ is shown in Fig.3.3.9. The thermopower gradually decreases from about 46 μV/K at 300 K to about 20 μV/k at about 120 K with decreasing temperature. The positive sign suggests that the dominant carrier is hole in this temperature region. Below 120 K, the thermopower rapidly decreases with decreasing temperature and changes its sign from plus to minus at about 100 K. The temperature seems to corresponds to the maximum of the gradient of the Arrhenius plot of the resistivity as shown in Fig. 3.3.10. It can be seen that the gradient decreases below about 100 K, though the data points are scattered. The apparent broad M-I transition observed around 310 K with the resistivity measurement for $(DIMET)_2AuI_2$ is considered not to correspond to the change in the band structure, though there is no data of the thermopower at 310 K for AuI_2 salt. The abrupt decrease at about 100 K corresponds to the change of the band structure, if the change is present.

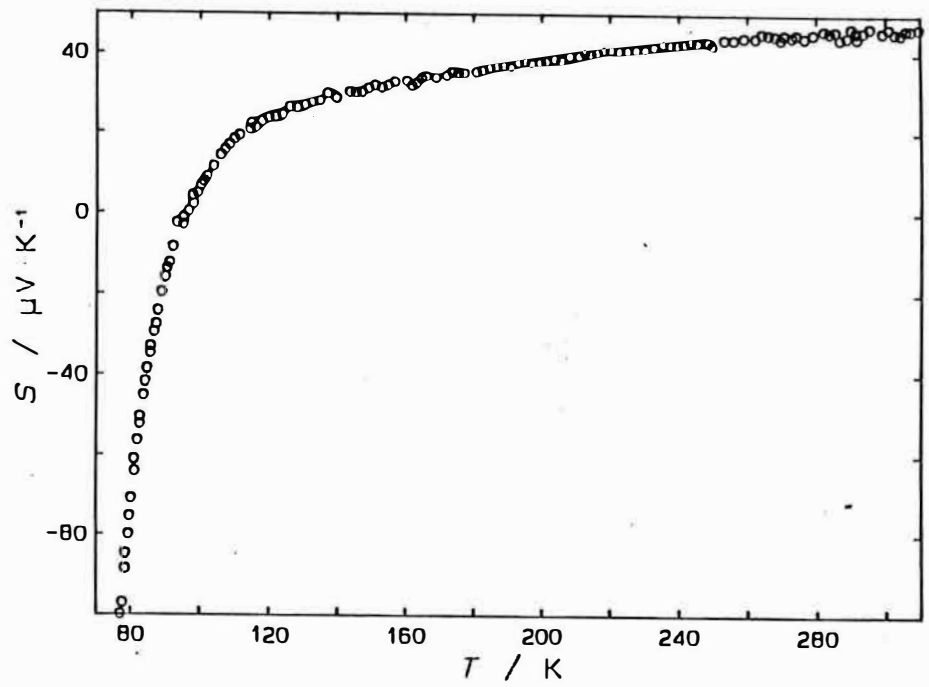

Fig. 3.3.9. Thermopower of $(DIMET)_2AuI_2$.

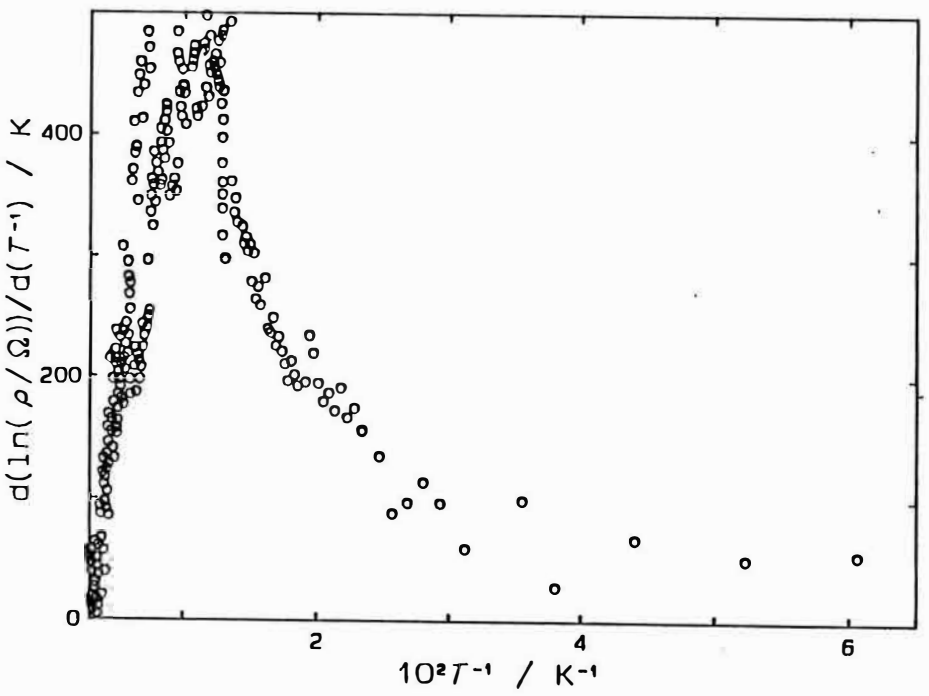

Fig. 3.3.10. Plot of slope in the Ahrrenius plot of resistivity of $(DIMET)_2AuI_2$ versus $1/T$.

References to Chapter 3

1 K. Kikuchi, K. Saito, I. Ikemoto, K. Murata, T. Ishiguro and K. Kobayashi, Synth. Metals, 27, B269(1988).

2 Y. Ishikawa, M. Sc. Thesis, Department of Chemistry, Faculty of Sc., Tokyo Metropolitan University(1989).

3 K. Kikuchi, Y. Ishikawa, K. Saito, I. Ikemoto, and K. Kobayashi, Synth. Metals, 27, B391(1988).

4 I. Ikemoto, K. Kikuchi, K. Saito, K. Kanoda, T. Takahashi, K. Murata, K. Kobayashi, Mol. Cryst. Liq. Cryst., 181, 185(1990).

5 K. Mortensene, J. M. Williams and H. H. Wang, Solid State Commun. 56, 105(1985).

6 K. Neriishi, M. Sc. Thesis, Department of Chemistry, Faculty of Sc., Tokyo Metropolitan University(1992).

7 K. Kanoda, T. Takahashi, K. Kikuchi, K. Saito, I. Ikemoto and K. Kobayashi, Synth. Metals, 27, B385(1988).

8 H. J. Pedersen, J. C. Scott, K. Bechgaad, Phys. Rev., B24, 5014(1981).

9 M. Ishibashi, M. Sc. Thesis, Department of Chemistry, Faculty of Sc., Tokyo Metropolitan University(1991).

10 K. Saito, Y. Ishikawa, M. Ishibashi, K. Kikuchi, K. Kobayashi and I. Ikemoto, Bull. Chem. Soc. Jpn., 63, 1865(1990).

11 K. Murata, K. Kikuchi, T. Takahashi, K. Kobayashi, Y. Honda, K. Saito, K. Kanoda, T. Tokiwa, H. Anzai, T. Ishiguro and I. Ikemoto, J. Mol. Electron., 4, 173(1988).

12 K. Kamio, M. Sc. Thesis, Department of Chemistry, Faculty of Sc., Tokyo Metropolitan University(1989).

13 K. Saito, H. Kamio, Y. Honda, K. Kikuchi, K. Kobayashi and I. Ikemoto, J. Phys. Soc. Jpn., 58, 4093(1989).

14 K. Kanoda, T. Takahashi, T. Tokiwa, K. Kikuchi, K. Saito, I. Ikemoto and K. Kobayashi, Phys. Rev. B38, 39(1988).

15 K. Murata, K. Kikuchi, Y. Honda, T. Komazaki, K. Saito, K. Kobayashi and I. Ikemoto, Springer Proceedings in

Physics(Heidelberg), 51, 234(1990).
16 M. Ishibashi, K. Murata, K. Kikuchi, K. Saito, I. Ikemoto and K. Kobayashi, Synth. Metals, 42, 2167(1991).
17 T. Mori and H. Inokuchi, J. Phys. Soc. Jpn. 57, 3674(1988).
18 H. Itoh, B. Sc. Thesis, Department of Chemistry, Faculty of Sc., Tokyo Metropolitan University(1991).
19 C. S. Jacobsen, K. Mortensen, M. Weger, K. Bechgaad, Solid State Commun., 38, 423(1981).
20 K. Murata, H. Anzai, G. Saito, K. Kajimura, T. Ishiguro, J. Phys. Soc. Jpn., 50, 3529(1981).
21 R. L. Greene, P. Haen, S. Z. Huang, E. M. Engler, M. -Y. Choi, P. M. Chaikin, Mol. Cryst. Liq. Cryst., 79, 183(1982).
22 H. Endres, R. Heid, H. J. Keller, I. Heinen and D. Schweitzer, Acta Cryst., C43, 115(1987).
23 L. Pauling, The Nature of the Chemical Bond, Cornell University press (Ithaca, 1960).

Chapter 4. Discussion

4.1 Dimensionality and superconductivity

It has been claimed that the dimensionality of the DMET salts in Group 4 is higher than those of Groups 1, 2, and 3 since the classification was made.[1] It is apparently strange that the insulating state has been found in the salts of Group 3 and not been found in those of Group 4, though the salts of the both groups have linear anions and isostructures. In this section, the dimensionality of the DMET salts of Groups 3 and 4 is discussed.

In Fig. 4.1, intercolumn and intracolumn short contacts between heteroatoms seen in isostructural DMET salts of Groups 3 and 4 at RT is represented as a solid line.[2-4] Each kind of short contact is symbolized as p, q, r and so on. The distances of these short contacts and the angles from the stacking axis to the normal to the molecular plane at RT are summarized in Table 4.1.

If short contacts exist between two molecules, it is considered that there is qualitatively strong interaction between the molecules for a certain extent. Larger number of short contacts mean stronger interaction. Furthermore, a shorter contact also means stronger interaction. In Table 4.1, the averages of the distances of the intracolumn and intercolumn short contacts and their ratio are also summarized as a criterion for the inter- and intracolumn interaction. Comparing the distances of the intracolumn contacts between Group 3 and Group 4 salts, no obvious difference is found. However, the distances of the intercolumn contacts of Group 4 seems shorter than those of Group 3. It suggests the stronger intercolumn interaction in Group 4 than those in Group 3. Because no obvious difference of the intracolumn interaction between Groups 3 and 4, the apparent difference of the intercolumn interaction also suggests the higher dimensionality in Group 4.

In Table 4.2, the transfer integrals obtained from the thermopower measurement is summarized for all metallic DMET salts studied. BF_4 salt is classified into Group 2, and $Au(CN)_2$ salt into

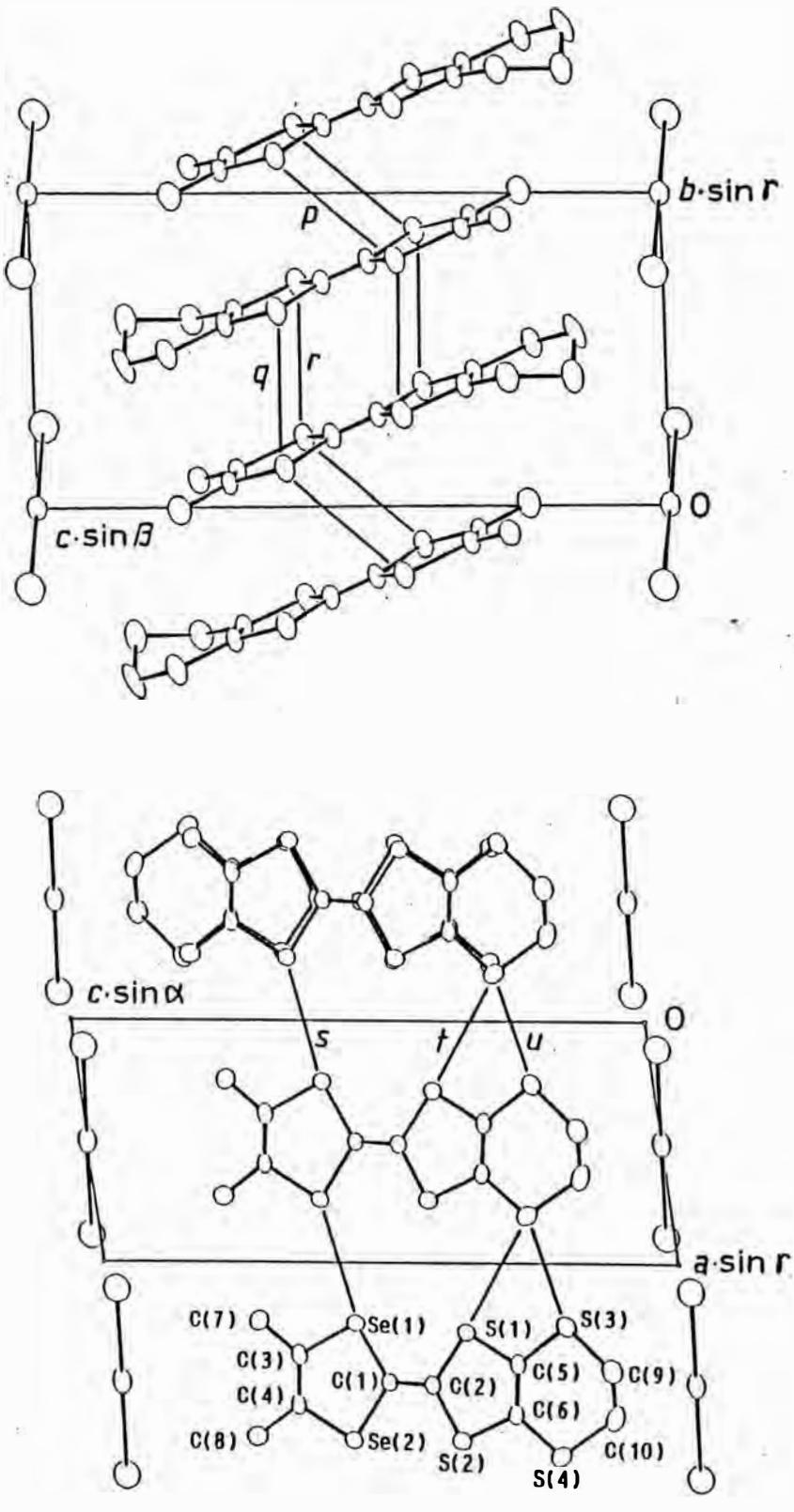

Fig. 4.1. Short contacts seen in the crystal structures of DMET salts in Groups 3 and 4.

Table 4.1. Distances of short contacts and tilted angles of DMET molecules in Fig. 4.1.

Group	anion	distance / Å						tilted angle / deg.
		intracolumn			intercolumn			
		p	*q*	*r*	*s*	*t*	*u*	
			((*p*+*q*+*r*)/3)			((*s*+*t*+*u*)/3)		
3	$Au(CN)_2$	3.983	3.819	3.837	3.884	3.672	3.580	22.2
			(3.880)			(3.712)		
	AuI_2	3.965	3.819	3.825	3.832	3.611	3.552	22.4
			(3.870)			(3.665)		
4	I_3	3.957	3.845	3.837	3.782	3.604	3.504	23.4
			(3.880)			(3.630)		
	IBr_2	3.949	3.837	3.841	3.774	3.589	3.494	23.2
			(3.876)			(3.619)		
	$AuBr_2$	3.964	3.810	3.822	3.824	3.608	3.534	22.6
			(3.865)			(3.655)		
	I_2Br	3.952	3.832	3.827	3.783	3.595	3.501	23.2
			(3.870)			(3.626)		

Table 4.2. Transfer integral t of each DMET salt from thermopower.

Group	anion	t / eV
2	BF_4	0.19 (a-axis)
		0.22 (b-axis)
3	$Au(CN)_2$	0.25 (T>180 K)
		0.21 (T<180 K)
4	I_3	0.19
	SCN	0.15

Group 3, I_3 and SCN salts into Group 4. The transfer integral t along the stacking direction reflects the magnitude of the intracolumn interaction. Below RT, t of $Au(CN)_2$ salt (0.25 eV) is larger than t's of I_3 and SCN salts (0.19 and 0.15 eV). Although these three salts are isostructural, the distinct difference of t are found. The larger t of $Au(CN)_2$ salt suggests stronger intracolumn interaction in this salt than that in I_3 and SCN salts. From the comparison of crystal structures above, the intercolumn interaction in Group 4 is considered to be stronger than that in Group 3. The smaller t's of Group 4 give the additional evidence of the higher dimensionality of Group 4 than Group 3. The result is consistent with the result from the reflectance spectra.[5,6] The lower dimensionality (stronger 1D character) is considered to be responsible for the existence of the insulating state in Group 3. In contrast, the higher dimensionality in Group 4 is advantageous to the superconductivity and the absence of the insulating state.

Because no obvious difference of the distances of the intracolumn short contacts are seen between Groups 3 and 4, the distinct difference of t's between the groups is apparently strange. However the tilted angle in Group 4 is somewhat larger than that in Group 3 as seen in Table 4.1. If the tilted angle becomes large, the overlap of HOMO's of facing molecules decreases. The slightly larger tilted angeles are probably responsible for the decrease in t's in Group 4.

One of the reasons of the higher dimensionality in DMET salts is attributed to the rather large side-by-side (intercolumn) interaction. Two of the three intercolumn short contacts are related to the ethylenedithio unit in the BEDT-TTF side of DMET molecule. A part of the higher dimensionality is, therefore, the reflection of the BEDT-TTF like character of DMET.

4.2 Dimensionality and metallic character

Although most of the DIMET salts previously reported are semiconducting,[7-9] some of the new DIMET salts, I_3, IBr_2, $Cu(NCS)_2$ and BF_4 salts, in this study show the metallic behavior down to about 40 K. The corresponding DMET salts, namely $(DMET)_2BF_4$, $(DMET)_2I_3$ and $(DMET)_2IBr_2$ are metallic down to low temperature. Although $(DMET)_2BF_4$ is semiconducting below about 35 K, $(DMET)_2I_3$ and $(DMET)_2IBr_2$ show the superconductivity below 0.47 and 0.58 K at ambient pressure. BF_4 salts of DMET and DIMET are isostructural as described in the previous chapter. Though the crystal structures of IBr_2 and $Cu(NCS)_2$ salts of DIMET has not been solved, $(DIMET)_2I_3$ is also isostructural to $(DMET)_2I_3$. The appearance of metallic behavior in these DIMET salts is reasonable when one consider the properties of the corresponding DMET salts. However other DIMET salts in this study do not show metallic behavior below RT, though each $(DIMET)_2AuCl_2$ and $(DIMET)_2AuI_2$ has the slight minimum of the resistivity around RT. $(DIMET)_2AuCl_2$ and $(DIMET)_2AuI_2$ are also isostructural to $(DMET)_2AuI_2$ and also $(DIMET)_2I_3$. ($(DMET)_2AuCl_2$ is not isostructural to these four salts, though this salt has a 1D column.) $(DMET)_2AuI_2$ is metallic down to 20 K at ambient pressure and shows superconductivity at 0.55 K under pressure of 5.0 kbar. In contrast to I_3 salts of DMET and DIMET, the distinct difference of the electrical properties between $(DMET)_2AuI_2$ and the corresponding DIMET salts is very strange.

For I_3, $AuCl_2$ and AuI_2 salts of DIMET, the inter- and intracolumn distances between sulfur atoms corresponding to the short contacts in DMET salts in Fig. 4.1 are summarized in Table 4.3 and also *t*'s of metallic DIMET salts in Table 4.4. In fact, there exist only two kinds of short S-S contact in these DIMET salts. The both short contacts are intercolumn contacts related to the ethylenedithio unit of DIMET molecule and they correspond to the contacts symbolized as t and u in Fig. 4.1. It is important that no short contact exists in the stack. The smaller *t*'s of DIMET salts than those of DMET salts reflect the absence of short contacts. As shown in Table 4.3, the intracolumn distances in I_3 salt seem larger than those in $AuCl_2$

Table 4.3. Distances between sulfur atoms of adjacent DIMET molecules in some DIMET salts. See Fig. 4.1.

anion	distance / Å					
	intracolumn			intercolumn		
	p	*q*	*r*	*s*	*t*	*u*
		((p+q+r)/3)			((s+t+u)/3)	
I_3	3.943	3.793	3.807	3.974	3.548	3.480
		(3.848)			(3.667)	
$AuCl_2$	3.901	3.780	3.809	4.026	3.589	3.539
		(3.830)			(3.718)	
AuI_2	3.916	3.763	3.781	4.000	3.548	3.514
		(3.820)			(3.687)	

Table 4.4. Transfer integral t of each DIMET salt from thermopower.

anion	t / eV
BF_4	0.10 (a-axis)
	0.14 (b-axis)
I_3	0.12
IBr_2	0.14
$Cu(NCS)_2$	0.15

and AuI_2 salts. Furthermore, the intercolumn distances in I_3 salt is shorter than those in $AuCl_2$ and AuI_2 salts. Considering in the same manner in the previous section, the dimensionality in I_3 salt is probably higher than that in $AuCl_2$ and AuI_2 salts. The apparently higher dimensionality in I_3 salt is, therefore, considered to be responsible for the metallic character of this salt. Opposite to I_3 salt, the lower dimensionality (stronger 1D character) in $AuCl_2$ and AuI_2 salt is considered to be responsible for the semiconducting behavior.

In radical salts, the on-site Coulomb repulsion energy U on the DIMET molecule (one ethylenedithio unit per molecule, no Se atom) is probably larger than that in BEDT-TTF (two ethylenedithio units per molecule) and DMET (containing Se atom) molecules, because the extension of HOMO of DIMET molecule must be smaller than those of BEDT-TTF and DMET molecules. On the other hand, the bandwidth W ($=4t$) is smaller in DIMET salts than that in DMET salts as shown in Table 4.4. The small W is probably appropriate to $AuCl_2$ and AuI_2 salts. The large U and the small W in DIMET salts are consistent with the weak temperature dependence of the thermopower and the semiconducting behavior of the resistivity of $(DIMET)_2AuCl_2$ and $(DIMET)_2AuI_2$ as mentioned in the previous chapter. If the dimensionality becomes higher, the condition of the on-site Coulomb repulsion should decrease. Under the assumption of the increase in the dimensionality from $AuCl_2$ and AuI_2 salts to I_3 salt, I_3 salt remains in the metallic character, though the small W are still held in I_3 salt. If the crystal structures of $(DIMET)_2IBr_2$ and $(DIMET)_xCu(NCS)_2$ are solved, this explanation will be confirmed though t's estimated for these salts are somewhat larger than that of I_3 salt.

For DMET salts in Groups 3 and 4, three kinds of short intercolumn and three kinds of short intracolumn contact exist. On the other hand, only two kinds of short intercolumn contact exist for DIMET salts which are isostructural to Groups 3 and 4 DMET salts. The difference between the crystal structures of the DMET and DIMET salts suggests that the decrease in the intracolumn interaction is

smaller than in the intercolumn interaction from the DMET salts to the DIMET salts. As a result, the dimensionality is considered to increase from the DMET salts to the DIMET salts. The decrease in the intracolumn interaction was experimentally confirmed through the measurement of the thermopower. As shown in Tables 2 and 4, the transfer integrals of DIMET salts are smaller than those of DMET salts. The evidence of the higher dimensionality of DIMET salts was also brought by the resistivity measurement with the Montgomery method. The ratio of the conductivities along the most to the second most conducting direction is about from 8 to 20 for both I_3 and IBr_2 salts.

The smaller W and the larger U in DIMET salts than in DMET salts is probably the obstacle against the electrical conduction. In fact, along the stacking direction, the conductivity of DIMET salts is from 1 to 10 S/cm, although that of DMET salts is from 10 to 100 S/cm. The metallic behavior in I_3, IBr_2, $Cu(NCS)_2$ and BF_4 salts of DIMET is, therefore, attributed to the higher dimensionality than DMET salts. Only for the dimensionality, DIMET salts are closer to quasi-2D BEDT-TTF salts than DMET salts. However the conductivity of DIMET salts are at least 10 times smaller than that of DMET and BEDT-TTF salts. Not only the absence of the superconductivity but also the less metallic character in DIMET salts are attributed to the small conductivity in spite of the relatively high dimensionality.

The dimensionality, the magnitude of the conductivity and the bandwidth are closely related to the appearance of the metallic or superconducting behavior in the low dimensional conductors.

4.3 The anomaly in the resistivity and the thermopower of $(DMET)_2Au(CN)_2$, $(DIMET)_2I_3$, $(DIMET)_2IBr_2$ and $(DIMET)_xCu(NCS)_2$.

In the semiconducting region of $(DMET)_2Au(CN)_2$, $(DIMET)_2I_3$, $(DIMET)_2IBr_2$ and $(DIMET)_xCu(NCS)_2$, the very similar anomaly in the resistivity and the thermopower was found in this study. Each of four salts undergoes the M-I transition at a low temperature. In the semiconducting regime, however, the slope of the resistivity in the Arrhenius plot decreases at a lower temperature T^* than T_{M-I} for $(DMET)_2Au(CN)_2$, $(DIMET)_2I_3$ and $(DIMET)_2IBr_2$, though the decrease is gradual in $(DIMET)_xCu(NCS)_2$. The thermopower of these salts below T_{M-I} also shows very similar behavior as shown in Fig. 4.2. The minimum of the thermopower at T^* is seen for all these salts.

The activation energy E_a estimated from the resistivity and the effective activation energy E_{eff} estimated from the thermopower are summarized for these salts in Table 4.5. The E_a's of $(DIMET)_xCu(NCS)_2$ are not shown because T^* is not clear in the resistivity. The ratios of electron-to-hole mobility b estimated using Eq.(2.14) are also summarized in the table. For these salts, the common variation in the band structure speculated from these quantities are described below.

On cooling, the band gap opens at T_{M-I}. This transition is an SDW transition confirmed with the ESR and NMR measurements for $(DMET)_2Au(CN)_2$, $(DIMET)_2I_3$ by Kanoda *et al.*[10,11] After the gap-opening, these salts becomes insulators. Below T_{M-I}, the dominant carrier is electron, namely the shape of the conduction band is more advantageous for electron to move than the valence band. At T^*, the band gap abruptly decreases and b becomes about a half of it, namely the contribution of electron to the conduction relatively decreases below T^*. A certain change in the band structure brings the relative decrease.

At present, no more detail of the change in the band structure can not be speculated. However, because these anomalies are very characteristic, if one measures the thermopower of a material that shows the change in the slope of the Arrhenius plot of the

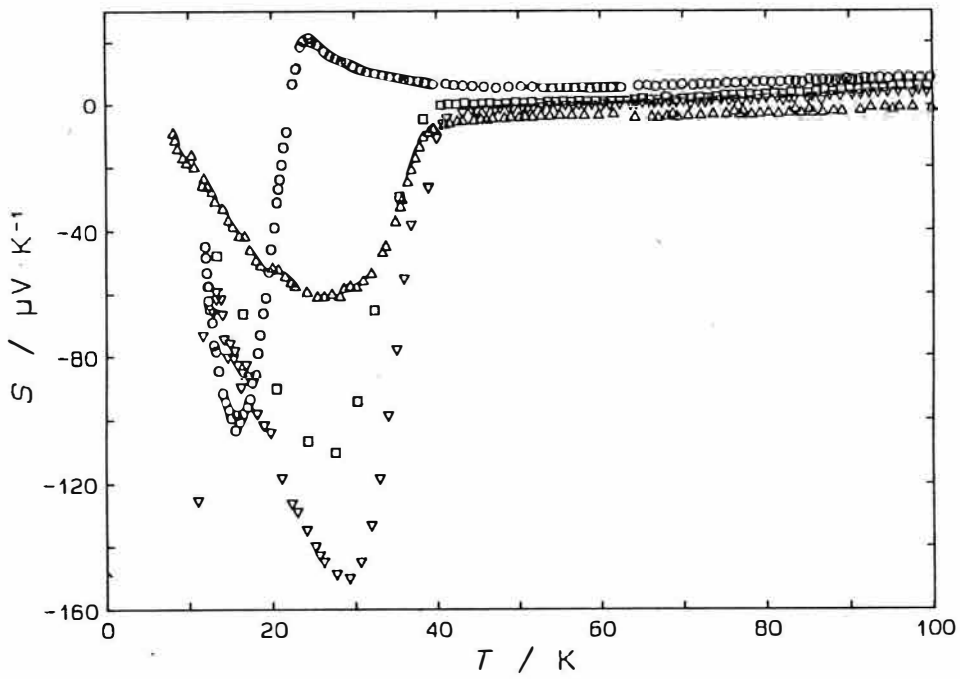

Fig. 4.2. Thermopower of $(DMET)_2Au(CN)_2$ (circles), $(DIMET)_2I_3$ (inverse triangles), $(DIMET)_2IBr_2$ (squares) and $(DIMET)_xCu(NCS)_2$ (triangles) below 100 K.

Table 4.5. E_a, E_{eff} and b of $(DMET)_2Au(CN)_2$, $(DIMET)_2I_3$, $(DIMET)_2IBr_2$ and $(DIMET)_xCu(NCS)_2$.

	$T > T^*$			$T < T^*$		
	E_a / meV	E_{eff} / meV	b	E_a / meV	E_{eff} / meV	b
$(DMET)_2Au(CN)_2$	4.1	-7.9	-3.2	0.28	1.9	-0.74
$(DIMET)_2I_3$	46	-20	2.5	6.0	2.9	1.0
$(DIMET)_2IBr_2$	80	-12	1.4	7.6	1.8	0.61
$(DIMET)_xCu(NCS)_2$	—	-8.5	—	—	0.8	—

resistivity like these, he probably finds the minimum of the thermopower at T^*.

Not only these anomalies, the complicated behavior was found in the SDW state of DMET and DIMET salts in this study, for example the stepwise variation in the ground state of $(DMET)_2BF_4$, $(DMET)_2ClO_4$ and $(DIMET)_2BF_4$. There is a possibility that these phenomena becomes interesting objects to be investigated.

References to Chapter 4

1 K. Kanoda, T. Takahashi, K. Kikuchi, K. Saito, I. Ikemoto and K. Kobayashi, Synth. Metals, 27, B385(1988).

2 Y. Ishikawa, M. Sc. Thesis, Department of Chemistry, Faculty of Sc., Tokyo Metropolitan University(1989).

3 S. Ito, B. Sc. Thesis, Department of Chemistry, Faculty of Sc., Tokyo Metropolitan University(1990).

4 I. Ikemoto, K. Kikuchi, K. Saito, K. Kanoda, T. Takahashi, K. Murata, K. Kobayashi, Mol. Cryst. Liq. Cryst., 181, 185(1990).

5 K. Kikuchi, K. Neriishi, K. Miyazaki, K. Saito, I. Ikemoto and K. Kobayashi, Synth. Metals, 42, 2275(1991).

6 K. Neriishi, M. Sc. Thesis, Department of Chemistry, Faculty of Sc., Tokyo Metropolitan University(1992).

7 R. Laversanne, E. Dupart and P. Delhaes, Mol. Cryst. Liq. Cryst., 137, 179(1986).

8 R. Laversanne, C. Coulon, J. Amiell, E. Dupart, P. Delhaes, J. P. Morand and C. Manigand, Solid State Commun., 58, 765(1986).

9 K. Bender, H. Endres, S. Gärtner, E. Gogu, R. Heid, I. Heinen, H. J. Keller, A. Kraatz and D. Schweitzer, Synth. Metals, 19, 559(1987).

10 K. Kanoda, T. Takahashi, K. Kikuchi, K. Saito, I. Ikemoto and K. Kobayashi, Synth. Metals, 27, B385(1988).

11 K. Kanoda, T. Takahashi, T. Tokiwa, K. Kikuchi, K. Saito, I. Ikemoto and K. Kobayashi, Phys. Rev. B38, 39(1988).

Chapter 5. Summary

The thermopower of typical DMET salts classified into the five groups were measured. For PF_6 and AsF_6 salts in Group 1, the semiconducting behavior was observed and it is consistent with the previous measurement of the resistivity. For BF_4 salt in Group 2, the thermopower was measured along two kinds of stacks. The M-I transition was detected at 35 K and it is consistent with the previous result of the resistivity measurements. From the thermopower, it was found that the bandwidth along the a-axis is larger than that along the b-axis. Furthermore, below T_{M-I} for the both directions, the complicated behavior was observed in the thermopower of BF_4 salt and the corresponding behavior was seen in the resistivity of BF_4 and ClO_4 salts. It suggests the complicated ground states of Group 2 salts at low temperatures. For Group 3, the thermopower of $Au(CN)_2$ salt was measured. A phase transition at 180 K was detected by the thermopower measurement. It was found that the transfer integral becomes smaller below the phase transition temperature. After the characteristic increase above the T_{M-I} 28 K, the thermopower of $Au(CN)_2$ decreases abruptly and changes the sign from plus to minus. In addition, it was also found that the thermopower has a sharp minimum at T^* (the temperature of the change in slope of the Arrhenius plot of the resistivity). The result suggests the change in the electronic structure of $Au(CN)_2$ salt in the SDW phase. For I_3 and SCN salts in Group 4, the metallic behavior of the thermopower was observed and no manifestation of the existence of the insulating phase was encountered. This is consistent with the results of the resistivity measurements. The transfer integrals of I_3 and SCN salts were obtained from the thermopower. Their magnitudes are smaller than that of $Au(CN)_2$ salt in Group 3. The higher dimensionality of the salts in Group 4 than those in Group 3 was confirmed through the thermopower measurement. The discussion concerning the dimensionality and the superconductivity in organic conductors was carried out using the results. For $AuBr_2$ salt in Group 5, the complicated temperature

dependence was observed. The behavior of the thermopower was found to depend on the orientation of the sample crystal strongly.

For DIMET salts, the measurements of the resistivity and the thermopower were made on the newly prepared salts, namely I_3. IBr_2, $Cu(NCS)_2$, $AuCl_2$, AuI_2, Br_3, $Ag(CN)_2$ (linear anions) and BF_4 salts. Some metallic salts, which are very rare among DIMET salts previously reported, were discovered through the resistivity measurement. The metallic salts of I_3, IBr_2, $Cu(NCS)_2$ and BF_4 salts undergo the M-I transition at about 40 K. The other salts were semiconducting below RT. In spite of the similarity in crystal structure of DIMET salts to corresponding DMET salts, the superconductivity was not found on these DIMET salts. The thermopower measurement, however, revealed the characteristic properties of these salts. I_3, IBr_2 and $Cu(NCS)_2$ salts show metallic behavior at RT and a M-I transition occurs at a lower temperature T_{M-I}. Below T_{M-I}, the thermopower of these salts abruptly decreases and changes its sign from plus to minus. Furthermore at a characteristic temperature T^*, these salts show a minimum of the thermopower and their thermopower turns to increase below T^*. Their resistivity changes the slope in the Arrhenius plot at T^*. These behaviors of the resistivity and the thermopower are similar to that observed for $(DMET)_2Au(CN)_2$. The discussion on these phenomena was made. In the metallic region of I_3, IBr_2 and $Cu(NCS)_2$ salts, the decrease in slope of thermopower versus temperature was observed below about 250 K, though the thermopowers is well fitted to the linear temperature dependence above about 250 K for each of the three salts. Referring to the result of the measurement of the anisotropy in resistivity with the Montgomery method, the possibility was pointed out that the change in the slope of the thermopower versus temperature is related to the cross-over of the dimensionality in these salts. Among the semiconducting DIMET salts, $AuCl_2$ and AuI_2 salts are isostructural to $(DIMET)_2I_3$, though the electrical properties of the two salts are very different from I_3 salt. The relation between the dimensionality and the metallic behavior in organic conductors was discussed.

Acknowledgements

I wish to thank Prof. Isao Ikemoto for his guidance. Although he is always busy, he gives us, students, valuable advice at every opportunity.

I am grateful to Dr. Kazuya Saito for guiding me zealously. The discussion with him has improved my ability to study science. Furthermore he kindly suggested me to write this master's thesis in English and corrected my mistakes. If he had been not, the thesis would has never become the style at present. Except due to the existence of the unknown true, my misunderstanding is responsible for all mistakes and errors in the thesis.

I also wish to acknowledge Dr. Koichi Kikuchi's guidance. His advice, especially on my preparation of the presentation at learned societies, was very valuable. This is also useful for the thesis.

I wish to thank Dr. Keio Toi and Dr. Toshiaki Shirakawa for their suggestion when I use personal computers and computer softs.

I am grateful to Messrs. Hiroyuki Kamio, Masayoshi Ishibashi, Hideki Saito, Tadashi Mochiduki and Ms. Keiko Neriishi for their help for the measurement. The new sample-holder and programs for the thermopower measurement were improved from Mr. Kamio's works. Mr. Ishibashi taught me most techniques to measure resistivity and so on. Mr. Tadashi Mochiduki supplied the sample crystals of DMET and DIMET radical salts. Mr. Hideki Saito and Ms. Keiko Neriishi helped me to determine the correspondence between the crystal axes and the growing edges of the crystals of $(DMET)_2BF_4$ and $(DIMET)_2BF_4$. The discussion with these people was not only useful for the study but also the stimulus in my life.

I wish to thank Messrs. Nobuo Nakahara, Hisanori Ueno, Hideyoshi Saito and Yasuhisa Yamamura, who helped me to finish writing the thesis on January 10.

Without all people above and others who helped me, I could not have completed this thesis.